Li and Mg isotopes as proxies for tracing element cycling in the Critical Zone

Dissertation

zur Erlangung des Grades eines
Doktors der Naturwissenschaften (doctor rerum naturalium)

am Fachbereich Geowissenschaften
der Freien Universität Berlin

vorgelegt von
Di Cai
Berlin 2021

Erstgutachter: Prof. Dr. Friedhelm von Blanckenburg
Freie Universität Berlin

Zweitgutachter: Prof. Dr. Xiao-ming Liu
University of North Carolina at Chapel Hill

Tag der Disputation: 03.02.2022

Eidesstattliche Erklärung

Hiermit erkläre ich, dass ich die vorliegende Dissertation selbstständig und ohne unzulässige Hilfe verfasst habe. Bei der Verfassung dieser Dissertation wurden keine anderen als die im Text und Literaturverzeichnis aufgeführten, Hilfsmittel und Quellen verwendet. Beiträge von Koautoren zu publizierten oder zur Publikation vorbereiteten Manuskripten sind im Vorwort (“Preface”) dieser Arbeit dargelegt. Ich versichere, dass die vorgelegte elektronische mit der schriftlichen Version der Dissertation übereinstimmt. Ein Promotionsverfahren zu einem früheren Zeitpunkt an einer anderen Hochschule oder einem anderen Fachbereich wurde nicht beantragt.

Potsdam, 18.11.2021

_____

Di Cai

Acknowledgements

I would like to express my deepest gratitude to all people who have helped and supported me during my past 4.5 years.

First of all, deepest appreciation to my supervisor Friedhelm von Blanckenburg, who accepted my application at the very beginning and brought me to this diverse and harmonious group. Thanks for all your effort, especially your scientific guidance, constructive discussions and feedbacks during my research. Without you, I would not have this opportunity to get access to the state-of-art instruments and conduct the frontier research for my PhD.

Secondly, I sincerely acknowledge the assistant from my co-supervisor Michael Henehan. Thanks for your patience in helping me out in the lab all the time and editing my manuscript. English writing is always a big obstacle for me. Thanks for helping me improve my writing skill.

My research is the following-up work of DFG priority program SPP 1685 "Ecosystem Nutrition—Forest Strategies for limited Phosphorus Resources". I'm grateful for all the members of SPP 1685 project, who instrumented the research site, collected the samples and background information, and made a lot of scientific achievements for following research. Special thanks are given to David Uhlig, for the pioneering work in this research site. Your papers and dissertation inspired me a lot. Your thorough comments on my manuscript also have significantly improved its quality.

I'd also like to express my great gratitude to technicians and lab managers of HELGES. A well organised lab has made my research life much easier. Many thanks to Jutta Schlegel and Josefine Holtz, who taught me the basic knowledge of chromatography and mass spectrometry, and are always helpful in the lab. I'm also very grateful to Daniel Frick, Tanya Goldberg and Patrick Frings, thanks for your timely help when I met troubles in the mass spectrometer lab. Johannes Glodny is acknowledged for support on mineral separation. Ralf Oeser is also acknowledged for showing me how to use the microwave digestion system, and Laura Krone for help on the German summary.

I'm proud of being a member of Earth Surface Geochemistry section at the GFZ, not only because of the frontier scientific questions investigated here but also the humorous atmosphere we have created. Thanks for all the group members, who are always so creative and warm hearted. Working in this environment is really enjoyable. Although we could not see each in face during pandemic, regular online meeting has successfully connected each other remotely. Special thanks are given to Coni Dettlaff for being so kind in dealing with all administration issues and preparing coffee and tea for every Tuesday's group meeting before Covid-19.

I would also like to pay my special regards to China Scholarship Council, who provided financial support for my living in Germany.

Finally, this study would not have been possible without the support from my parents. Thanks for cheering me up in this depressing COVID-19 pandemic. Your continuous love and encouragement are my emotional anchor.

Summary

The Critical Zone (CZ) is the thin, near-surface zone of terrestrial Earth, extending from the canopy of trees to the groundwater table. Within this system, coupled chemical, biological, physical, and geological processes operate together to support life at the Earth's surface. A major consideration in Critical Zone research is quantitatively predicting mass transfer fluxes between different compartments like soil, bedrock, water and biomass, and evaluating the influence of environmental forces on mass transfer. Elements (e.g., Li, Mg, Ca, Sr) concentrations and their isotopes have been widely employed to quantify mass transfer. Critical Zone processes, including primary mineral dissolution, secondary mineral formation, adsorption/desorption, biological recycling, are generally associated with different fractionation factors for a specific isotopic system. Therefore, measured isotope ratios along with concentrations could fingerprint the reaction pathways and magnitude of Critical Zone processes.

In this study, I have chosen the stable isotopes of Lithium (Li) and Magnesium (Mg) isotope tools to investigate Critical Zone processes. Mg and Li constitute nutritive and non-nutritive elements, respectively, Conventwald (the Black Forest, south Germany) was chosen as the research site as this site has been intensively monitored. By comprehensive sampling (including plant tissues, soil, bedrock, saprolite, subsurface flow, groundwater, creek water and wet precipitation samples), Critical Zone processes encompassing different time scales were investigated, e.g. how rock was converted into soil, how water chemistry evolves from precipitation to runoff and how biomass recycle nutritive elements. In addition, effort was made to balance Li, Mg isotope budgets at the catchment scale.

The Mg isotopic composition (the $^{26}Mg/^{24}Mg$ ratio expressed as $\delta^{26}Mg$ in permil) is similar between soil and regolith samples, and is higher than that of bedrock. This was attributed to preferential dissolution of amphibole and formation of secondary minerals during pedogenesis. Mg hosted in neoformed secondary minerals accounts for ~ 50% of total Mg in the soil as calculated by mass balance. Water samples did not show seasonal variability, despite large variation in dissolved Mg concentration. Subsurface flow samples have similar $\delta^{26}Mg$ values to the regolith exchangeable fraction at the respective sampling depths. Groundwater and creek water also show $\delta^{26}Mg$ values that are identical to those of the exchangeable fraction in the deep regolith. I suggest that cation-exchange processes in the regolith buffer $\delta^{26}Mg$ of creek water at our study site. To further explore this hypothesis, adsorption and desorption experiments using soil samples from our study site were carried out. The results showed negligible Mg isotope fractionation during adsorption-desorption, supporting our hypothesis that water $\delta^{26}Mg$ is in equilibrium of corresponding exchangeable $\delta^{26}Mg$ in this study site. The large pool of Mg in the exchangeable fraction of the deep regolith (>3 m) is isotopically light and presents most likely the Mg residue in soil water that entered the exchangeable pool after secondary mineral

formation - a process which often favours heavy Mg isotopes. The exchangeable fraction in the shallow regolith (0-3 m depth) shows a strong imprint of biological cycling. Plant uptake of Mg starts from ~3m, which drives the exchangeable $\delta^{26}Mg$ more negative towards the surface, but super-imposed on this the plant-recycled isotopically-heavy Mg is returned to the soil, enriching the exchangeable fraction of the top ~1.5m of soil in heavy Mg isotopes. Mg isotopes thus provide an exact depth image of the geogenic (weathering) and the organic (bio-cycled) nutrient cycle. At the catchment scale, dissolved Mg exported by creek water relative to the total export of solute and particulate Mg is 41 ± 11% as calculated by an isotope balance equation.

Li isotopes show different behaviour in the Critical Zone as compared to Mg isotopes. Li fluxes calculation show that wet precipitation and plant uptake have negligible impact on Li cycling in the catchment. Therefore, the $^{7}Li/^{6}Li$ ratio (expressed as $\delta^{7}Li$ in permil) is a good tracer for abiotic weathering. Both subsurface flow and creek water show seasonal variation in $\delta^{7}Li$, while groundwater exhibits negligible $\delta^{7}Li$ variation. Along with measurement of bedrock, bulk regolith, clay-sized fraction, vegetation and the exchangeable fraction of regolith, I suggest that $\delta^{7}Li$ variation in different water reservoirs indicate different chemical evolution pathways. $\delta^{7}Li$ in shallow subsurface flow (0-15 cm) become more positive with increasing Li concentration, and a binary mixing process could be identified with two endmembers being throughfall and pre-event soil solution. During rainfall events, dilute precipitation (enriched in ^{6}Li) flushed old, concentrated soil solution (enriched in ^{7}Li) retained in the soil matrix, and thus a mixing pattern was seen in $1/Li$-$\delta^{7}Li$ space. Groundwater exhibits negligible $\delta^{7}Li$ variation despite Li concentration and groundwater table fluctuations, which most likely reflects a buffering effect of deep exchangeable pool. This interpretation is similar to the one I offer to explain the invariance of $\delta^{26}Mg$ in groundwater. The only difference is that isotope fractionation occurs during Li exchange, as groundwater is ~ 4 ‰ heavier than the corresponding exchangeable pool $\delta^{7}Li$, while negligible fractionation is observed for Mg isotopes. In creek water samples, $\delta^{7}Li$ covaried with proportion of Li remaining in the solution. This fractionation could be attributed to Li incorporation or adsorption to secondary minerals during downstream transport, favouring ^{6}Li. Surprisingly, despite the heavy $\delta^{7}Li$ exported in dissolved form, saprolite and soil are almost isotopically identical to bedrock. A reservoir or flux enriched in ^{6}Li is missing. Several potential factors are discussed to account for this isotope imbalance and the potential reservoir or fluxes are listed. As separated clay-sized fraction from soil is enriched in ^{6}Li, it is likely that fine particulates that are preferentially exported by subsurface flow could be the missing flux.

In summary, contrasting Mg and Li recycling regimes were observed in this research. As anticipated, Mg was more involved in biological recycling compared to Li. Primary minerals in the bedrock showed homogenous $\delta^{7}Li$ but heterogeneous $\delta^{26}Mg$,

and therefore preferential dissolution of hornblende induced $\delta^{26}Mg$ variation in the weathering regolith but not for $\delta^{7}Li$. The biggest difference between $\delta^{7}Li$ and $\delta^{26}Mg$ variation is seen in water samples: subsurface flow, groundwater and creek water showed negligible seasonal variation in $\delta^{26}Mg$, but this is not the case for $\delta^{7}Li$. I attribute the invariance of water $\delta^{26}Mg$ to the buffering effect of exchangeable pool. By contrast, only groundwater exhibited invariant $\delta^{7}Li$. While this might also reflect the buffering effect of exchangeable pool, large $\delta^{7}Li$ variability in subsurface flow and creek water requires different explanations. Two-endmember mixing and further Li incorporation into secondary minerals were put forward to explain $\delta^{7}Li$ variation in subsurface flow and creek water respectively. For both elements, secondary mineral formation is the most important process fractionating isotopic composition of water at this study site.

Zusammenfassung

Die kritische Zone (Englisch: Critical Zone, CZ) ist die dünne, oberflächennahe Schicht der festen Erde, die sich von den Baumwipfeln bis zum Grundwasserspiegel erstreckt. Innerhalb dieser Zone wirken gekoppelte chemische, biologische, physikalische und geologische Prozesse zusammen, und schaffen dadurch die Bedingungen für Leben auf der Erdoberfläche. In der Erforschung der kritischen Zone sind die quantitative Berechnung des Massentransportflusses zwischen den verschiedenen Komponenten Boden, Grundgestein, Wasser und Biomasse, sowie die Messung von Umwelteinflüssen auf den Massentransport wesentliche Aspekte. Zur Quantifizierung dieses Massentransports wurden häufig Elementkonzentrationen (z.B. von Li, Mg, Ca, Sr) und deren stabile Isotope eingesetzt. Grundsätzlich sind mit den Prozessen in der kritischen Zone, zu denen die Auflösung von Primärmineralen, Bildung von Sekundärmineralen, Adsorption und Desorption und biologisches Recycling gehören, verschiedene Fraktionierungsfaktoren für bestimmte stabile Isotopensysteme verbunden. Daher können die gemessenen Isotopenverhältnisse zusammen mit den Konzentrationen einen Nachweis über Reaktionswege und Ausmaß der Prozesse in der kritischen Zone liefern.

In dieser Studie habe ich zur Untersuchung von Prozessen in der kritischen Zone die Systeme der stabilen Isotope von Magnesium (Mg) und Lithium (Li) ausgewählt, wobei Mg als ein Nährstoff für Pflanzen gilt, während Li kaum aufgenommen wird. Das Untersuchungsgebiet Conventwald (Schwarzwald, Süddeutschland) wurde ausgewählt, da dort bereits intensive Beobachtungen durchgeführt wurden. Eine umfassende Beprobung einschließlich Pflanzengewebe, Boden, unverwittertes Gestein, Saprolith, unterirdischer Wasserfluss, Grundwasser, Bachwasser und Niederschlagswasser ermöglicht die Untersuchung von Prozessen in der kritischen Zone. Prozesse in dieser Zone laufen auf verschiedenen Zeitskalen ab, wie beispielsweise die Umwandlung von Gestein in Boden, die Änderung der Wasserchemie vom Niederschlag zum Abfluss oder das Nährstoffrecycling der Biomasse. Zusätzlich zu diesen Untersuchungen habe ich ermittelt, ob ein Gleichgewicht der Isotopenhaushalte von Li und Mg im Einzugsgebiet besteht.

Die Isotopenzusammensetzung der stabilen Isotope des Mg (das Verhältnis $^{26}Mg/^{24}Mg$ wird ausgedrückt durch $\delta^{26}Mg$ in Promille) ist ähnelt sich in Boden- und Regolithproben aber ist höher als im unverwitterten Gestein. Dies kann auf die bevorzugte Auflösung von Amphibol und die Bildung von Sekundärmineralen während der Verwitterung zurückgeführt werden. Das in den ausgefällten Sekundärmineralen enthaltene Mg macht in der Massenbilanz etwa 50% des gesamten Mg im Boden aus. In den Wasserproben zeigen sich keine saisonalen Schwankungen, obwohl die Konzentration des gelösten Mg stark variiert. Proben aus dem Bodenwasser weisen ähnliche $\delta^{26}Mg$ Werte wie die austauschbare Fraktion des Regoliths in den jeweiligen Beprobungstiefen auf. Im Grund- und Bachwasser

sind die δ^{26}Mg Werte ebenfalls identisch mit der austauschbaren Fraktion des tiefen Regoliths. Vermutlich puffern Kationenaustauschprozesse im Regolith das δ^{26}Mg des Bachwassers an unserem Untersuchungsstandort. Um diese Hypothese zu untersuchen, wurden Adsorptions- und Desorptionsexperimente an Bodenproben durchgeführt. Die Ergebnisse zeigen eine vernachlässigbare Mg Isotopenfraktionierung während Adsorption und Desorption. Das stützt unsere Hypothese, dass sich das δ^{26}Mg des Wassers im Gleichgewicht mit dem zugehörigen austauschbaren δ^{26}Mg befindet. Der große Mg Pool in der austauschbaren Fraktion des tiefen Regoliths (>3 m) ist isotopisch leicht und stellt höchstwahrscheinlich die Mg Rückstände im Bodenwasser dar, die nach der Sekundärmineralbildung in den austauschbaren Pool gelangten – ein Prozess, der häufig schwere Mg Isotope bevorzugt. Die austauschbare Fraktion des flachen Regoliths (0-3 m) zeigt deutliche Spuren des biologischen Kreislaufs. In ~3 m Tiefe beginnt die Mg Aufnahme durch Pflanzen, wodurch das austauschbare δ^{26}Mg zur Oberfläche hin negativer wird. Durch die Zurückführung von isotopisch schwerem Mg in den Boden wird dieses Signal überlagert, so dass die austauschbare Fraktion in den oberen ~1.5m des Bodens mit schweren Mg Isotopen angereichert wird. Daher liefern Mg Isotope ein exaktes Tiefenprofil des geogenen (Verwitterung) und organischen (biologisches Recycling) Nährstoffkreislaufs. In der Größenordnung des Einzugsgebiets beträgt der Export von gelöstem Mg durch das Bachwasser im Verhältnis zum Gesamtexport von gelösten und partikulärem Mg 41 ± 11%, berechnet mit einer Isotopen Massenbilanz.

Die stabilen Isotope des Li Isotope zeigen ein anderes Verhalten in der kritischen Zone als Mg. Die Berechnung der Li Flüsse zeigt, dass Niederschlag und Pflanzenaufnahme einen vernachlässigbaren Einfluss auf den Li Kreislauf im Einzugsgebiet haben. Daher ist das ^{7}Li/^{6}Li Verhältnis (ausgedrückt durch δ^{7}Li in Promille) ein guter Indikator für abiotische Verwitterung. Der Fluss von sowohl Bodenwasser als auch Abfluss zeigt saisonale Schwankungen in δ^{7}Li, wobei im Grundwasser die δ^{7}Li Schwankungen vernachlässigbar sind. Zusammen mit den Messungen von Proben des unverwitterten Gesteins, Regoliths, der tongroßen Fraktion, Vegetation und der austauschbaren Fraktion des Regoliths nehmen wir an, dass die δ^{7}Li Schwankungen in verschiedenen Wasserreservoiren unterschiedliche chemische Entwicklungswege aufzeigen. Im Bodenwasser (0-15 cm) wird δ^{7}Li mit zunehmender Li Konzentration höher; ein binärer Mischungsprozess mit den zwei Endgliedern - Baumkronendurchlass und Bodenlösung durch Wasser von vorherigen Niederschlagsereignissen - konnte bestimmt werden. Während Niederschlagsereignissen spült verdünnter Niederschlag (angereichert in ^{6}Li) alte, konzentrierte Bodenlösung (angereichert in ^{7}Li), die in der Bodenmatrix gespeichert ist, aus, wodurch ein Mischungsmuster im 1/Li-δ^{7}Li Raum zu beobachten ist. Das Grundwasser weist trotz der Li Konzentrationen und Veränderungen des Grundwasserspiegels vernachlässigbare Schwankungen von δ^{7}Li auf, die wahrscheinlich auf eine Pufferwirkung des tiefen austauschbaren Pools

zurückzuführen sind. Diese Interpretation ist ähnlich zu der, die ich zur Erklärung der Invariabilität von δ^{26}Mg im Grundwasser gebe. Der einzige Unterschied ist, dass beim Austausch die Li Isotope fraktioniert werden, da das Grundwasser ~ 4 ‰ schwerer ist als der dazugehörige austauschbare δ^{7}Li Pool, während die Isotopenfraktionierung für Mg vernachlässigbar ist. In Proben des Bachwassers kovariiert δ^{7}Li mit dem Li Anteil, der in Lösung verbleibt. Diese Fraktionierung kann auf den Einbau von Li oder die Adsorption an Sekundärminerale während des Abwärtsflusses zurückgeführt werden, bei dem ^{6}Li bevorzugt wird. Überraschenderweise sind Saprolith und Boden isotopisch nahezu identisch zum unverwitterten Gestein, obwohl schweres δ^{7}Li in der gelösten Form exportiert wird. Um das Isotopenungleichgewicht zu erklären, fehlt ein Reservoir oder Fluss, der in ^{6}Li angereichert ist. Einige potenzielle Faktoren, die dieses Ungleichgewicht erklären können, werden erörtert und potenzielle Reservoire und Flüsse aufgelistet. Es ist wahrscheinlich, dass der bevorzugte Transport von feinen Partikeln durch den unterirdischen Wasserfluss der fehlende Fluss ist, da die abgetrennte tongroße Fraktion des Bodens in ^{6}Li angereichter ist.

In dieser Studie wurden die gegensätzlichen Recycling-Regime Mg und Li untersucht. Mg ist im Vergleich zu Li wie erwartet stärker involviert in biologisches Recycling. Primärminerale im Grundgestein wiesen ein homogenes δ^{7}Li, aber heterogenes δ^{26}Mg auf, daher können wir annehmen, dass die bevorzugte Auflösung von Hornblende zu Variationen in δ^{26}Mg, aber nicht in δ^{7}Li führt. Der größte Unterschied der δ^{7}Li und δ^{26}Mg Schwankungen ist in den Wasserproben sichtbar: unterirdischer Wasserfluss, Grundwasser und Bachwasser zeigten vernachlässigbare saisonale Schwankungen in δ^{26}Mg, was aber nicht für δ^{7}Li zutrifft. Die Invariabilität von δ^{26}Mg im Wasser führe ich auf den Puffereffekt des austauschbaren Pools zurück. Im Gegensatz dazu weist nur Grundwasser invariables δ^{7}Li auf. Während das ebenfalls die Pufferwirkung des austauschbaren Pools reflektieren könnte, benötigt die große Variabilität in δ^{7}Li im tiefen Wasserfluss und Bachwasser andere Erklärungen. Als Erklärung für diese Variabilität wurde ein binärer Mischungsprozess und weiterer Einbau von Li in Sekundärminerale vorgeschlagen. Für beide Elemente ist die Sekundärmineralbildung der wichtigste Prozess, der für die Fraktionierung der Isotope in den Wassern am Untersuchungsstandort verantwortlich ist.

Preface

This PhD thesis includes 4 chapters and is a cumulative collection of an introductory chapter, two scientific studies and a conclusion chapter. Below, I provided more information of each chapter, and the co-authors that are involved. Submission status is also provided.

Chapter 1 is the introduction chapter. This chapter introduces the concept of the Critical Zone and the application of isotope tools in the Critical Zone research. Research gaps are identified, and the objectives of this study are set. Mg and Li isotopes were chosen as the proxies and isotopic fractionation mechanisms of these two elements are reviewed. This chapter also provides a detailed description of methods used for isotope ratio determination, and an introduction to the research site.

Chapter 2 presents the first scientific study with the title: "Mg isotopic composition of runoff is buffered by the regolith exchangeable pool". This chapter was submitted to the journal Geochimica et Cosmochimica Acta. Co-authors involved in this study are Michael Henehan, David Uhlig and Friedhelm von Blanckenburg. This study reports the Mg isotopic composition of different compartments of the Critical Zone at the Conventwald research site and focuses on the mechanisms driving Mg isotopes fractionation during weathering. This study was designed by Friedhelm von Blanckenburg and me. David Uhlig collected samples. I conducted laboratory work. All co-authors contributed to data interpretation. I prepared the manuscript with the help of all co-authors.

Chapter 3 presents the second scientific study with the title "Identifying pathways for dissolved Li from its isotopic composition during weathering in a temperate forested catchment". This study is prepared for further submission to a scientific journal. This study focusses on the Li isotopic composition of different compartments of the research site and discusses the potential driving forces fractionating Li isotopes in the course of weathering. Friedhelm von Blanckenburg and I designed the research. I conducted the laboratory work and wrote the manuscript. Friedhelm von Blanckenburg, Michael Henehan and David Uhlig helped with data interpretation and revised the manuscript.

Chapter 4 is the final synthesis of the research. It summarizes the work that has been done and research results of previous chapters. It also provides implications for future Critical Zone research.

List of Figures

List of tables

Table of Contents

Chapter 1

Introduction

The Earth's Critical Zone (CZ) is defined as the thin layer of the Earth's surface and near-surface terrestrial environment from the top of the vegetation canopy (or atmosphere–vegetation interface) to the bottom of the weathering zone (or freshwater–bedrock interface) (National Research Council, 2001; Brantley et al., 2007). Critical Zone science is the study of integrated Earth surface processes (such as weathering, hydrology, geochemistry, and ecology) at multiple spatial and temporal scales and across anthropogenic gradients. These processes impact mass and energy exchange necessary for biomass productivity, chemical cycling, and water storage. Research topics within the Critical Zone framework include regolith development, streamflow formation, landscape evolution, biosphere-lithosphere interaction and so on.

The Critical Zone can be divided into several compartments, for example: unweathered bedrock, saprolite, soil, plant biomass, soil water, groundwater, and river water (Bouchez et al., 2013). Some compartments can be further divided into several sub-compartments for research purposes, for example, bulk soil is composed of primary minerals, secondary minerals, organic matter, etc. A key consideration of Critical Zone research is mass transfer between different compartments, which can often be ascertained through measuring the chemical composition of – and partitioning of elements between – these compartments.

However, elemental concentration is not always a perfect tracer of the Critical Zone processes at work. The concentration of a specific element varies due to either physico-chemical reactions of this element or other dilution/enrichment factors. For example, the major elements concentrations in soil water and runoff are controlled by both evapotranspiration and reactions, concentration alone could not disentangle these two processes. Normalising to a conservative tracer (like Cl) is generally applied in field research (e.g. Lemarchand et al., 2010; Tipper et al., 2012). Similarly, to evaluate the net gain or loss of a particular element of a weathering regolith, normalizing to an immobile element (like Zr) is always applied (e.g. Brimhall and Dietrich, 1987). However, Cl and Zr or other assumed conservative elements are not always ideally conservative when examined closely (e.g. Rodstedth et al., 2003; Bastviken et al., 2007; Bern and White, 2011), which hinders our interpretation on geochemical processes based on concentration data alone. In this case, the isotopic composition of a single element could provide extra information regardless of dilution or enrichment factor.

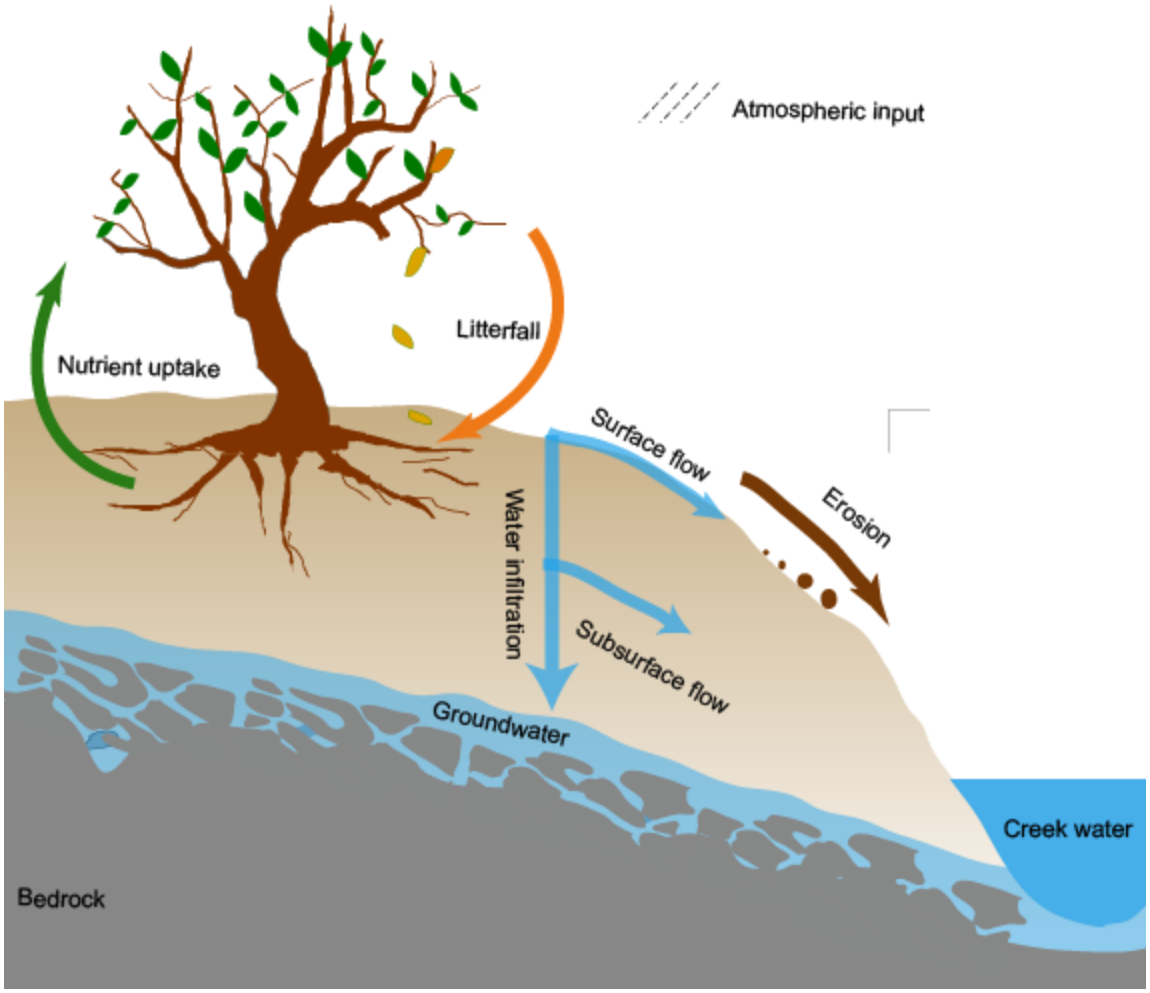

Fig. 1-1 Sketch of the Critical Zone in this study. Major compartments and different processes are shown.

For example, isotope ratios could be either used to identify the source of a specific element if negligible fractionation occurs, or to trace biogeochemical reactions if the associated fractionation factor is well constrained. Another disadvantage of relying on elemental concentrations as a sole tracer of Critical Zone processes is the measurement precision. Typical uncertainty of trace elements measurement (by ICP-MS) and major elements (by ICP-OES) is about 5 %, which may not always be sufficient to answer research questions. To overcome these drawbacks, the measurement of isotopes has been developed into powerful tracer in the recent years. The measured isotope values are the ratio of two isotopes rather than absolute concentration and the precision is generally much higher compared to concentration measurement, with precision being better than 0.5‰ to 0.05‰ for most commonly used isotopes (e.g. Li, Mg, Si, Ca, etc.).

In the past, accurate determination of isotope ratios was only possible for a few elements like H, O, S, C, N (generally light elements). Thanks to the development

of mass spectrometry technology – in particular the advent of Multi-collector Inductively Coupled Plasma Mass Spectrometry (MC-ICPMS) – accurate determination of many new isotopes such as Li, Mg, Si, Ca is now possible. These isotopes are often called non-traditional isotopes, so as to differentiate with the aforementioned light elements. Since then, the geochemical behaviour of most elements could be better understood. In the Critical Zone research, the application of novel isotopes in tracing biological recycling and chemical weathering has achieved many new scientific findings and has also been proven powerful tracers. Here, development of these research was reviewed, and research gaps were also constrained, as a guide for this work.

1.1. Metal isotopes as a tracer for chemical weathering processes

Chemical weathering solubilize cations from minerals and these soluble elements are transported to the ocean by rivers and groundwater. In the ocean, Ca, Mg is removed in combination with HCO_3^- to form carbonate minerals. Ultimately, this process not only modifies chemical composition of continent and ocean but also regulates atmospheric CO_2 and thus also climate (Berner, 1992; Gaillardet et al., 1999; Kump et al., 2000). It is notable that only weathering of Mg and in particular Ca from silicate minerals results in net removal of CO_2 from atmosphere, and it is silicate weathering rather than carbonate weathering that exerts a major long-term control on atmospheric CO_2 (Berner, 1992). Early chemical weathering research focused mainly on the element concentrations and fluxes in river water, and environmental factors that control water-rock interaction. Lithology, topography, climate (temperature and runoff), and vegetation cover are all thought be majors factors governing weathering rate and regimes as revealed by previous studies (e.g. Berner, 1997; White et al., 1999; Riebe et al., 2001; Maher, 2010). In recent years, accurate measurement of metal(loid) isotopes has provided more constraints on a specific element's behaviour during weathering and have shed new light on the feedback between climate change and continental weathering. Among the various isotopic systems (e.g. Ca, Mg, K, Sr, Li, Si, etc) which have been investigated, Ca, Mg and Li have attracted particulate interest, since the transformation of Mg(Ca) silicates on the continent to carbonate in the ocean plays the central role in consuming CO_2 during weathering, and since Li is mainly hosted in silicate minerals thus also a good silicate weathering tracer. Generally, the mechanisms (or environmental factors) inducing isotope fractionations are firstly investigated and subsequently isotope composition of geological reservoirs or archives were used to reconstruct weathering process or weathering history. For example, Li incorporation/adsorption into secondary minerals is thought to be the major process fractionating Li isotopes during weathering and the Li isotopic difference between river water and sediments mainly reflects the fractionation of Li dissolved compared to the Li incorporated (e.g. Huh et al., 1998; Vigier et al., 2009; Dellinger et al., 2015; Li et al., 2020). Weathering-limited regions (mountainous areas where weathering is limited by kinetics of mineral dissolution) and transport-limited

regions (tectonically quiescent landscapes where weathering results in complete dissolution of minerals) are both characterized by less fractionated Li isotopes in the river water (Dellinger et al., 2015). This is due to little secondary mineral formation and secondary mineral dissolution in the two regimes respectively. And thus, Li isotopes could be used to depict weathering regimes (kinetic or transport limited) of different catchments. More importantly, using foraminifera archives, Misra and Froelich, (2012) reconstructed the evolution of the Li isotope composition of seawater from 70 Ma ago to present, which has stimulated modelling endeavours for tracing continental weathering history in the Cenozoic (e.g. Bouchez et al., 2013; Wanner et al., 2014; Li and West, 2014; Vigier and Goddéris, 2015; Caves Rugenstein et al., 2019). Although these modelling results sometimes differ in their interpretation, Li isotopes have proven a unique and powerful tracer for weathering process. Unlike Li, Mg (and also Ca) are also subject to biological influence, which raises extra uncertainty for weathering studies. Weathering profile research has identified secondary mineral formation as major controlling factor fractionating Mg isotopes in soil (Teng et al., 2010; Liu et al., 2014), but Mg isotope signatures of soil water and river water also indicate the non-negligible role of bioactivity (e.g. Bolou-Bi et al., 2010; Tipper et al., 2010; Uhlig et al., 2017). Similarly, application of Ca isotopes has indicated that Ca stable isotope fractionation observed in watersheds is primarily biological in origin (Wiegand et al., 2005; Page et al., 2008; Holmden and Bélanger, 2010; Bullen and Chadwick, 2016). Therefore, in contrast to Li isotopes which are a good tracer for abiotic weathering, Mg and Ca are isotopes are also subject to fractionation during bio-cycling, a topic we discuss in the following section.

1.2. Metal isotopes as a tracer for nutritive elements recycling by plants

Macronutrients for plants include N, P, K, S, Ca and Mg. Studies of biological recycling of nutritive elements span more than 100 years (Attiwill and Adams, 1993 and reference therein). Early research mainly focused on measurement of element pools in plants and soil, and also uptake and return (via litter fall) of elements between these two compartments (Attiwill, 1968; Vitousek and Sanford, 1986; Anderson, 1988; Attiwill and Adams, 1993 and reference therein). Later, C, O, N isotope tools were developed and widely applied to forest science, which greatly expanded our understanding of processes like photosynthesis (e.g. O'Leary, 1988), water uptake (e.g. Ehleringer and Dawson, 1992), and nitrogen utilization (e.g. Martinelli et al., 1999). In recent years, accurate determination of metal isotopes has made tracing metal nutritive element recycling possible. The major questions investigated using these isotope techniques include 1) identifying the source (or depth) from which plant uptake metal nutrients, 2) how plant activity affects chemical weathering (by e.g. accelerating chemical weathering rate or controlling runoff chemistry). Tracing nutrient sources is crucial as it reveals how an ecosystem maintains a healthy nutrient inventory. Radiogenic Sr isotopes were amongst the first to be applied in field studies, followed by Mg and Ca isotopes. However,

conclusions differ between studies. Drouet et al., (2005) estimated that most Ca uptake happened at the forest floor (from atmospheric input) in two Belgian forests by using radiogenic Sr isotopes. Similarly, application of stable and radiogenic Ca isotope in a north-eastern USA forest (Farkaš et al., 2011) also indicated Ca uptake mostly originated from the shallow soil layer. Shallow Mg uptake was also inferred from a labelled ^{26}Mg spiking experiment (van der Heijden et al., 2015) in a French forest. By contrast, radiogenic Sr and Ca isotope evidence has shown deep uptake in the mineral soil layer in other settings (Dijkstra and Smits, 2002; Brandtberg et al., 2004; Berger et al., 2006). Recently, Uhlig et al., (2020) suggest that nutrient uptake could even reach ~3 m depth, based on radiogenic Sr and ^{10}Be/^{9}Be isotopes. Therefore, the depth at which metal nutrients are taken up by plants remains somewhat poorly constrained, which has hindered our understanding of the sources (i.e., atmospheric input or deep weathering input) that replenish the nutrient pool.

Another important application of metal isotopes is evaluating biological influence on weathering. Plants and their associated fungal activity are thought to be able to enhance weathering to constantly liberate nutrients from rock. The mechanisms by which they accelerate weathering include penetration of roots which expand fractures (e.g. Roering et al., 2010; Pawlik et al., 2016; Hasenmueller et al., 2017), acidification of the rhizosphere that increases mineral solubility (e.g. Lucas, 2001; Schöll et al., 2006; Brantley et al., 2011), and root-associated fungi directly altering mineral surfaces (e.g. Jongmans et al., 1997; Bonneville et al., 2009; Frey et al., 2010). Investigations of biological influence on weathering of rocks have been carried out from nano scale to field scale and fractionation of metal isotopes (especially Mg and Ca) are identified in many biological processes. From nano scale, ectomycorrhizal fungi can mobilise and accumulate Mg, K, and P from mineral particles (Bonneville et al., 2009; Gerrits et al., 2020; Wild et al., 2021) and Mg is also fractionated during the uptake process (Fahad et al., 2016; Pokharel et al., 2017, 2019). The direction and magnitude of Mg fractionation depends on the fungal species. Growth experiments have confirmed the fractionation of most metal elements, like Mg, Ca, Fe, Zn, etc., by plants (e.g. von Blanckenburg et al., 2009). Field research, however, is more complicated. Mg and Ca isotope signatures of soil solution under forests have indicated the influence of bio-uptake or litter decomposition superimposed on abiotic weathering (Holmden and Bélanger, 2010; Tipper et al., 2010; Hindshaw et al., 2011; Opfergelt et al., 2014; Mavromatis et al., 2014). But whether this signal could be seen in the outlet runoff and how to quantify this influence is less constrained. Bolou-Bi et al., (2010) suggested that decomposition of litterfall could directly contribute Mg to runoff during high discharge. Systematic Ca isotope investigation also have shown direct bio-cycled Ca input to runoff (Cenki-Tok et al., 2009). More quantitatively, using Mg isotope mass balance, Uhlig suggested that 50-100% of Mg released by chemical weathering was taken up by trees in a Sierra Nevada catchment. However, using stable and radiogenic Sr isotope, Oeser and von Blanckenburg, (2020) concluded

that silicate weathering rates are not sensitive to plant growth in the "EarthShape" research sites (sites defining a north–south gradient in precipitation and primary productivity). Therefore, more comprehensive and quantitative work need to be done to evaluate biological influence on chemical weathering.

1.3. Constraining the scientific questions for this research

Based on the review above, I have chosen Mg and Li isotopes, constituting a nutritive element and a non-nutritive element respectively, to trace Critical Zone processes. Three main scientific questions will be investigated in detail.

1.3.1. Tracing water chemical evolution from rainfall to runoff

Riverine water chemistry is extensively investigated, as weathering products are transported mainly by rivers (Gaillardet et al., 1999). However, rivers integrate various processes taking place in a basin and it is always hard to disentangle detailed mechanisms dictating water chemistry, due to complex interplay between hydrology and biogeochemistry. To better constrain water chemistry evolution, a comprehensive sampling strategy is required. This could be achieved by sampling water from rainfall to subsurface flow and groundwater and eventually to runoff, representing the whole water infiltration pathway. This comprehensive sampling allows for the evaluation of dissolution kinetics and shifting equilibrium with respect to primary and secondary mineral phases (Jin et al., 2011). In addition to spatially high-resolution sampling, time-series water sampling is also a good-way to single hydrological control out from other environmental factors. An enigma regarding element export in small catchments is that river water fluxes respond promptly to rainfall inputs, but ion concentration do not decrease so much as discharge increases. The question "where the extra elements come from" has led to long hours pondering hydrochemical data (Kirchner, 2003). To date, various mechanisms have been put forward to explain such concentration-discharge relationships, including exchange reactions (Clow and Mast, 2010; Kim et al., 2017), mixing of waters from different sources (Bouchez et al., 2017; Torres et al., 2017), transport or kinetic reaction control (Maher, 2010; Torres and Baronas, 2021), and the influence of colloids (Trostle et al., 2016), to name a few. The emerging application of Li and Mg isotopes as tools in weathering studies in recent years has the potential to shed new light on this issue (Tipper et al., 2012; Fries et al., 2019). Combined with our comprehensive water sampling strategy, this question will be further investigated in this study.

1.3.2. Tracing nutrient uptake depth and investigating how weathering replenishes nutrient pool

In eroding ecosystems, the nutrient pool experiences continual nutrient loss in the form of plant litter erosion, subsurface flow drainage and surface water runoff (Scatena and Lugo, 1995; Chaudhuri et al., 2007; Scalley et al., 2012). To avoid exhaustion of the nutrient inventory, some replenishing processes are required. Dust input has been suggested as the external nutrient input balancing nutrient loss in

some studies (e.g. Chadwick et al., 1999; Aciego et al., 2017). However, the flux of nutrient input by dust is not always sufficient to balance nutrient loss. Rejuvenation of the landscape by erosion, and associate chemical weathering, is thought to be another important process balancing nutrient loss (Porder et al., 2007; Buendía et al., 2010). From a geochemical perspective, Uhlig and von Blanckenburg, (2019) developed this weathering-uptake-recycling concept and called it the coupled "organic nutrient cycle and geogenic nutrient pathway". The "organic nutrient cycle" comprises a set of strategies for re-utilization plant litter and organic matter and requires rapid nutrient turnover, while the "geogenic nutrient pathway" means slow release of "new" mineral nutrients from the mineral soil and bedrock through chemical weathering. This feedback mechanism was demonstrated by means of measurements of inventories and fluxes (Uhlig and von Blanckenburg 2019) and verified in a subsequent study, in which Uhlig et al. (2020) fingerprinted the depth of the geogenic nutrient source by the isotope proxies $^{87}Sr/^{86}Sr$ and $^{10}Be(meteoric)/^{9}Be$. However, both studies lack direct evidence that elements hosted in the bioavailable fraction of topsoil can be attributed to biological uplift. The key question is whether there is any direct geochemical index one could use to trace nutrient weathering, uptake, and recycling? In this study, Mg isotopes will be applied as a tool to explore this issue.

1.3.3. Balancing Mg, Li isotopes recycling in the Critical Zone

A challenge of the Critical Zone science is to interpret CZ processes over both short and long timescales. The turnover time of a specific element differs in different compartments, because of different inventory size and input-output fluxes. For example, for typical soil production rates of 320 to 450 $t/km^2/y$, residence times of soil are around 10^3 to 10^5 years (Dixon and von Blanckenburg, 2012). By contrast, the residence time of water is much shorter. Mean residence time of base flow is around 0.8 to 3.3 years in mountainous areas, depending on the catchment size (McGuire et al., 2005). The elemental inventory in regolith is also much higher than that of the water bodies. As a result, regolith samples shows negligible chemical composition variation on decadal time scales, but water samples exhibit measurable variation even on storm-event time scales. If soil may be considered the weathering residue, and river water the instantaneous weathering product, their chemical evolution should be coupled, i.e., compared to the bedrock, soil should be depleted in the elements that water samples are enriched in. However, systematic application of isotopes in catchment studies have shown a different story. In a catchment in France (Lemarchand et al., 2010), the regolith shows identical Li isotope composition compared to the bedrock, despite runoff being substantially enriched in ^{7}Li. Not only Li, for other elements like Mg, similar discrepancies have been observed. Ma et al., (2015) observed that both soil and stream have lighter Mg isotope composition than bedrock in an instrumented site in USA. Bolou-Bi et al. (2012), Tipper et al. (2012), and Uhlig et al. (2017) also found isotopically light riverine Mg isotopes but bulk soil that was almost isotopically indistinguishable to

bedrock. Therefore, this apparently decoupled behaviour requires further investigation.

1.4. An introduction to Mg isotopes

Mg is an alkaline earth element and the fourth most abundant element (MgO = 25.5 %) on Earth (after O, Fe and Si). Mg has three stable isotopes, ^{24}Mg, ^{25}Mg, and ^{26}Mg. The isotopic ratios are reported in δ-notation:

$$\delta^{X}Mg=[(^{X}Mg/^{24}Mg)_{sample}/(^{X}Mg/^{24}Mg)_{Standard}-1] \quad (1.1)$$

where X= 25 or 26, and the standard typically used as a reference being DSM3 (Galy, 2001). δ^{X}Mg is expressed in permil. Large Mg isotope variation (>7 ‰ for δ^{26}Mg) has been observed within terrestrial samples, with carbonate minerals preserving the lightest values (reaching -5.6 ‰) and weathered silicates being amongst the heaviest (reaching 1.8 ‰). Mechanisms and magnitudes of Mg isotope fractionation during biological weathering, magmatic differentiation metamorphic dehydration processes etc. have been extensively studied (see Teng, 2017 for a recent review). This thesis focuses on Critical Zone processes, especially silicate catchment weathering. Detailed fractionation mechanisms are reviewed in more detail below.

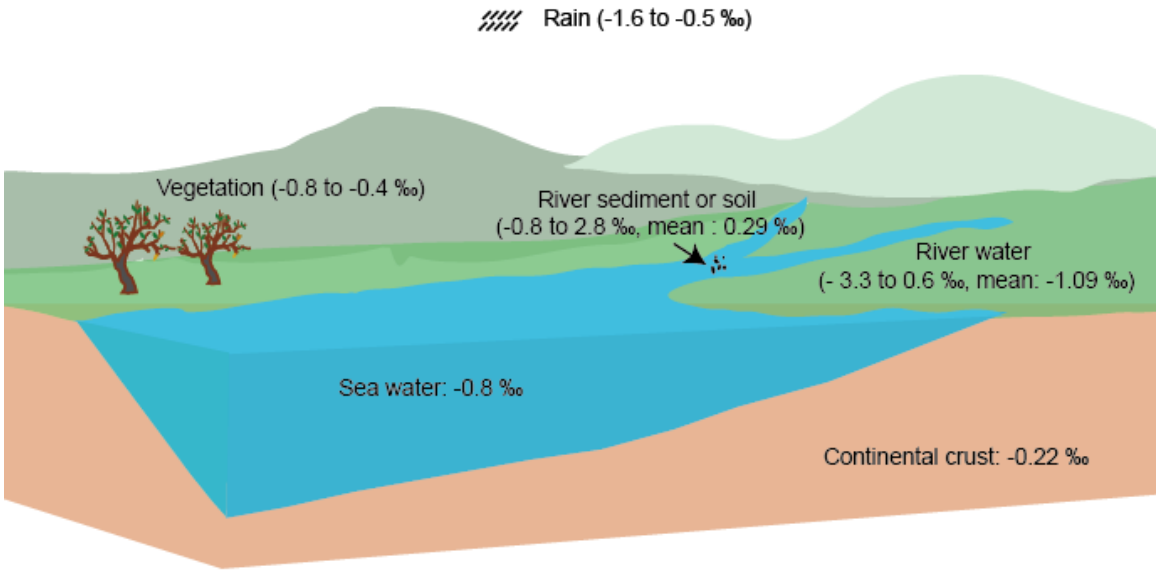

Fig. 1-2 Mg isotopic composition of major terrestrial reservoirs. Compiled data from Teng, (2017) and Hindshaw et al., (2020) and reference therein.

1.4.1. Mg isotope fractionation during plant uptake

Investigation of Mg isotope fractionation by plant uptake were carried out via both growth experiments and field research. Generally, plant (wheat, rye grass, clover etc.) growth experiments have identified preferential uptake of heavy isotopes (Black et al., 2008; Bolou-Bi et al., 2010; Wang et al., 2020). Plant tissues also exhibit heterogeneous δ^{26}Mg, suggesting fractionation also occurs during

translocation. On average, isotopic fractionation between bulk plants and source ($\varepsilon^{26}Mg_{plant\text{-}source}$) is 0.59 ± 0.39‰ (Pokharel et al., 2018).

Field studies of Mg isotope fractionation in plants are more complicated, as the $\delta^{26}Mg$ of nutritive source material is hard to determine. Commonly, soil porewater solution or exchangeable fraction is regarded as the Mg source, and many authors (e.g. Opfergelt et al., (2012); Mavromatis et al., (2014); Chapela Lara et al., (2017); Uhlig et al., (2017)) have found heavier $\delta^{26}Mg$ in plant tissues than that of the Mg source. The averaged fractionation factor ($\Delta^{26}Mg_{plant\text{-}source}$) across these studies is 0.16 ± 0.14‰, somewhat lower than that observed in hydroponic experiments. Kimmig et al. (2018) suggest that the presence of mycorrhizal fungi is also an important factor affecting fractionation of Mg isotopes during plant growth, as lab experiments have verified that magnitude and sign of Mg isotope fractionation can vary depending on the species of fungi cultured and the culture medium (Fahad et al., 2016; Pokharel et al., 2017).

1.4.2. Mg isotope fractionation during mineral and rock dissolution

Mg isotope fractionation has been observed during both rock and mineral dissolution. Ryu et al., (2011) show that different primary minerals within fresh granite can have distinct $\delta^{26}Mg$ values, with three Mg-bearing minerals spanning a 1.53‰ range in $\delta^{26}Mg$. $\delta^{26}Mg$ of the leaching output solution mainly reflects conservative mixing of heterogenous minerals rather than fractionation. Two olivine dissolution experiments conducted in a closed system (Maher et al., 2016; Pokharel et al., 2019) have found preferential release of ^{24}Mg at initial stage, following by congruent dissolution in the later stage. In both studies, this preferential release of ^{24}Mg was attributed to a kinetic effect associated with the formation of a Mg-depleted layer that develops as protons exchange for Mg^{2+}. Wimpenny et al., (2010) dissolved glass basalt and olivine in a mixed through-flow reactor and observed that output solutions became progressively lighter in Mg isotope with time, a result distinct to former two studies. The contrasting results might be due to different setups of these experiment, where Wimpenny et al., (2010) used a flow-though reactor and Maher et al., (2016) and Pokharel et al., (2019) performed batch experiments. However, the exact mechanism accounting for different dissolution patterns of Mg isotopes in flow-through and batch reactors is yet to be answered. It is likely that the minerals were always being exposed to fluid out of equilibrium with the solid in flow through experiments, whereas in a batch reactor it is always going to be getting closer to equilibrium. Another important factor controlling Mg isotopes dissolution is the Mg coordination difference. Ryu et al., (2016) dissolved biotite in a plug flow reactor and leaching solutions during biotite dissolution are enriched in light isotopes, which was attributed to preferential release of light Mg from exchangeable sites compared to octahedrally-bound structural Mg.

1.4.3. Mg isotope fractionation during secondary mineral formation

A handful of lab experiments and theoretical modelling studies have investigated Mg isotope fractionation during silicate mineral precipitation, but the results vary. Wimpenny et al., (2014) synthesized brucite ($Mg(OH)_2$; viewed as an analogue for octahedrally-coordinated Mg clays) and the precipitated minerals are enriched in heavier isotopes than the corresponding solution. Similarly, Ryu et al., (2016) synthesized lizardite and kerolite, with these neoformed minerals found to be significantly enriched in heavy isotopes ($\alpha_{clay\text{-}solution}$=1.00059 ± 0.00014). By contrast, Li et al., (2014) also synthesised brucite at lower temperature (<45 °C) and observed fractionation in the opposite direction to that seen by Wimpenny et al., (2014), with light Mg isotopes being preferred by precipitated brucite. Hindshaw et al., (2020) synthesized stevensite and saponite and the result is consistent with the research of Li et al., (2014) with light Mg isotopes preferentially incorporated in precipitated minerals. Given the contradictory nature of these lab experiment results, theoretical modelling research would be helpful to gain a better understanding. Colla et al., (2018) used density function theory to evaluate the isotope fractionation between brucite and aqueous Mg and predicted that brucite should be enriched in heavy isotopes. Using first principal simulation, Wang et al., (2019) also suggest that both brucite and lizardite should be enriched in heavy Mg isotopes relative to dissolved Mg. The discrepancy of these modelling and laboratory experiments suggests that Mg isotopes fractionation during silicate mineral precipitation might not be governed by a single factor, with both kinetic and equilibrium effects at work during the precipitation process.

1.4.4. Mg isotope fractionation during adsorption and desorption

The evidence for Mg isotope fractionation during adsorption and desorption is also not conclusive. In a tropical, mafic weathering profile, Huang et al., (2012) explained observed patterns of $\delta^{26}Mg$ change with saprolite depth as a product of isotopic fractionations during adsorption and desorption, namely: preferential adsorption of isotopically-heavy Mg onto kaolin minerals, and conversely preferential desorption of heavy Mg isotopes from the upper saprolite profile. The former process is thought to be driven by the difference in coordination environment between absorbed Mg and dissolved Mg in pore water and the latter process is evidenced by the observation that heavy Mg isotopes are eluted earlier during chromatography. Similarly, Opfergelt et al., (2014) and Pogge von Strandmann et al., (2012) suggest that heavy Mg isotopes are preferentially taken up by the exchangeable complex of Iceland basalt soil, leaving the corresponding pore water enriched in light Mg isotopes. By contrast, Jacobson et al., (2010) tentatively suggest preferential uptake of light Mg isotopes during Mg-for-Na ion exchange in a calcite aquifer setting. Finally, Uhlig et al., (2017) compared the Mg isotopic composition ($\delta^{26}Mg$) of stream water and the exchangeable fraction of soil, and favoured the interpretation that no isotope fractionation occurs during adsorption-desorption processes. Given the complexity of natural systems, such empirical field

results would benefit from comparison with observations from controlled experiments. However, very few such experiments have been carried out to date. In a clay formation experiment, Wimpenny et al., (2014) reacted synthetic smectite and natural clays with pure $MgCl_2$ solution of a known isotopic composition. After reaction, exchangeable Mg retained by clays had almost identical or slightly lighter (maximum ~0.1 ‰) $\delta^{26}Mg$ than the original pure $MgCl_2$ solution, suggesting the uptake of Mg onto clays is associated with negligible Mg isotope fractionation. Similarly, after synthesis of stevensite and saponite, Hindshaw et al., (2020) observed the exchangeable Mg of the synthesised mineral to have $\delta^{26}Mg$ lower than, or within error of, the initial solution. If these findings are more universally applicable, it would throw doubt on the aforementioned assertions of Huang et al. (2012), Opfergelt et al. (2014) and Pogge von Strandmann et al. (2012). As yet, however, empirical experimental knowledge is limited to a few isolated clay minerals.

1.5. An introduction to Li isotopes

Lithium is the lightest alkaline element with an atomic number of three and an atomic mass of 6.94. Lithium has two stable isotopes: ^7Li and ^6Li with abundance of 92.4 % and 7.6 % respectively. Due to the large mass difference between ^7Li and ^6Li (~17 %), huge Li isotope fractionation has been observed in natural terrestrial samples. The ratio of Li isotopes is reported in delta notation:

$$\delta^7Li=[(^7Li/^6Li)_{sample}/(^7Li/^6Li)_{Standard} -1] \qquad (1.2)$$

and is expressed in permil (‰) where the standard is referred to as LSVEC (Li carbonate, Flesch et al., 1973). As with Mg, I review possible processes fractionating Li isotopes in the Critical Zone in detail below.

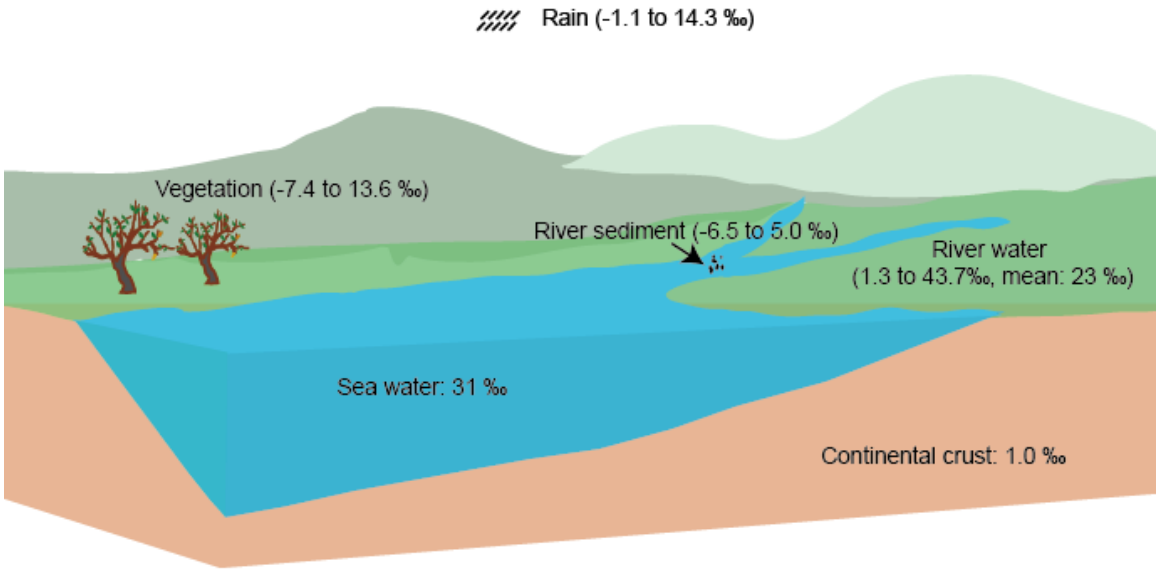

Fig. 1-3 Li isotopic composition of major terrestrial reservoirs. River water compiled by Hindshaw et al., (2019). Continental crust from Teng et al., (2004). Vegetation from (Lemarchand et al., 2010; Clergue et al., 2015; Li et al., 2020; Steinhoefel et al., 2021). River sediments from (Huh et al., 2001; Millot et al., 2010; Dellinger et al., 2014, 2015; Liu et al., 2015; Wang et al., 2015; Weynell et al., 2021). Rain from (Pistiner and Henderson, 2003; Lemarchand et al., 2010; Clergue et al., 2015)

1.5.1. Li isotopes fractionation during plant uptake

As aforementioned, Li is generally regarded as a non-nutritive element. To date, no hydroponic growth experiment has been done to investigate Li isotope fractionation during plant uptake, and few field studies that do exist and have reached different conclusions. Lemarchand et al., (2010) and Clergue et al., (2015) compared δ^7Li of plant tissues and shallow soil solution from forested catchments and found no significant difference, suggesting that vegetation does not seem to fractionate Li isotopes, and that vegetation cycling has little influence on the Li budget at the catchment scale. By contrast, Li et al., (2020) investigated Li geochemistry in vegetation and regolith profiles developed in humid and arid sites in Hawai'i and found that δ^7Li in plant tissues is lighter than both exchangeable and reducible soil fractions (regarded as the source of Li to vegetation). They suggest that organic matter acts as an underestimated host of ^{6}Li in soils, which is supported by experimental humus-Li complexation. In summary, existing evidence from field studies is inconclusive as to whether or not biological activity fractionates Li isotopes, and future plant growth experiments are needed if we are to better understand this issue.

1.5.2. Li isotope fractionation during dissolution of rocks and minerals

Experimental studies have found different dissolution regimes including 1) congruent dissolution of Li isotopes (Pistiner and Henderson, 2003; Wimpenny et al., 2010); 2) preferential dissolution of ^{6}Li (Pistiner and Henderson, 2003; Zhang et al., 2021a) and 3) transition from preferential dissolution of ^{6}Li to congruent dissolution (Verney-Carron et al., 2011; Li et al., 2021). Various mechanisms accounting for the preferential dissolution of ^{6}Li were proposed. For example: heterogeneity of primary mineral δ^7Li (Pistiner and Henderson, 2003), diffusion (through leached layer) induced kinetic fractionation (Verney-Carron et al., 2011; Li et al., 2021) and preferential breaking of ^{6}Li-O bond or preferential leaching of ^{6}Li from AlO_6 octahedral sites (Zhang et al., 2021a). In field research, the heterogeneity of primary mineral δ^7Li should be taken into account as revealed by Zhang et al., (2021b), while diffusion induced kinetic fractionation should be minimal as compared to secondary mineral formation (Verney-Carron et al., 2011) in low temperature conditions (like in the Critical Zone).

1.5.3. Li isotope fractionation during secondary mineral formation

Secondary mineral formation is regarded as the most important driver of Li isotope fractionation in the earth surface environment. However, due to the difficulty of silicate mineral synthesis, little experimental work has been done to determine Li isotope fractionation during Li incorporation into secondary minerals. Vigier et al., (2008) synthesized smectite, determining a $\Delta^7Li_{clay\text{-}solution}$ of -10‰ ± 1.3‰ at temperatures lower than 90 °C. Hindshaw et al., (2019) synthesized stevensite and saponite at ambient temperature and found an average difference between the residual solid and initial solution ($\Delta^7Li_{clay\text{-}solution}$) for these synthesized layer silicates of -16.6 ± 1.7‰ at 20 °C. The experimentally determined fractionation factors are similar and these values are generally consistent with $\Delta^7Li_{clay\text{-}solution}$ deduced from field research (16 to 24‰, e.g. Bouchez et al., 2013; Dellinger et al., 2015; Hindshaw et al., 2019).

1.5.4. Li isotope fractionation during adsorption and desorption

Isotope fractionation during Li adsorption onto minerals is largely dependent on the complexation mechanism. Pistiner and Henderson (2003) conducted Li adsorption experiments onto smectite and gibbsite, which yielded contrasting results. For smectite, negligible isotope fractionation was observed, but for gibbsite fractionations reaching 14 ‰ were seen. For smectite, outer-sphere complexation (which involves physical adsorption without chemical bond alteration) is predominant, while adsorption onto gibbsite involves inner-sphere chemisorption and Li incorporation into lattice. Following this work, Wimpenny et al., (2015) conducted more detailed Li adsorption experiments with gibbsite, with results consistent with Pistiner and Henderson (2003). Apart from gibbsite, large isotope fractionation during Li adsorption onto kaolinite has also been observed. Zhang et al., (2021) reacted kaolinite with artificial seawater and revealed a partition coefficient between fluid and kaolinite of up to 28, with an isotopic fractionation of 24 ‰. Similarly, Li and Liu (2020) demonstrated liquid-solid Li isotope fractionation during adsorption onto kaolinite of up to 36 ‰, with up to 99 % of initial Li being adsorbed on kaolinite in batch Li adsorption experiments.

1.6. Analytical methods

1.6.1. Extraction of the exchangeable fraction

The exchangeable fraction consists of elements that form weak electrostatic bonds between the hydrated surfaces of phyllosilicates, oxyhydroxides minerals, or organic matter. This fraction is thought to be representative of soil solution chemistry and is also thought to be the cation source for plants. To extract this fraction, we used a traditional NH_4OAc extraction method (Schollenberger and Simon, 1945). Soil and saprolite samples were first oven-dried and sieved to <2 mm. 2 g of the selected samples were accurately weighed and added to 15 ml acid-cleaned polypropylene centrifuge tubes pre-filled with 14 ml 1 M NH_4OAc solution. Samples were then agitated, and the resulting suspensions shaken on a hotdog roller

at 60 rpm for 3 hours. After reaction, the suspensions were centrifuged at 4200 rpm for 30 min, before the supernatant was pipetted off into a syringe and filtered through a 0.2 μm acetate filter. Solutions were then split into two separate aliquots for major element concentration and isotope analysis.

1.6.2. Separation of the clay-sized fraction from bulk soil and saprolite

In order to evaluate the chemical composition of precipitated secondary minerals, the clay-sized fraction of bulk saprolite and soil was extracted. Following the exchangeable fraction extraction procedure, NH_4OAc-extracted soil and saprolite samples were rinsed with Milli-Q (18.2 MΩ) water twice. Clay-sized fractions of these samples were then extracted by centrifuge following the USGS method (Poppe et al., 2012). Briefly speaking, 10 ml Milli-Q water was added to the sample containing centrifuge tubes and these tubes were put in the ultrasonic bath for 5 mins to homogenize the suspension. Centrifuge speed and time was calculated using the equation provided by Poppe et al., (2012). After centrifuging, clay-sized fraction contained in the supernatant liquid was poured into Teflon beakers for further oven drying and acid digestion.

1.6.3. Separation of primary minerals from bedrock

To evaluate the homogeneity of the Mg and Li isotopic composition of different minerals in the bedrock, primary minerals were also separated. Bedrock was first crushed and then sieved to 125 μm -1 mm. The felsic minerals (mainly quartz, and feldspar in this study) were first separated out using a magnet separator. Magnetic hornblende, chlorite, and biotite were then hand-picked under binocular microscope. Chlorite and biotite were secondary minerals metamorphosed from hornblende.

1.6.4. Acid digestion of samples

Soil, saprolite, extracted clay-sized fraction, separated minerals and bedrock were dissolved by (ultrapure) acid digestion. 1.2 ml concentrated HNO_3 and 2 ml HF were added to ~50 mg of sample material in 7 ml Teflon beakers. These beakers were then put (closed) on the hotplate overnight at a temperature of ~120 °C, before being evaporated to near dryness. Concentrated HCl and HNO_3 were applied successively to remove F^-. Aqua regia was also used to assist digestion when residues were present after HCl and HNO_3 treatment. Plant sample digestion was assisted by microwave (MLS start). Prior to analysis, the plant samples were oven-dried (60 °C, 24 h) and crushed. 100-500 mg (dry mass) of plant material was weighed directly into Teflon vessels. A mixture containing 5 mL of Milli-Q water, 4 mL of ~14 M HNO_3, and 3 mL of 30% H_2O_2 was used to digest plant material. The microwave procedure was then run by gradually heating for 12.5 min to 200 °C, holding the temperature for 17.5 min and venting for another 18 min to allow cooling and degassing. Digested plant material was then transferred into 22 mL PFA vials and evaporated to dryness.

1.6.5. Major element concentration and trace element concentration measurement

Major elements analyses were done using an axial ICP-OES (Varian 720ES). Before ICP-OES analysis, aliquots from the acid digestions were diluted gravimetrically in 0.3 mol/L (M) HNO_3 containing Cs as ionisation buffer (1000 ppm) to achieve matrix-matching to the calibration standards, which in turn were made from a mixture of ICP standards. To assess the uncertainty of the analytical results, we evaluated the precision and accuracy of replicate analyses of reference materials processed along with the samples in this study and also replicate dissolutions and analyses of different rock reference materials from independent dissolution replicates. The results of these measurements and comparison to published measurements indicate uncertainties close to 5 % relative for most elements.

Li concentration was measured by iCap Q-ICP-MS (Thermo Fisher). Similar to major element measurement, acid digestions were diluted gravimetrically in 0.3 M HNO_3 to 4 ml with a dilution factor ranging from 1 to 200. Diluted solution generally had a Li concentration of 0.5 to 10 ppb. An internal standard (in this case 5 ppb Rh) was added to the sample by online addition using a prepFAST autosampler system. The procedure blank was routinely monitored in a measurement sequence and the value was generally lower than 0.05 ppb. The precision and accuracy were also evaluated by replicate analyses of reference materials. Uncertainties are close to 5 % for most samples except for some water samples and plant samples. Uncertainties for plant samples and water samples having low Li concentration (<1 ppb) was generally higher (~10 %).

1.6.6. Mg isotope composition measurement

The digested solutions were dried again and taken up in 1 M HNO_3 for cation exchange chromatography. The chromatography procedure is similar to that described in Pogge von Strandmann et al. (2011) and Uhlig et al. (2017). 2.8 ml of exchange resin Bio-Rad AG-50W-X12 (200-400 mesh) was loaded in Spectrum 104704 MiniColumns. After resin cleaning and conditioning, 200 µL solution (containing ~10µg Mg) was introduced on resin bed and matrix elements ware eluted by subsequent washing with 31ml 1 M HNO_3 acid. Next, Mg was collected with 10 ml 2 M HNO_3. The purified Mg fractions were evaporated to dryness and taken up in 1 mL of 0.3 M HNO_3. Purity and quantitative Mg yield check was done by Q-ICP-MS.

Table 1-1 Procedures for Li and Mg purification

Procedure	Li chromatography		Mg chromatography	
	Eluent	Volume (ml)	Eluent	Volume (ml)
Cleaning	6N HCl	30	6N HCl	30
	MQ-H_2O	30	MQ-H_2O	5
Pre-conditioning	0.2N HCl	7	1N HNO_3	5

Sample loading	0.2N HCl	0.5	1N HNO_3	0.2
Fixing	0.2N HCl	0.5	1N HNO_3	1
Eluting matrix	0.2N HCl	25	1N HNO_3	25
Split 1	0.2N HCl	1	2N HNO_3	1
Collection	0.2N HCl	23.5	2N HNO_3	10
Split 2	0.2N HCl	1	2N HNO_3	1
Cleaning	6N HCl	30	6N HCl	30

Mg isotope ratios were measured on a MC-ICP-MS (Thermo Scientific Neptune) equipped with a Jet Interface pump and a quartz-glass spray chamber (double-pass cyclone Scott-type, Thermo stable introduction system, SIS) with a 100 μL/min self-aspirating PFA nebulizer for sample introduction at the Helmholtz Laboratory for the Geochemistry of the Earth Surface (HLGES) at GFZ Potsdam. All samples were measured by standard-sample-standard bracketing technique, with DSM3 as bracketing standard to correct for instrumental mass bias. Samples and standards were diluted in 0.3 M HNO_3 to 500 ppb Mg, corresponding to a ~10 V signal on a Faraday cup equipped with a 10^{11} Ω amplifier. 20 cycles were measured in 1 block and 4 replicates were run for each sample. The reference material Cambridge-1 (a pure Mg solution), was ran with every analytical run to gauge machine behaviour (i.e. intermediate reproducibility). In addition, reference materials SLRS-6 (river water), SRM2709a (soil) were ran with each column set and monitored to gauge external reproducibility.

1.6.7. Li isotope composition measurement

The digested solutions were dried and taken up in 0.2 M HCl for cation exchange chromatography. 3.0 mL of Bio-Rad AG-50W-X12 (200-400 mesh) was loaded in BRAND 50 ml pipette PP columns (I.D. 6.4 mm, resin height 9.32 cm in MQ-H_2O). The matrix was eluted with 26 ml 0.2 N HCl and Li was collected in 23.5 ml 0.2 N HCl. The purified Li fractions were evaporated to dryness and taken up in 1 mL of 0.3 N HNO_3. Purity and quantitative Li yield was verified by Q-ICP-MS (Thermo Scientific iCAP).

Lithium isotope ratio measurements were done on an MC-ICP-MS equipped with a Jet Interface (Jet sample and X skimmer cones) at HLGES. Sample solutions were nebulized into an ESI Apex desolvating sample introduction system. Instrumental mass bias was corrected using the sample-standard-sample bracketing technique. Prior to analysis the Li concentration in the sample solutions were adjusted to match the bracketing standard solution (L-SVEC) at 20 ng/mL in 0.2 M HNO_3 (e.g. Millot et al., 2004). Samples were measured two to three times during each session. An individual measurement consisted of 10 cycles of 4.2 s integration time, with ^{7}Li and ^{6}Li signals detected simultaneously (in Faraday cups L4 and H4, equipped with $10^{11}\Omega$ amplifiers). Background signals were monitored with 0.2 M HNO_3 and

subtracted on-peak from sample signal intensities. Reference materials L-SVEC and in house Li_2CO_3 were ran with every analytical run to gauge machine behaviour (i.e. intermediate reproducibility). SLRS-6 (river water), SRM2709a (soil), BHVO-2 (basalt) were routinely monitored to gauge external reproducibility.

1.7. Geological setting and sample collection

The research site is "Conventwald" (48°02′0N, 7°96′0E), located in the Black Forest, south Germany.

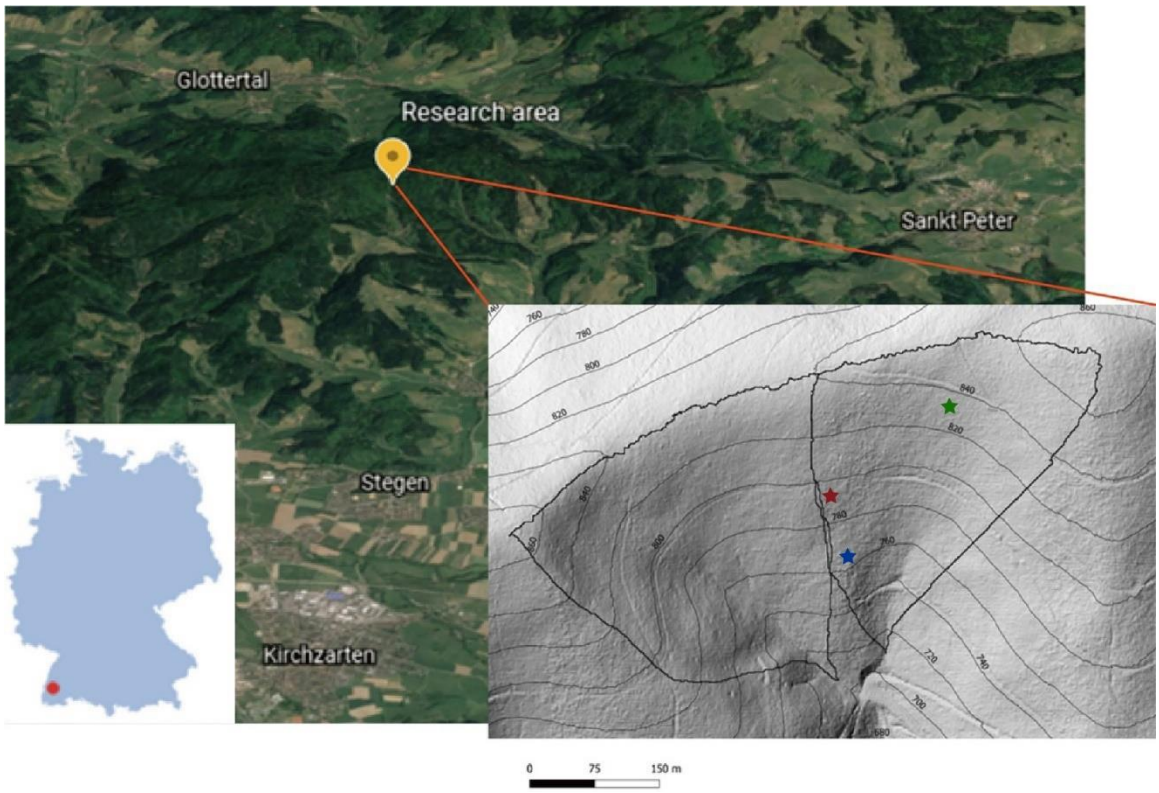

Fig. 1-4: Location (Google maps) and topography (generated from lidar data, provided by David Uhlig) of study area "Conventwald". Black lines are catchments delineations. Red, blue and green stars denote sampling locations of drilling core, creek water and groundwater respectively.

This site is a well-drained temperate forest, underlain by metamorphosed sedimentary rock. The monitored creek catchment has an area of 0.077 km² and the average elevation was ~840 m above sea level (a.s.l.). Mean annual temperature at the study site was 6.8 ˚C, and mean annual precipitation was 1395 mm/a. Weathered bedrock was found at ~7 m and massive, unweathered bedrock was encountered at ~16 m during a core-drilling campaign (Uhlig and von Blanckenburg, 2019). The regolith is mantled by weakly developed soil and covered by

mixed deciduous and coniferous forests. Although the study site was not glaciated during Quaternary, periglacial slope deposits developed during the last glacial maximum. The uppermost meter of soil has a rock fragment content of ~70%. The parallel-aligned relict periglacial deposits to the slope also function as a basal layer and set water flow pathways, which redirect preferential infiltrating flow into lateral subsurface flow. This research site is part of the long-term forest ecosystem monitoring program "*International Co-operative Program on assessment and monitoring of air pollution effects on forests (ICP Forest Level II)*" and is also the study site of the DFG priority program SPP 1685 "*Ecosystem Nutrition—Forest Strategies for limited Phosphorus Resources*". Therefore, this site is well instrumented and detailed background information is available (Table 1-2).

Table 1-2 Background information of this study area

Study site	Conventwald
Longitude	48°1.20222'N
Latitude	7°57.93996'E
Altitude (m.a.s.l)	733-863
Slope (°)	17 (south-facing)
Mean annual temperature (°C) [a]	6.8
Mean annual precipitation (mm) [a]	1749
Main vegetation type	*Fagus sylvatica*, *Picea abies*
Soil type (WRB)[b]	Dystric Cambisol
Lithology	Paragneiss
Denudation rate (t/km^2/yr)[c]	125 ± 11 (SE)
Weathering rate (t/km^2/yr)[c]	71 ± 19 (SE)
Erosion rate (t/km^2/yr)[c]	54 ± 15 (SE)

a: data from Forest Research Institute of Baden-Wuerttemberg

b: WRB (World Reference Base for Soil Resources)

c: measured with cosmogenic in situ ^{10}Be (Uhlig and von Blanckenburg, 2019)

Shallow regolith (<3 m) was sampled at depths increment of 20 cm from a 3 m trench and deep regolith (>3 m) was retrieved using diesel-powered wireline core-drilling to 20 m depth (Uhlig and von Blanckenburg, 2019). Time series water samples were collected from 01.03.2015 to 25.02.2016. Rainwater and throughfall were collected biweekly in a bulk container covered by a netting mesh. Creek discharge was collected daily at midnight by autosampler. Groundwater was sampled daily by autosampler (Sohrt et al., 2019). Groundwater table level was monitored by a pressure probe installed in 8.5m below the surface. Lateral subsurface flow from subsurface flow collectors (see Bachmain and Weiler, 2012), collecting water at three depths intervals: 0-15 cm, 15-150 cm, and 150-320 cm.

Due to limited water samples collected for 150-320 cm subsurface flow, we only analyzed the other two shallow subsurface flow samples in this study. All the water samples were acidified and stored at 4 ˚C before analysis. Living wood, beech leaves and spruce needles were collected from representative mature and young trees.

Fig. 1-5 Field work photos showing how samples were collected (Photo 2 credit to David Uhlig)

Chapter 2

Mg isotopic composition of runoff is buffered by the regolith exchangeable pool

[Note: A revised version of this chapter was published in the journal Geochimica et Cosmochimica Acta. Cai, D., Henehan, M.J., Uhlig, D., von Blanckenburg, F., 2022. Mg isotope composition of runoff is buffered by the regolith exchangeable pool. Geochimica et Cosmochimica Acta 321, 99-114. DOI: 10.1016/j.gca.2022.01.011]

Abstract

In a small, forested catchment underlain by gneiss (Conventwald, Black Forest, Germany), we found that the magnesium isotope composition (δ^{26}Mg) of creek water did not show seasonal variability, despite large variation in dissolved Mg concentration. To investigate the potential controlling factors on water δ^{26}Mg, we studied Mg isotopes on solid samples (bedrock, bulk soil, clay-sized fraction of soil, separated minerals, the exchangeable fraction of regolith) and water samples comprising time series of creek water, groundwater and subsurface flow. Subsurface flow from 0-15 cm depth (-0.80 ± 0.08 ‰) and 15-150 cm depth (-0.66 ± 0.17 ‰), groundwater (-0.55 ± 0.03 ‰), and creek water (-0.54 ± 0.04 ‰) are all enriched in light Mg isotopes compared to bedrock (-0.21 ± 0.05 ‰). Subsurface flow samples have similar δ^{26}Mg values to the regolith exchangeable fraction at the respective sampling depths. Groundwater and creek water also show δ^{26}Mg values that are identical to those of the exchangeable fraction in the deep regolith. We suggest, therefore, that cation-exchange processes in the regolith buffer δ^{26}Mg of creek water at our study site. To further explore this hypothesis, adsorption and desorption experiments using soil samples from our study site were carried out. The results showed negligible Mg isotope fractionation during adsorption-desorption, supporting our hypothesis. Thus, the exchangeable pool can be sampled at high depth resolution to reconstruct fluid Mg isotope composition. The large pool of Mg in the exchangeable fraction of the deep regolith (>3 m) is isotopically light and presents most likely the Mg residue in soil water that entered the exchangeable pool after secondary mineral formation - a process which often favours heavy Mg isotopes. However, the exchangeable fraction in the shallow regolith (0-3 m depth) shows a strong imprint of biological cycling. Mg isotopes thus provide an exact depth image of the geogenic (weathering) and the organic (bio-cycled) nutrient cycle.

2.1. Introduction

Magnesium (Mg) is a major element in the interior of the Earth and at its surface, the terrestrial hydrosphere, the oceans, and is intensely cycled through the biosphere. The use of Mg stable isotopes as a tracer to decipher biogeochemical processes in

natural systems has developed in the last two decades into a powerful tool (Schmitt et al., 2012; Teng, 2017), especially in the Critical Zone which encompasses the near-surface earth, extending from the top of the vegetation canopy down to groundwater.

Laboratory experiments have documented Mg isotope fractionation by both biotic and abiotic processes. Biologically, uptake of Mg by plants generally favours heavy Mg isotopes, and Mg translocation within plants can further fractionate Mg, as demonstrated in growth experiments (Black et al., 2008; Bolou-Bi et al., 2010) and in field studies (e.g. Bolou-Bi et al., 2012; Uhlig et al., 2017). Abiotic processes are also capable of fractionating Mg isotopes significantly. For example, during the dissolution of olivine, lighter Mg isotopes are preferentially leached at initial stage (Wimpenny et al., 2010; Maher et al., 2016; Pokharel et al., 2019). Granite dissolution experiments show preferential dissolution of isotopically distinct primary minerals (Ryu et al., 2011). Secondary mineral formation is generally thought to favor heavy Mg isotopes, as revealed in brucite (an analogue of octahedrally-coordinated Mg clays), lizardite and kerolite synthesis experiments (Wimpenny et al., 2014; Ryu et al., 2016). In contrast, experimental precipitation of brucite in another study (Li et al., 2014) and precipitation of stevensite and saponite (Hindshaw et al., 2020) found that light Mg isotopes were preferentially incorporated. The direction of Mg isotope fractionation during secondary incorporation is controlled by the difference in bond length between clay octahedral sites and dissolved Mg (Li et al., 2014; Hindshaw et al., 2020), but also a kinetic effect cannot be ruled out. Compared to the aforementioned processes, less well documented is Mg sorption-desorption and associated isotope fractionation. In an adsorption experiment (Wimpenny et al., 2014), Mg retained by clays had almost identical or by only ~0.1‰ more negative δ^{26}Mg values than the original Mg solution, suggesting the adsorption of Mg onto clays is associated with little or no Mg isotope fractionation. Similarly, after synthesis of stevensite and saponite, Hindshaw et al., (2020) observed the exchangeable Mg of the synthesized mineral to have δ^{26}Mg lower than, or within error of, the initial solution.

As with these lab experiments under controlled conditions, field studies on river water Mg isotopic composition show similar complexity. Isotopically lighter Mg in river water compared to the silicate bedrock it drains has been reported, with secondary mineral formation (favoring heavy Mg isotopes) thought to be the reason for this fractionation (Tipper et al., 2006a, b, 2008; Brenot et al., 2008; Ma et al., 2015; Dessert et al., 2015). Conversely, however, secondary mineral formation incorporating isotopically light Mg is also inferred in other catchments (Pogge von Strandmann et al., 2008). Lab experiments have identified both fractionation directions during secondary mineral formation (e.g. Wimpenny et al., 2014; Li et al., 2014), suggesting these hypotheses are not incompatible. There have also been cases where observed isotopic fractionation in natural catchment waters could not be attributed to the formation of secondary minerals. For example, in Greenland,

river waters were found to be too dilute to form secondary minerals, with negative δ^{26}Mg values in river water instead reflecting preferential dissolution of calcite (Wimpenny et al., 2011). Elsewhere, δ^{26}Mg of soil at an instrumented catchment in the Sierra Nevada did not significantly differ from bedrock, despite the creek water draining the catchment being significantly enriched in ^{24}Mg (Uhlig et al., 2017). Instead, at this site, negative δ^{26}Mg values in creek water may be driven by the preferential uptake of heavy Mg isotopes by plants (Uhlig et al., 2017).

Given the complexity of natural watersheds (that vary in lithology, climate and vegetation cover), conclusions drawn from field studies can be more useful if a particular controlling factor can be singled out. To this end, time series of water samples can be used (e.g. Tipper et al., 2012). Such time series water samples could be collected over discrete storm events (Chapela Lara et al., 2017; Fries et al., 2019) such that short-term hydrological change is the main factor driving variation. Alternatively, they can be collected in different seasons (Bolou-Bi et al., 2012; Tipper et al., 2012; Mavromatis et al., 2014; Uhlig et al., 2017; Hindshaw et al., 2019; Novak et al., 2021) to investigate biological and longer-term hydrological effects. However, the response of δ^{26}Mg to discharge varies between studies. In the studies of Fries et al. (2019) and Hindshaw et al. (2019), Mg concentration and isotopic composition changed little compared to discharge variation, while in other studies (e.g. Bolou-Bi et al., 2012; Mavromatis et al., 2014), a clear correlation was found between discharge and δ^{26}Mg. Variation in δ^{26}Mg over short-lived or seasonal fluctuations in discharge were either attributed to mixing of Mg from different depths or the combined effect of more than one process (Tipper et al., 2012; Mavromatis et al., 2014; Chapela Lara et al., 2017).

In this study, to fill gaps in our understanding of Mg isotopic fractionation during weathering processes, we conducted a comprehensive study in a small, forested catchment underlain by felsic metamorphic rock (Conventwald, the Black Forest, Germany). Along with measurements of δ^{26}Mg of bedrock, bulk regolith, clay-sized fraction, and exchangeable fraction of regolith, we investigated the potential controlling factors on water Mg isotopic composition. We collected time series samples of not only stream water but also groundwater and subsurface flow from 0-15 cm and 15-150 cm below the surface. We suggest that the vertical exchangeable Mg isotope distribution is due to weathering imprinted by biological cycling. Exchange reactions in our catchment are a primary control on water chemistry as δ^{26}Mg values of water are like those of the exchangeable fraction at depths where it was collected. To further interrogate this finding, a batch of adsorption and desorption experiments using soil samples from our study site were carried out, indicating negligible fractionation during exchange process. This combination of field research and lab experiments informs about processes fractionating Mg in the Critical Zone – with the role of the exchangeable pool highlighted as particularly important – and further verifies the potential of Mg isotopes as a tool in tracing continental weathering process.

2.2. Geological setting

Samples were collected from an instrumented forest "Conventwald" (48°02′0N, 7°96′0E), located in the Black Forest, southern Germany. This study site is part of the long-term forest ecosystem monitoring program "International Co-operative Program on assessment and monitoring of air pollution effects on forests (ICP Forest Level II)" and represents also one among the study sites of the DFG priority program SPP 1685 "Ecosystem Nutrition—Forest Strategies for limited Phosphorus Resources". The monitored creek catchment has an area of 0.077 km² and the average elevation was ~840 m a.s.l.. Mean annual temperature of the study site was 6.8 ˚C, and mean annual precipitation was 1395 mm/a. The underlying bedrock is paragneiss, which was developed from metamorphosed sedimentary rock in the Precambrian. Weathered bedrock was found at ~7 m depth and unweathered bedrock was encountered at ~16 m depth during a core-drilling campaign. The main Mg-hosting minerals in the bedrock include hornblende, chlorite, biotite. Based on microscopic investigations, chlorite and biotite are secondary minerals originating from hornblende alteration. The soil type is a hyperdystric skeletic folic Cambisol with a loamy or sandy loamy texture and a mor-type moder forest floor atop. A detailed description is provided by Lang et al. (2017). Although the study site was not glaciated during the Quaternary. Periglacial slope deposits developed during the last glacial maximum. The uppermost meter of soil had a rock fragment content of ~70%. The vegetation is mainly composed of European beech *(Fagus sylvatica*, ~40%) and Norway spruce (*Picea abies*, ~45%). Previous element budget calculations for this site were presented by Uhlig and von Blanckenburg, (2019). The result for Mg is shown in Fig. 2-1 for reference.

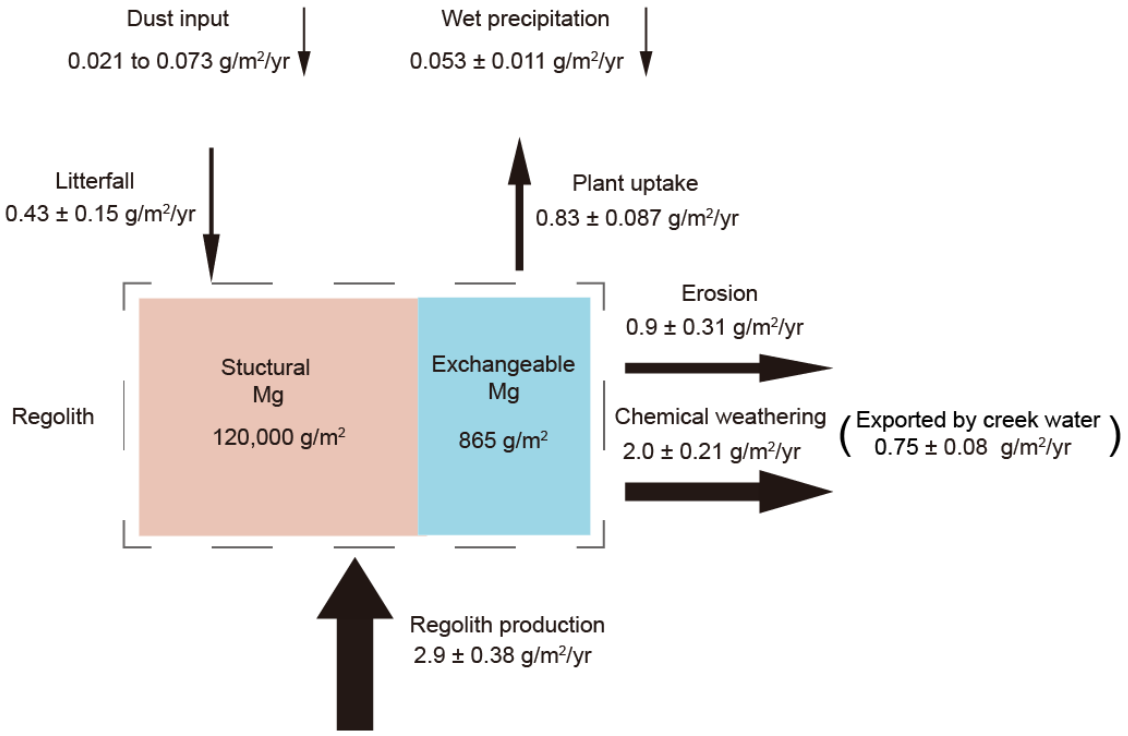

Fig. 2-1 Mg inventories and fluxes of this catchment. Data from Uhlig and von Blanckenburg (2019) and Uhlig et al. (2020). Arrow width corresponds to the flux magnitude. Chemical weathering rate is evaluated from denudation rate and chemical depletion factor in the soil. Mg exported by creek water is evaluated from creek discharge and Mg concentration in the creek water.

2.3. Methods

2.3.1. Sampling

The sampling strategy was presented in detail by Uhlig and von Blanckenburg (2019) for regolith samples and Sohrt et al. (2019) for water samples. Briefly, shallow regolith was sampled at depth increments of 20 cm in a 3 m deep trench. Deeper regolith beyond 3 m was retrieved using diesel-powered wireline core-drilling to ~20 m. Time series water samples were collected from 01.03.2015 to 25.02.2016. Open rainfall and throughfall were collected biweekly in bulk container coved by a netting mesh. Creek discharge was collected daily at midnight by autosampler. Groundwater was sampled daily by an autosampler. The groundwater table level was monitored by a pressure probe installed 8.5 m below the surface. Subsurface flow from subsurface flow collectors (see Bachmain and Weiler 2012) was collected at three depths intervals: 0-15 cm, 15-150 cm, and 150-320 cm. Due to limited availability of water samples from 150-320 cm subsurface flow, we only analysed the other two shallow subsurface flow samples in this study. All the water samples

were acidified and stored at 4 ˚C before analysis. Living wood, beech leaves and spruce needles were collected from representative mature and young trees.

2.3.2. Extraction of the exchangeable fraction, separation of the clay-sized fraction and primary minerals

Soil and saprolite samples were first oven-dried and sieved to < 2 mm. Two grams of the selected samples were accurately weighed and added to 15 ml acid-cleaned polypropylene centrifuge tubes pre-filled with 14 ml of a 1 M NH_4OAc solution. Samples were agitated, and the resulting suspensions shaken on a hotdog roller at 60 rpm for 3 hours. After reaction, the suspensions were centrifuged at 4200 rpm for 30 min, before the supernatant was pipetted off into a syringe and filtered through a 0.2 μm acetate filter. Solutions were then split into two separate aliquots for major element concentration and Mg isotope analysis. Afterward, the NH_4OAc-extracted soil and saprolite samples were twice rinsed with Milli-Q water. The clay-sized fractions of these samples were then extracted by centrifugation following the USGS method (Poppe et al., 2012). To evaluate the Mg isotopic composition of different minerals in bedrock, the main Mg-hosting minerals were separated. Bedrock was first crushed and then sieved to 125 μm - 1 mm. The felsic minerals (mainly quartz, and feldspar in this study) were first removed using a magnet separator. Hornblende, chlorite, and biotite were hand-picked under a microscope. Chlorite and biotite grains, formed from metamorphosed hornblende, generally contained trace relicts of hornblende.

2.3.3. Mg isotopes adsorption-desorption experiment using topsoil

In order to investigate whether Mg isotopes fractionate during adsorption and desorption, we conducted a series of batch experiments using topsoil collected at 5 cm depth from our study site. Prior to the batch experiments, the exchange kinetics of Mg on the soil surface was investigated, to evaluate reaction time required to reach equilibrium. Two aliquots of 3 g untreated soil samples were soaked in 30 ml pH-neutral $CaCl_2$ (30 μg/g) and $MgCl_2$ (14 μg/g) solutions, respectively. During reaction, 0.5 ml aliquots of solution were pipetted out after 0.5 h, 1 h, 2 h, 4 h and 40 h for Mg concentration measurement. The results of this preliminary experiment indicate that the exchange reaction was rapid, with near-equilibrium reached within 2 - 4 hours (Fig. 2-2). In the following experiment, soils were reacted with solution for 3 hours: long enough to reach near equilibrium, but not too long so as to avoid potential dissolution of structural Mg in the soil. In the Mg desorption experiment, circumneutral Milli-Q water (pH 6.2), acidified Milli-Q water (pH 3.2) and $CaCl_2$ solutions of different concentration and pH were reacted with untreated soil to desorb exchangeable Mg. After reaction for 3 hours, the suspensions were centrifuged, before the supernatant was pipetted off into a syringe and filtered from remaining solids for major element concentration and Mg isotope analysis. Procedures for the Mg adsorption experiment were largely identical to those of the

Mg desorption experiment, except that $MgCl_2$ solutions were used instead of $CaCl_2$ solutions. Similarly, untreated soil samples were immersed in neutral $MgCl_2$ solutions ([Mg] of 0.6 to 61 µg/g) or acidic $MgCl_2$ solutions ([Mg] of 0.6 to 19 µg/g). A detailed description of experimental procedures can be found in the Appendix to this chapter.

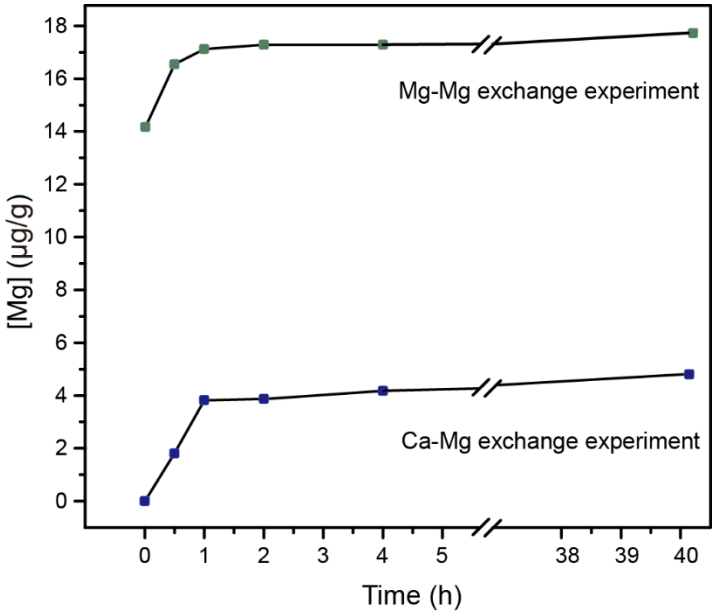

Fig. 2-2 Kinetics of Mg exchange, as demonstrated by the concentration of Mg in filtered aliquots of soil suspension solution (see text for details). In both our Ca-Mg and Mg-Mg exchange experiments, near-equilibrium was reached in 2 - 4 hours.

2.3.4. Instrumental methods

All measurements were performed in the Helmholtz Laboratory for the Geochemistry of the Earth Surface (HELGES) at GFZ Potsdam. Detailed analytical description could be seen in Chapter 1. Soil, saprolite, the extracted clay-sized fraction, primary minerals, and bedrock were dissolved by acid digestion using a mixture of concentrated HF and HNO_3 in PFA vials. Aqua regia was also applied to assist digestion after HF and HNO_3 treatment. Elemental concentrations of the filtered supernatant, water samples, and acid digested solution were analysed by inductively coupled plasma optical emission spectrometry (ICP-OES, Varian 720-ES) following published protocols (Schuessler et al., 2016). Relative uncertainties are better than 5% for Mg based on repeat analyses of the international reference materials SLRS-6 (river water, NRC CNRC), SRM2709a (soil, USGS) and synthetic in-house standards. The chromatography procedure for Mg purification is described in detail in the supporting information and is the same as that used in Uhlig et al. (2017). Mg isotopes were measured via multicollector inductively coupled plasma mass spectrometry (MC-ICPMS, Thermo Neptune) using DSM3 as

bracketing standard to correct for instrumental mass bias. Analytical results are reported relative to DSM3 in delta notation (Table S2-1 to S2-6), $\delta^{x}Mg_{sample} = [(^{x}Mg/^{24}Mg)_{sample} / (^{x}Mg/^{24}Mg)_{DSM3} - 1] \times 10^{3}$, where x = 26 or 25. Reference materials Cambridge-1 (pure Mg solution), SLRS-6 (river water), SRM2709a (soil), SRM1515 (apple leaves) are routinely monitored, yielding values of -2.60 ± 0.07‰ (n=24), -1.24 ± 0.14‰ (n=11), -0.16 ± 0.04‰ (n=8), -1.20 ± 0.04‰ (n=3) respectively, which agree well with previously published values (e.g. Shalev et al., 2018).

2.4. Results

2.4.1. δ^{26}Mg in bulk regolith, separated minerals, clay-sized fraction and exchangeable fraction

Primary Mg-bearing minerals include primary hornblende and secondary biotite and chlorite originating from hornblende alteration. Both biotite (-0.08 ± 0.05‰) and chlorite (-0.13 ± 0.09‰) are slightly enriched in heavy Mg isotopes compared to hornblende (-0.21 ± 0.05‰). Non-magnetic felsic minerals (mainly feldspar and quartz) containing relatively little Mg (contributing less than 10% of total Mg in bedrock) exhibit significantly more negative δ^{26}Mg values (-0.42 ± 0.07‰). Bulk bedrock shows similar Mg isotopic composition to hornblende, consistent with being the major host phase of Mg. δ^{26}Mg of soil and saprolite shows little variation and is on average 0.2‰ more positive than bedrock. τ_{Zr}^{Mg}, calculated as $\frac{[Mg]_{sample}/[Zr]_{sample}}{[Mg]_{bedrock}/[Zr]_{bedrock}} - 1$ (Brimhall and Dietrich, 1987), using Zr as the reference element as justified in Uhlig and von Blanckenburg (2019), suggests ~ 70% loss of Mg in the regolith (Fig. 2-3). δ^{26}Mg of the clay-sized fraction is ~0.1‰ more positive than bulk regolith from which it was extracted (Fig. 2-4). Meanwhile, the exchangeable fraction of the regolith exhibits systematic variation throughout the profile: a decreasing trend in δ^{26}Mg with depth is observed from 0-1.5 m depth, followed by an increasing trend to -0.52‰ to ~3 m, and below 3 m depth values are largely invariant (Fig. 2-4). The Mg concentration of the exchangeable fraction relative to the Mg concentration of bulk soil amounts to <0.1 % and is thus a negligible contribution to the δ^{26}Mg of bulk soil.

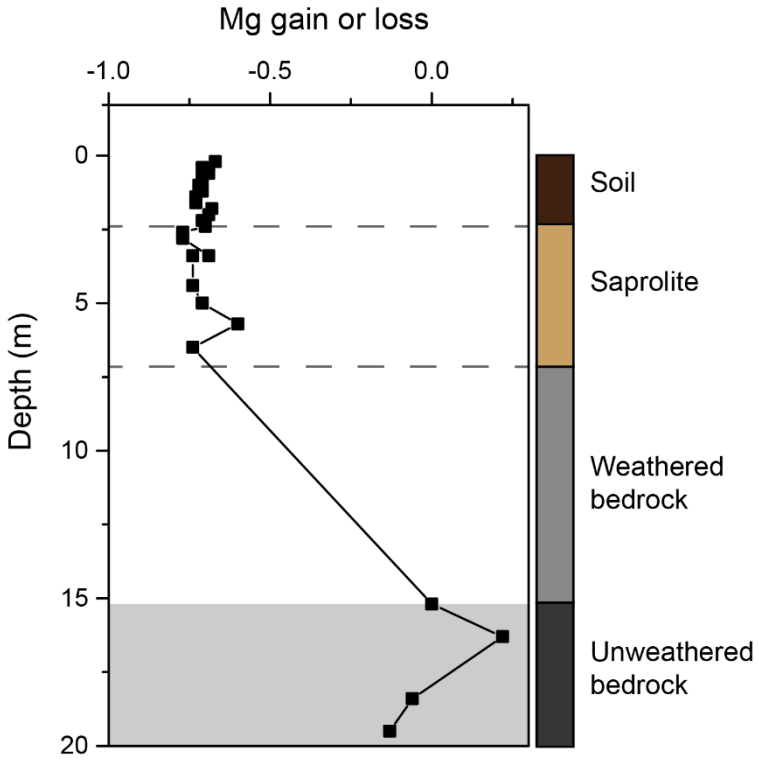

Fig. 2-3 Mg gain or loss (τ_{Zr}^{Mg}) of the regolith.

2.4.2. δ^{26}Mg of plant samples

Plant samples show heterogeneous δ^{26}Mg among species and tissue types (Fig. 2-4). Beech tree ring samples span a wide range of δ^{26}Mg variation from -0.61 ‰ to -0.39 ‰. Twigs and leaves are generally more enriched in heavy Mg isotopes than the trunk. Based on Mg allocation in beech tree tissues (4 %, 10 %, 69 % and 17 % for foliage, branch, trunk, and roots, respectively, Feger, 1997), the estimated δ^{26}Mg of bulk beech tree is -0.40 ±0.12 ‰ (root was not considered as it was not sampled, and it only contributed to 17 % of Mg budget). Spruce needles (-0.74 ‰ to -0.87 ‰) are slightly enriched in ^{24}Mg compared to exchangeable Mg. This value is similar to the data reported for needles in a Vosges Mountains Forest (Bolou-Bi et al., 2012) and is amongst the most negative δ^{26}Mg values compiled for biological samples by Pokharel et al. (2018).

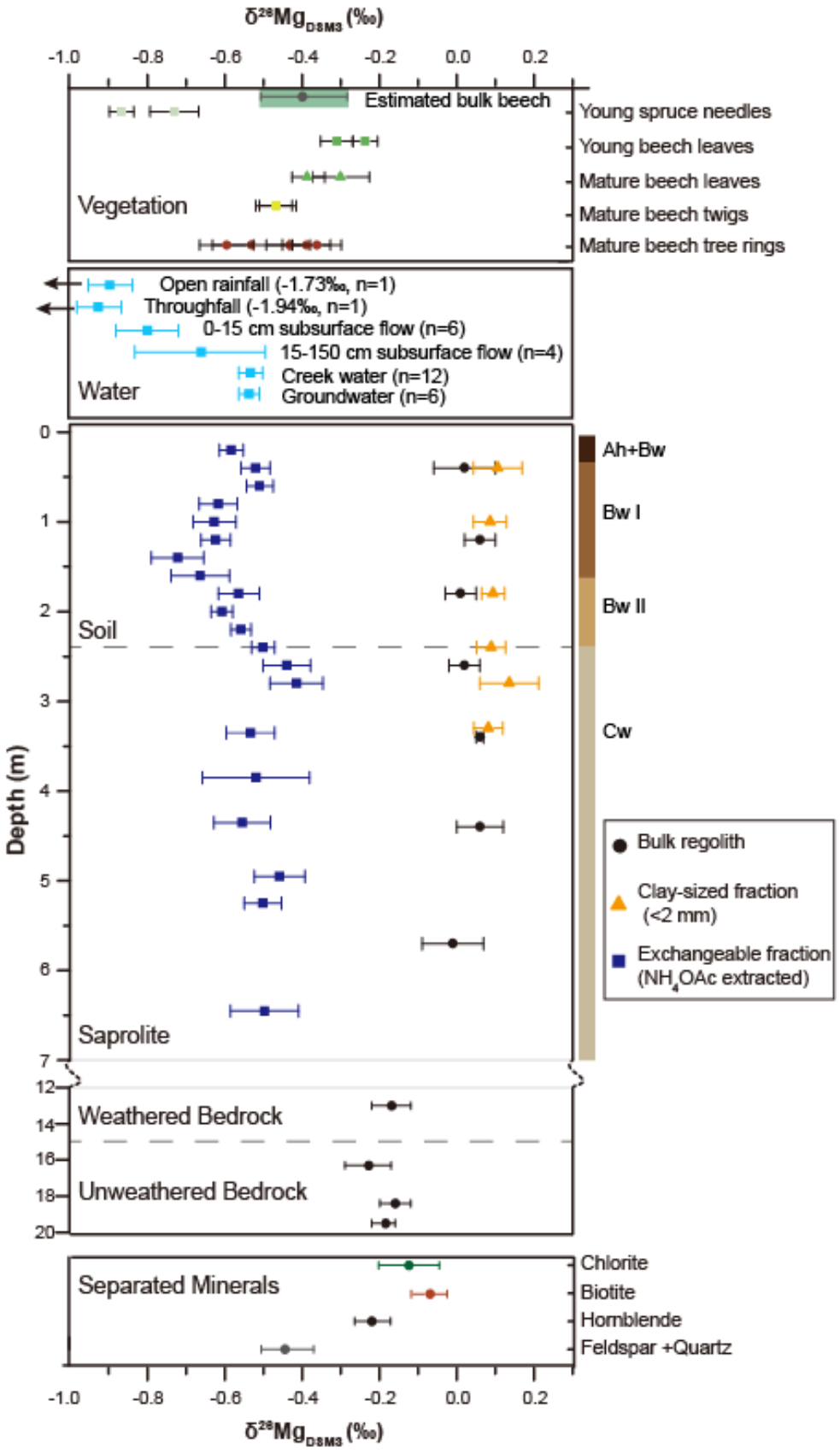
δ²⁶Mg_DSM3 (‰)
-1.0
-0.8
-0.6
-0.4
-0.2
0.0
0.2
Estimated bulk beech
Young spruce needles
Young beech leaves
Mature beech leaves
Mature beech twigs
Mature beech tree rings
Vegetation
Open rainfall (-1.73‰, n=1)
Throughfall (-1.94‰, n=1)
0-15 cm subsurface flow (n=6)
15-150 cm subsurface flow (n=4)
Creek water (n=12)
Groundwater (n=6)
Water
Depth (m)
0
1
2
3
4
5
6
7
12
14
16
18
20
Soil
Saprolite
Weathered Bedrock
Unweathered Bedrock
Ah+Bw
Bw I
Bw II
Cw
Bulk regolith
Clay-sized fraction (<2 mm)
Exchangeable fraction (NH4OAc extracted)
Separated Minerals
Chlorite
Biotite
Hornblende
Feldspar +Quartz
δ²⁶Mg_DSM3 (‰)

Fig. 2-4 δ^{26}Mg of bulk regolith, separated minerals, clay-sized fraction, exchangeable fraction, water samples and plant samples. Ah, Bw, Cw: Soil horizons according to IUSS/ISRIC/FAO 2006. For water samples, error bars represent two standard deviations of the mean value of time series samples. For other samples, error bars represent two standard deviations of four replicate measurements (similarly hereafter).

2.4.3. Mg concentration and δ^{26}Mg of time series water samples

Subsurface water flow collected from 0-15 cm depth show the largest variation in Mg concentration ([Mg]) among all water samples, ranging from 17 to 184 μmol/l, which is expected due to dilution with open rainfall or condensation through evaporation. δ^{26}Mg, however, shows little variation (-0.80 ± 0.08 ‰ mean ± 2SD, n = 6) across different seasons and hydrological conditions. Despite the shallow depth at which the subsurface flow was collected, these δ^{26}Mg values are significantly more positive than the open rainfall (-1.73 ± 0.03 ‰) and throughfall (-1.97 ± 0.03 ‰). Similarly, negative δ^{26}Mg values of open rainfall were also observed in a Swiss Alps catchment and the negative value might reflect the interaction of carbonate dust and open rainfall (Tipper et al., 2012). The lighter Mg isotopes in throughfall may reflect the leaching of isotopically light Mg from the canopy such as the unbonded Mg contained in cells that is depleted in ^{26}Mg as compared to Mg in Chlorophyll or other bonded Mg forms (Pokharel et al., 2018). Subsurface flow collected from 15-150 cm depth shows relatively smaller [Mg] variation, ranging from 19 to 49 μmol/L and on average, values are lower than for the 0-15 cm depth section. With the exception of one subsurface flow sample from 15-150 cm depth collected in August, which has identical δ^{26}Mg values (-0.84 ± 0.03 ‰) to that collected from the 0-15 cm depth section, subsurface flow samples collected from 15-150 cm depth show consistently more positive δ^{26}Mg values than their shallower counterparts (-0.62 ± 0.04 ‰, n = 3).

Groundwater [Mg] is generally twice as high in concentration as 15-150 cm subsurface flow, and ranges between 65 and 99 μmol/L. Despite changing [Mg], δ^{26}Mg values of groundwater remain invariant (-0.55 ± 0.03 ‰, n = 6). However, although discharge variations span 3 orders of magnitude, [Mg] at low flow is only 5 times higher than that seen during high flow periods. Intriguingly, despite the large variability in discharge and [Mg] over the sampling period, no corresponding change in creek water δ^{26}Mg was observed (-0.54 ± 0.04 ‰, n = 12), with values remaining identical to that of groundwater.

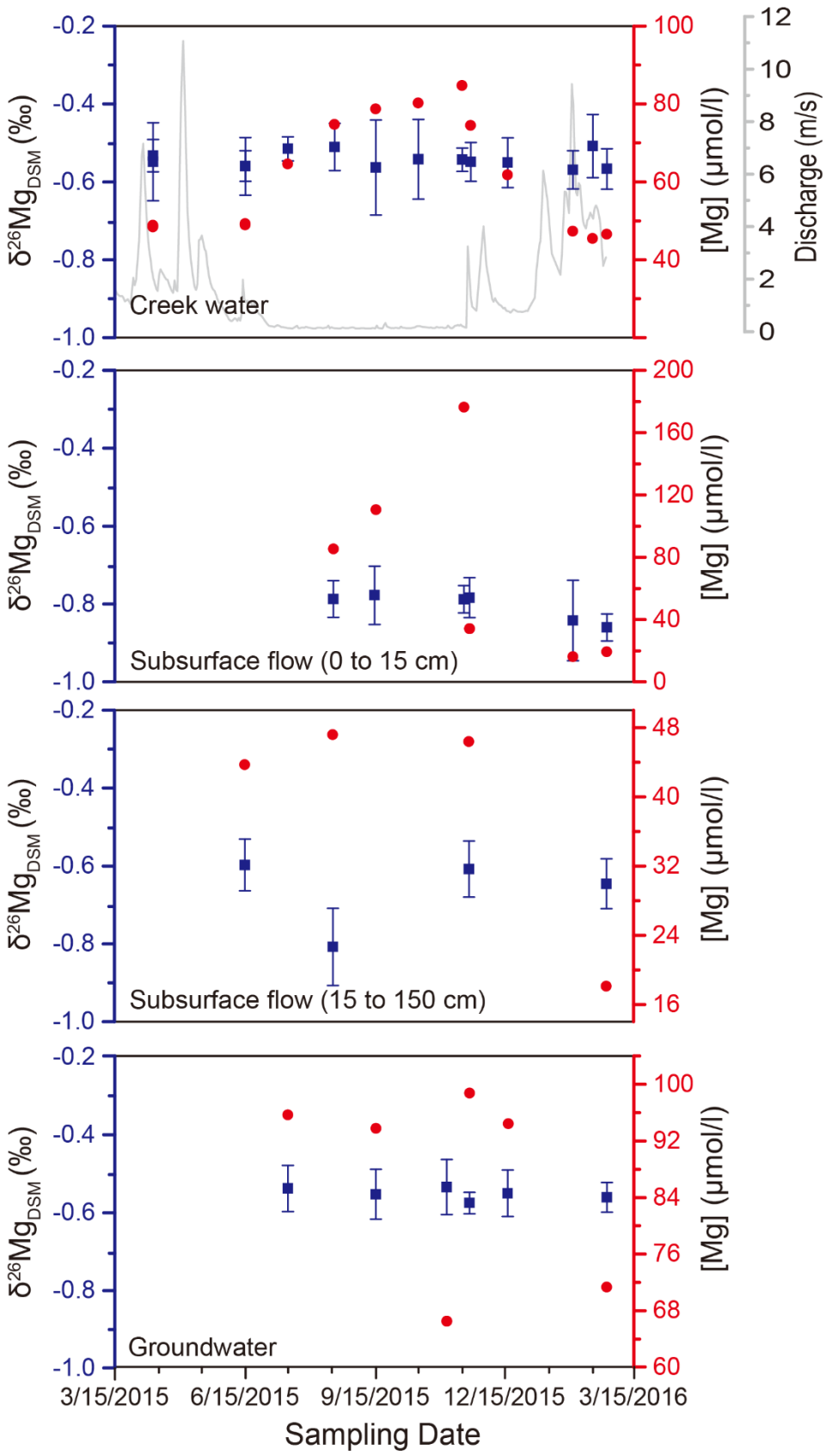
δ26MgDSM (‰)
-0.2
-0.4
-0.6
-0.8
-1.0
[Mg] (µmol/l)
Discharge (m/s)
Creek water
Subsurface flow (0 to 15 cm)
Subsurface flow (15 to 150 cm)
Groundwater
3/15/2015
6/15/2015
9/15/2015
12/15/2015
3/15/2016
Sampling Date

Fig. 2-5 $\delta^{26}Mg$ (left axis) and [Mg] (right axis) of time-series water samples including creek water, subsurface flow and groundwater sampled from a well at 8 m depth. The grey curve in the background of the uppermost panel shows the creek discharge.

2.4.4. Adsorption and desorption experiment on topsoil

Assuming excess NH_4OAc could extract all the exchangeable Mg from soil, we found that 20 % of Mg was desorbed with circumneutral Milli-Q water (pH 6.2) and 32 % was desorbed with Milli-Q acidified to pH 3.2 with a few drops of distilled HNO_3. In both acidic and circumneutral conditions, increasing [Ca] in solution could exchange more Mg, although the increase in Mg desorbed with higher Ca input is considerably weaker at low pH compared to circumneutral pH (Fig. 2-6a). Importantly, however, despite the difference in the amount of Mg desorbed, the $\delta^{26}Mg$ of all reacted solutions remain almost identical or slightly more negative (< 0.1 ‰) than that of bulk soil exchangeable Mg (Fig. 2-6b), suggesting the exchangeable Mg was congruently released to the solutions with little or no fractionation.

Patterns of Mg adsorption (and desorption) equilibrium after soil was reacted with $MgCl_2$ solutions are shown in Fig. 2-6. Data points above the 1:1 line indicate increasing $[Mg]_{solu}$ after reaction, thus a net desorption, while those below the 1:1 line suggest net adsorption during the experiment (Fig. 2-6c). This result suggests that desorption and adsorption on natural soil depends on both solution pH and input solution Mg concentration. After reaction, regardless of whether adsorption or desorption was dominant, exchangeable Mg had $\delta^{26}Mg$ values that were almost identical to solution Mg (Fig. 2-6d), suggesting that isotope fractionation is negligible.

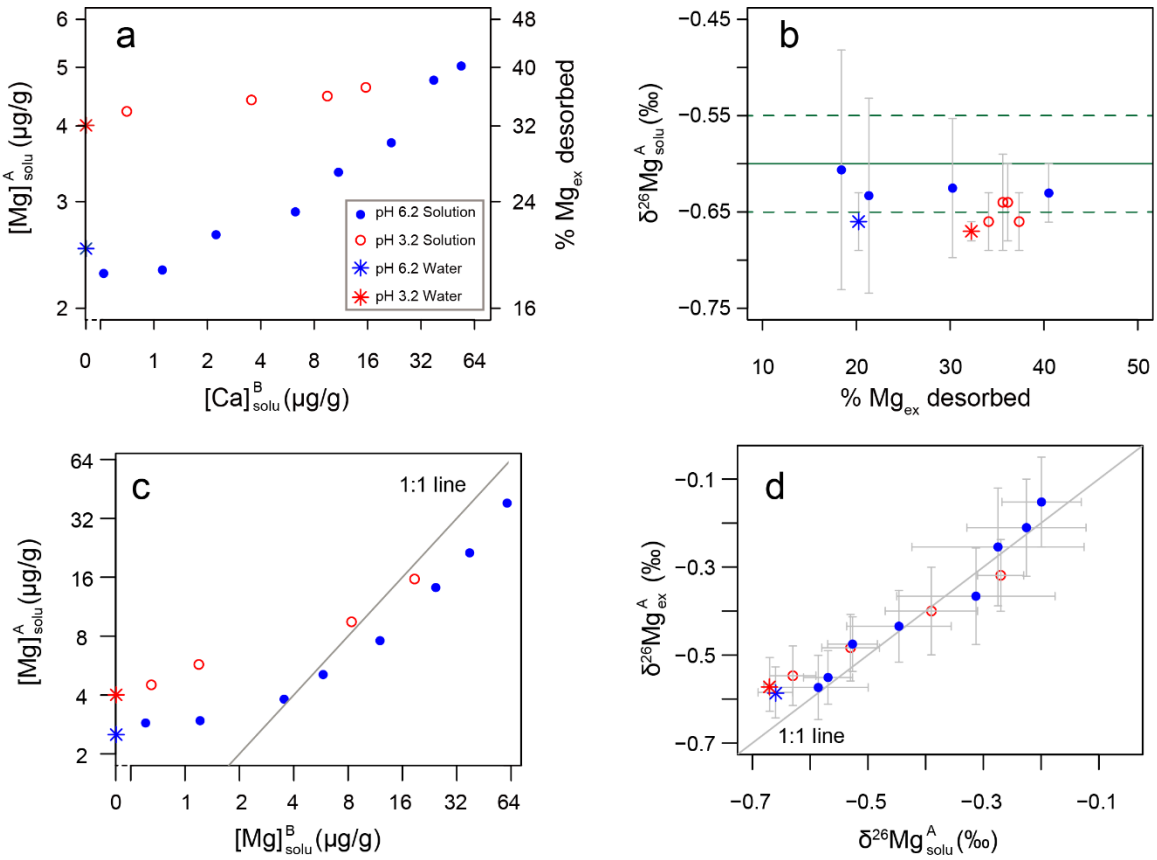

Fig. 2-6 Adsorption-desorption experiment result. **Panel a)** depicts the influence of solution [Ca] on the amount of Mg desorption. $[Ca]^{B}_{solu}$ denotes Ca concentration in the solution before reaction. $[Mg]^{A}_{solu}$ denotes the Mg concentration in the solution after reaction. The second y-axis (right) shows the percentage of total exchangeable Mg that is desorbed. Note x and y axes are in log scale. The star symbols denote circumneutral or pH 3.2 water. **Panel b)** shows the relationship between the proportion of Mg desorbed and the isotopic composition of desorbed Mg ($\delta^{26}Mg^{A}_{solu}$). Horizontal solid and dashed lines represent the isotopic value of bulk exchangeable Mg and its analytical uncertainty (2SD). The data suggests that Mg was released with no or little fractionation. **Panel c)** Mg concentrations in solutions before ($[Mg]^{B}_{solu}$, x-axis) and after ($[Mg]^{A}_{solu}$, y-axis) reaction respectively. Data points above the 1:1 line imply desorption while points below the line imply adsorption. Note x and y axes are in log scale. **Panel d)** Mg isotope composition of solution ($\delta^{26}Mg^{A}_{solu}$) and absorbed fraction ($\delta^{26}Mg^{A}_{ex}$) after reaction. The data points are generally distributed along the 1:1 line, indicating negligible fractionation between solution Mg and exchangeable Mg after reaction.

2.5. Discussion

2.5.1. The absence of isotope fractionation during an adsorption-desorption experiment using topsoil

Our lab experiment results suggest that soil exchangeable Mg is congruently desorbed to solution without isotope fractionation, regardless of pH, solution chemistry or proportion of Mg released. Similarly, no or very small (<0.1 ‰) fractionation was observed in Mg adsorption experiments, even though pH exerted a strong influence on sorption-desorption equilibrium. We infer that Mg adsorption is non-specific in the sense that it does not involve changes in inner-sphere complexation. The rationale is as follows: if Mg were adsorbed as an inner-sphere complex, then isotopic fractionation might be expected during the process of dehydration and formation of covalent bonds. For example, molecular dynamics simulations of Mg isotope fractionation amongst aqueous Mg species predict fractionations in the range of one to several per mil (Schott et al., 2016). In this case, hydrated Mg, typically represented as $Mg[H_2O]_6^{2+}$ in molecular dynamics simulations (Trivedi and Axe, 2001), is electrostatically attracted to the surface without undergoing dehydration and forming chemical bonds, and thus no isotope fractionation occurs. That Mg is readily exchanged by Ca lends support to this interpretation. This study and Charlet and Sposito (1989) showed that Mg adsorption is depressed when solution electrolyte concentration increases, a characteristic of non-specific sorption mechanism.

2.5.2. Mg isotope fractionation in regolith: preferential dissolution and secondary mineral formation

In the upper ~7 m of bulk regolith $\delta^{26}Mg$ is ~ 0.03 ‰, a value in between the $\delta^{26}Mg$ of remaining primary minerals (biotite and chlorite) and the clay-sized fraction (Fig. 2-4), and on average 0.2 ‰ more positive than bedrock. In previous field studies, secondary mineral formation has been widely assumed to be the main factor fractionating soil Mg isotopes (e.g. Teng et al., 2010; Liu et al., 2014). However, we observed that minerals separated from bedrock do show Mg isotope heterogeneity. Among the main Mg-bearing minerals, biotite and chlorite are more enriched in ^{26}Mg than hornblende. Thus, differential dissolution of primary minerals might cause the observed depletion in ^{24}Mg in regolith. Indeed, X-ray diffraction analyses suggests that hornblende, the Mg phase with low $\delta^{26}Mg$ (-0.21 ‰) is abundant in the bedrock but undetectable in the upper 7 m of regolith (Uhlig and von Blanckenburg, 2019), suggesting it has been dissolved due to its higher solubility. Therefore, the more positive Mg isotope composition we observed in soil and saprolite might be due to dissolution of hornblende. However, biotite (-0.13 ‰) and chlorite (-0.08 ‰), the remaining two Mg carriers, are still isotopically lighter than the bulk soil and saprolite (0.03 ± 0.06 ‰, n = 6) by ~0.1 ‰. We thus explore next whether secondary mineral formation is setting the increase in $\delta^{26}Mg$ from bedrock to regolith.

The clay-sized fractions were extracted from regolith and this fraction yields δ^{26}Mg of 0.10 ± 0.04 ‰ (n = 6), a value more positive than bulk regolith and separated minerals. Because the clay-sized fraction is composed of truly neoformed secondary minerals and fine primary minerals, δ^{26}Mg of the truly neoformed secondary minerals are assumed to be even more positive than its measured values. An upper approximation of the relative amount of neoformed secondary minerals can be estimated by a simple mass balance (equation 1),

$$\delta^{26}Mg_{soil} = (1 - f_{secondary}) \times \delta^{26}Mg_{primary} + f_{secondary} \times \delta^{26}Mg_{secondary} \quad (2.1)$$

where $\delta^{26}Mg_{primary}$ represent the mean δ^{26}Mg value of biotite and chlorite (-0.11 ‰), $\delta^{26}Mg_{secondary}$ is the most positive δ^{26}Mg value of our separated clay-sized fraction (0.12 ‰), and $f_{secondary}$ is the relative proportion of neoformed secondary minerals. Given that $f_{secondary}$ amounts to ~52 %, half of the soil Mg is hosted in secondary minerals. The incorporation of heavy Mg isotopes into clays is also supported by the low δ^{26}Mg value in fluid and the exchangeable fraction; a topic we return to in section 2.5.3.

In summary, we suggest that the positive δ^{26}Mg value of the upper regolith is due to a combination of 1) dissolution of isotopically lighter hornblende and 2) secondary mineral formation further fractionate regolith towards more positive δ^{26}Mg values.

2.5.3. The source and vertical distribution of isotopically lighter exchangeable Mg

The vertical distribution of the exchangeable Mg concentration and Mg isotope composition in this study can be divided into two parts: From 0 to 3 m, showing a bulge pattern with low Mg concentrations and more negative δ^{26}Mg values in the center of the bulge; and from below 3 m depth, where exchangeable Mg concentration and δ^{26}Mg are almost invariant (Fig. 2-7). Whereas the vertical distribution of element concentrations in the exchangeable fraction has been explained in previous studies through supply from atmospheric deposition (Opfergelt et al., 2012), dissolution of primary minerals, and biological cycling (Jobbágy and Jackson, 2001; James et al., 2016; Uhlig and von Blanckenburg, 2019; Yu et al., 2020), the depth distribution of the Mg isotope composition remains poorly constrained.

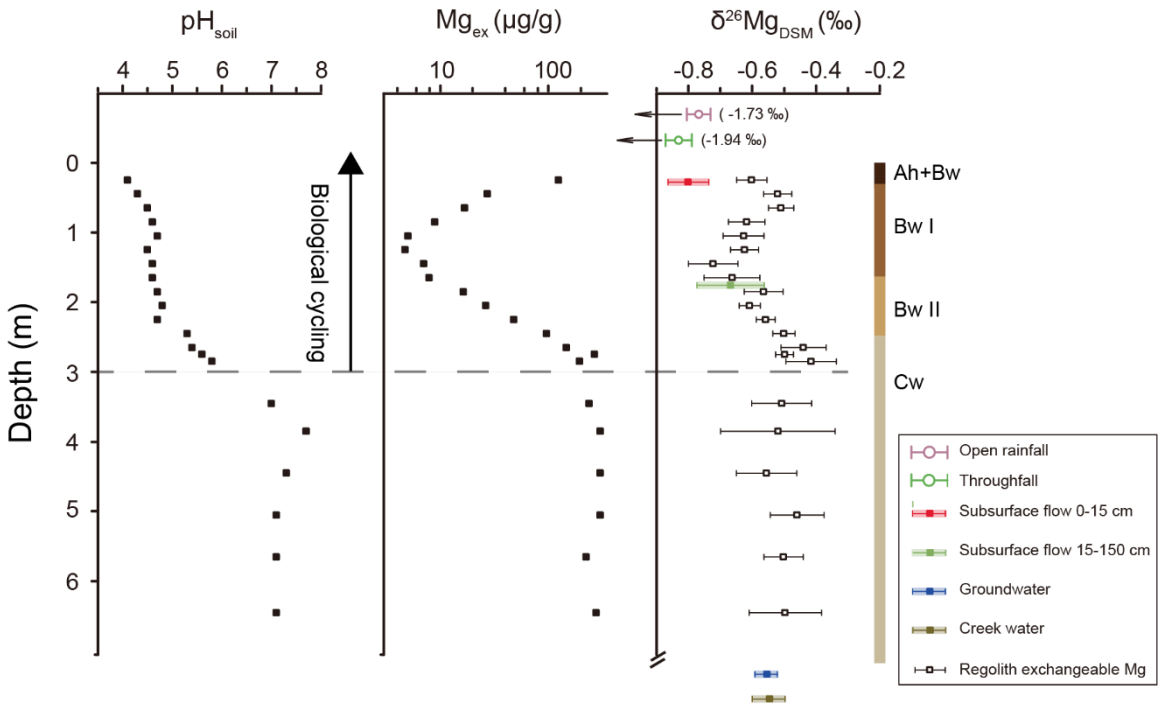

Fig. 2-7 Vertical distribution of pH, exchangeable Mg concentration (µg/g, 1M NH_4OAc extracted Mg in 2 g regolith) and exchangeable Mg isotopic composition. The bulged distribution of exchangeable [Mg] and $\delta^{26}Mg$ in the shallow depth (0 – 3 m) is attributed to chemical weathering imprinted by biological cycling (see text for detail). $\delta^{26}Mg$ of water samples including open rainfall (n = 1), throughfall (n = 1), subsurface flow from 0-15 cm (n = 6), subsurface flow from 15-150 cm (n = 4), groundwater (n = 6), and creek water (n = 14) was also shown for comparison with the exchangeable $\delta^{26}Mg$.

a) Influence of biological cycling on the exchangeable Mg concentration and isotopic composition variation at shallow depth (0 to 3 m)

In eroding settings, forest ecosystems experience a permanent loss of organic-bound mineral nutrients. Thus, long-term nutrition of forest ecosystems can only be sustained if the organic nutrient cycle is coupled to the geogenic nutrient pathway (Uhlig and von Blanckenburg 2019). This feedback mechanism was demonstrated by means of measurements of inventories and fluxes by Uhlig and von Blanckenburg (2019) and verified in a subsequent study, in which Uhlig et al. 2020 fingerprinted the depth of the geogenic nutrient source by the isotope proxies $^{87}Sr/^{86}Sr$ and $^{10}Be(meteoric)/^{9}Be$. However, both studies lack direct evidence that elements hosted in the exchangeable fraction of topsoil can be attributed to biological uplift. Our new dataset comprising the paired analyses of Mg concentrations and isotope compositions allows for an assessment of the biological nutrient uplift hypothesis (Jobággy and Jackson 2004).

The depth profile of the Mg concentration of the exchangeable fraction was described earlier in Uhlig and von Blanckenburg (2019). In brief, the interplay of soil mineralogy (e.g., clays and oxides) and organic matter (e.g. humus), and the soil pH explains the vertical depth profile of exchangeable Mg concentrations. Importantly, the increasing Mg concentrations from 1.5 m depth to topsoil was attributed to biological uplift, which agrees with the studies of Jobbágy and Jackson (2001, 2004). In this case, Mg is utilized by trees at depth (1.5 - 3 m) with heavy Mg isotopes being favored, which agrees with results from $^{87}Sr/^{86}Sr$ and $^{10}Be(meteoric)/^{9}Be$ used as nutrient uptake tracer in Uhlig et al. (2020). The Mg is then cycled through trees and a fraction is ultimately returned to the forest floor via annual litterfall. As Mg is not significantly re-utilized from organic matter in this study site (Uhlig and von Blanckenburg 2019), isotopically heavy Mg liberated from decomposing plant litter or organic matter may re-enter the pool of the exchangeable fraction.

In support of this suggested mechanism, the increase of both $[Mg_{ex}]$ and $\delta^{26}Mg_{ex}$ from 1.5 m to the forest floor is consistent with the observation that beech leaves (representing plant litter) are enriched in heavy Mg isotopes. Even though Uhlig and von Blanckenburg (2019) concluded that trees do not set the stoichiometry of the exchangeable fraction of the upper three meters of soil, their general statement may not hold for elements such as Mg that are not significantly re-utilized. In summary, we conclude that $\delta^{26}Mg_{ex}$ of the top 3 m of our profile is first set by secondary mineral formation (see below), to be then overprinted by Mg uptake by trees (at 1.5 to 3 m depth) and biological uplift of Mg (in the top 1.5 m).

b) Source of light exchangeable Mg isotopes in the deep (>3 m) regolith

The exchangeable fraction of deep regolith (>3 m) is characterized by high Mg concentration and negative $\delta^{26}Mg$ values. That the exchangeable fraction is isotopically lighter than bulk regolith was observed in previous studies (e.g., Opfergelt et al., 2012; Chapela Lara et al., 2017; Uhlig et al., 2017). Opfergelt et al. (2012) attributed this phenomenon to isotope fractionation during successive adsorption-desorption processes. However, our adsorption-desorption experiment using topsoil from our study site shows negligible isotope fractionation. Therefore, other factors need to be considered. Both open rainfall and throughfall are enriched in isotopically light Mg, but this isotope signature is not likely transferred to several meters depth as demonstrated by a labeling experiment with an artificial ^{26}Mg spike (van der Heijden et al., 2013). In addition, the inventory of the exchangeable Mg pool is more than 10^3 times higher than the annual influx of Mg by atmospheric deposition (Fig. 2-1). Thus, the large exchangeable Mg pool should originate from weathering of the regolith rather than from atmospheric input. Felsic minerals (feldspar and quartz) exhibit $\delta^{26}Mg$ values similar to exchangeable Mg (Fig. 2-4),

but the Mg concentration in these minerals is too low to be a primary Mg source, amounting to less than 10 % relative to biotite and chlorite. Moreover, biotite is more soluble than the felsic minerals (e.g., 1.5×10^{-10} mol/g/s for biotite compared to 6.6×10^{-11} mol/g/s for plagioclase in a granite dissolution experiment, Ganor et al., 2004). The light exchangeable Mg isotopes thus does not originate from the preferential dissolution of felsic minerals. Carbonate minerals are known to have the most negative δ^{26}Mg values in environmental samples (Saenger and Wang, 2014), but microscopic and XRD analyses (Uhlig and von Blanckenburg, 2019) failed to identify the presence of carbonate minerals at this site. Eliminating these factors, the most likely process driving exchangeable Mg isotopes to negative values is secondary mineral formation as discussed in section 2.5.2. It is likely that the Mg residue in soil water entered the exchangeable pool after secondary mineral formation. This is evidenced by former clay synthesis experiments (Hindshaw et al., 2020), which showed 17 - 33 % Mg entered exchangeable sites (compared to Mg in bulk solid) of precipitated stevensite and saponite.

2.5.4. Exchangeable fraction as first order control on runoff water chemistry

It is intriguing that the subsurface flow, groundwater, and creek water show negligible seasonal variation in δ^{26}Mg despite large variations in Mg concentration (Fig. 5). A buffering process appears to set the isotope ratio of Mg, but not its concentration. Importantly in this regard δ^{26}Mg values of water agree with those of the exchangeable fraction at their respective sampling depth (Fig. 2-7), in agreement with our lab experiment indicating negligible isotope fractionation during adsorption-desorption (Fig. 2-6). We thus hypothesize that the exchangeable fraction is the first order control on water chemistry in this study site (Miller et al., 1993), and infiltrating water recharging the groundwater reservoir is likely buffered by this large exchangeable pool.

Even at 1.5 m depth, where exchangeable Mg concentration is much lower than that of deep regolith, collected time-series subsurface flow samples exhibit uniform δ^{26}Mg that correspond to exchangeable δ^{26}Mg (Fig. 2-7). Only in the 0-15 cm subsurface water δ^{26}Mg deviate from the exchangeable pool, being on average ~ 0.2 ‰ more negative (Fig. 2-7). A potential explanation for this discrepancy is the contribution of throughfall, which has a very negative δ^{26}Mg value. Given the short water flow path length scale of about 15 cm the timescale for desorption may be too low to fully buffer diluted rainwater.

Even more intriguingly, Mg in time-series creek water samples also exhibits minimal isotope variation (Fig. 2-5, 2-8b). The concentration-discharge relationship (or C-Q relationship; Fig. 2-8a) for Mg can be described by the power law equation $C=aQ^b$, with a and b being fitted parameters (Godsey et al., 2009). A log-log slope (b-value) of zero represents chemostasis (Godsey et al., 2009) meaning the concentration of a given solute remains constant regardless of discharge, and a b-value of -1 indicates pure dilution behavior. Thus, a b-value of -0.49 for Mg in this

study indicates moderate buffering of Mg. That Mg concentrations are buffered at high discharge has been observed before (e.g., Godsey et al., 2009; Clow and Mast, 2010; Kim et al., 2014). However, the Mg source that sets the buffering process is subject to debate (e.g., Maher, 2010; Trostle et al., 2016; Torres et al., 2017; Kim et al., 2017; Torres and Baronas, 2021). Our isotope data sheds light onto this issue. That creek water has almost identical δ^{26}Mg to exchangeable δ^{26}Mg of deep regolith strongly supports the hypothesis that it is the interaction between water and the exchangeable pool in deep regolith that buffers Mg at high discharge (e.g. Campbell et al., 1995; Jin et al., 2011; Kim et al., 2017).

We can quantify the capacity of the exchangeable pool to buffer the Mg concentration in creek water, by comparing the exchangeable Mg pool with the Mg export flux by creek water. Using pool size and flux data from Fig. 2-1, the exchangeable Mg hosted in the upper 7 m of regolith – if not replenished – would last for about 1200 years before being exhausted. This is a rough estimation as exchangeable Mg is also involved in biological recycling (section 5.3.1) and secondary mineral formation (section 5.3.2). Chemical weathering flux as evaluated from the denudation rate and the chemical depletion factor of Mg in soil (Uhlig and von Blanckenburg 2019) is more than twice as high as dissolved Mg export flux derived from empirical measurement of creek water. It is feasible therefore, that the exchangeable pool may be continuously replenished by Mg liberated from mineral dissolution, such that it can over millennia buffer the Mg export by creek water. On short time scales, exchangeable Mg rapidly interacts with soil water and reaches near equilibrium within hours (Fig. 2-2). Thus, the reservoir of exchangeable Mg likely presents the source that buffers water chemistry on both short and long timescales. We suggest therefore that the buffered Mg concentration and invariance of δ^{26}Mg observed in other studies (e.g., Hindshaw et al., 2019; Fries et al., 2019; Novic et al., 2021) might also be due to the same exchange reactions.

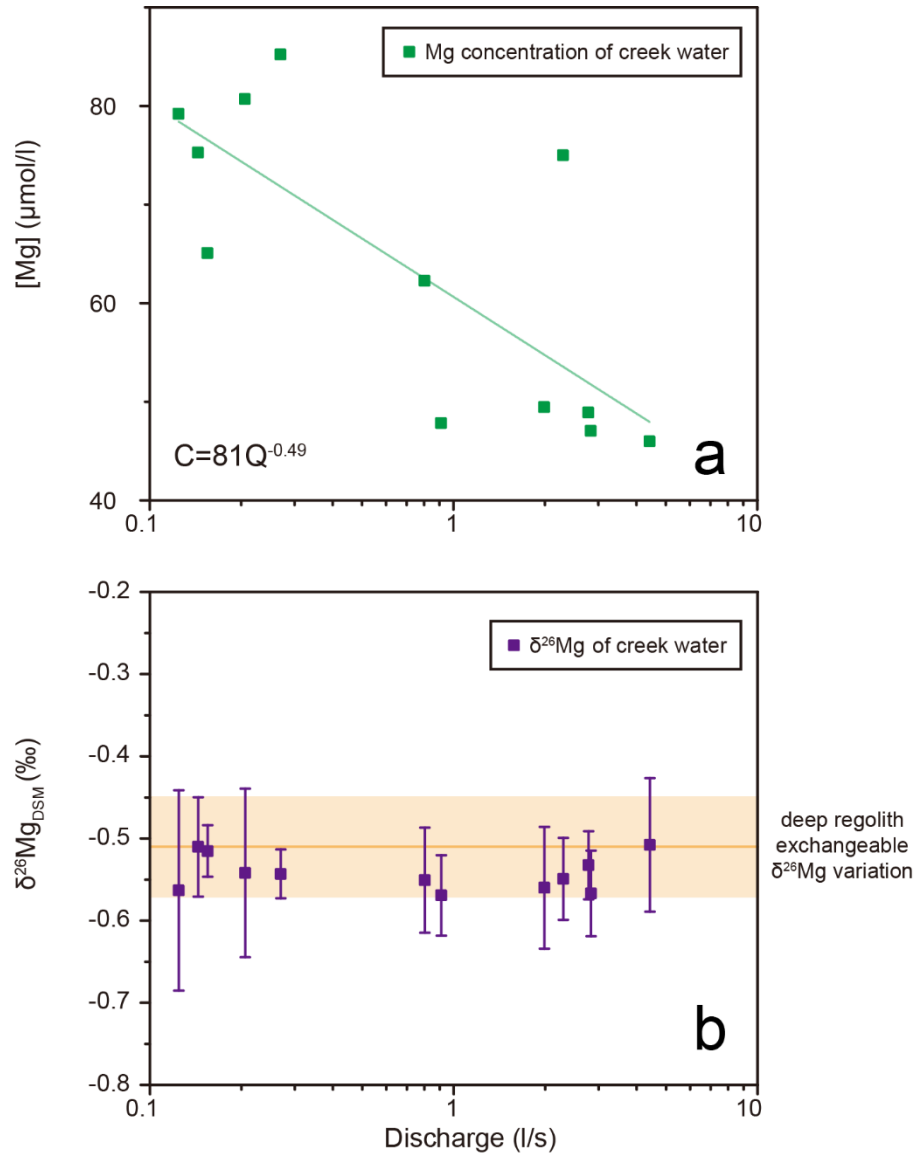

Fig. 2-8 a: Concentration-Discharge (C-Q) relationship of Mg. Fitted curve is $C=81Q^{-0.49}$, which suggests Mg concentration is slightly buffered during high discharge. **b**: δ^{26}Mg-Discharge relationship of creek water samples. Horizontal line and shaded area mean the averaged and variation (2SD) of deep regolith (>3m) exchangeable δ^{26}Mg.

2.5.5. Quantifying dissolved Mg loss by elemental and isotope mass balance

In the Critical Zone, bulk soil integrates the long-term weathering process, whereas water chemistry is an instantaneous weathering product. Using an isotope mass balance approach, Bouchez et al. (2013) developed an isotope model that quantifies the relationship between the weathering flux of the element of interest and the total denudation flux solely by metal isotopes (equation 2.2).

$$w^{Mg} = \frac{\delta^{26}Mg_{regolith} - \delta^{26}Mg_{rock}}{\delta^{26}Mg_{regolith} - \delta^{26}Mg_{water}} \quad (2.2)$$

In equation 2.2, w^{Mg} is the fraction of dissolved Mg export relative to the total export of solute and particulate Mg. $\delta^{26}Mg_{regolith}$, $\delta^{26}Mg_{rock}$, and $\delta^{26}Mg_{water}$ are the δ^{26}Mg of regolith, bedrock and water, respectively. The calculated w^{Mg} is 41 ± 11 %, indicating that ~41 % of total denuded Mg occurs in dissolved form, while the remainder is eroded in particulate form. w^{Mg} can also be evaluated by calculating the relative mass loss of Mg from regolith (τ_{Zr}^{Mg}, Fig. 2-4). This method gives a value of 71 ± 17 %. The results derived from these two methods are roughly consistent, indicating the robustness of using both methods for evaluation of Mg weathering intensity in the Critical Zone.

2.6. Conclusion

We hypothesize that the exchangeable fraction exerts the main control on the Mg isotope composition of creek water. Several lines of evidence support this hypothesis: first, results of our laboratory adsorption-desorption experiment show that isotope fractionation during the adsorption-desorption processes is negligible (a corollary of this is that the exchangeable fraction of regolith Mg records the Mg isotope composition of porewater fluids). Second, creek water records δ^{26}Mg values identical to those of the exchangeable fraction in the deep regolith. Thirdly, the pool size of exchangeable Mg suffices over millennia to buffer creek water. Mg isotope mass balance suggests that 41 ±11% of Mg loss is in the dissolved form, roughly consistent with the calculation based on τ_{Zr}^{Mg} (71 ± 17%).

We also demonstrated that the vertical distribution of both exchangeable Mg concentration and isotopic composition can be reconstructed at high resolution in the Critical Zone. Deep regolith hosts substantial amounts of exchangeable Mg sourced from abiotic weathering processes. At shallower depth, in contrast, biological recycling exerts significant influence with deep bio-uptake reaching up to ~3m. This large pool of deep geogenic exchangeable Mg sustains nutrient loss from the forest floor on long time scales.

Acknowledgements

The authors are grateful for funding from the German National Science Foundation Priority Program 1685 “Ecosystem nutrition: forest strategies for limited phosphorus resources” and to Friederike Lang for coordination and discussion. Di Cai is grateful for funding by a CSC scholarship. Johannes Glodny is acknowledged for support on mineral separation. Finally, the authors are grateful to the analytical support provided by Jutta Schlegel, Josefine Holtz and Daniel Frick.

2.7. Appendix

2.7.1. Procedure for adsorption and desorption experiments

The topsoil sample (~5 cm depth) used for adsorption and desorption experiments was collected from this study site. The concentration and isotopic composition of soil exchangeable Mg was determined prior to the experiment via extraction using 1 M NH_4OAc, yielding a concentration value of 124 μg/g and isotopic value of -0.6 ± 0.05 ‰. This magnesium fraction is thought to be reactive in the sorption-desorption experiments.

2.7.2. Mg desorption experiment

We used 14 aliquots of the topsoil sample to run two series of desorption experiments. In the first series, circumneutral $CaCl_2$ solutions were added to 9 topsoil aliquots at Ca concentrations from 0 (pure Milli-Q water) to 54 μg/g. In the second series, acidic $CaCl_2$ solutions (pH adjusted to 3.2 with HNO_3) were added to 5 topsoil aliquots at Ca concentrations of 0 to 16 μg/g. Specifically, in both series of desorption experiments 1 g of topsoil was accurately weighed into 15 ml acid-cleaned polypropylene centrifuge tubes, 10 ml of $CaCl_2$ solution was added, samples were agitated and shaken on a hotdog roller at 60 rpm for 3 hours. Then, the suspensions were centrifuged at 4200 rpm for 30 min, the supernatant was pipetted off into a syringe and passed through a 0.20 μm acetate filter.

2.7.3. Mg adsorption experiment

Using $MgCl_2$ instead of $CaCl_2$, the adsorption experiment was otherwise conducted in the same way as the desorption experiment. The Mg concentration of circumneutral $MgCl_2$ solutions ranged from 0.6 to 61 μg/g, and of acidic $MgCl_2$ solutions (pH=3.2) from 0.6 to 19 μg/g.

2.7.4. Mass balance calculations

Element concentrations and Mg isotopic compositions were analyzed on solutions after adsorption-desorption experiments. Thus, concentration and isotopic composition of the exchangeable fraction, which interacted with the $CaCl_2$ and $MgCl_2$ solutions, were calculated by the mass balance equations (2-A-1) to (2-A-4).

For the desorption experiments, the only Mg source is the exchangeable Mg. Thus, the Mg concentration and Mg isotope composition of the exchangeable fraction can be calculated from equation (2-A-1) and (2-A-2), where $[\mathrm{Mg}]^{\mathrm{A,B}}_{\mathrm{ex,solu}}$ is the Mg concentration of either the exchangeable fraction (ex) or the solution (solu) before the experiment (B) and after the experiment (A), m_{soil} is the mass of soil, m_{solu} is the mass of solution and $\delta^{26}\mathrm{Mg}^{\mathrm{A,B}}_{\mathrm{ex,solu}}$ is the Mg isotope composition of either the exchangeable fraction or the solution.

$$[Mg]^{B}_{ex} \times m_{soil} = [Mg]^{A}_{ex} \times m_{soil} + [Mg]^{A}_{solu} \times m_{solu} \quad \text{(2-A-1)}$$

$$\delta^{26}Mg_{ex}^{B} \times [Mg]_{ex}^{B} \times m_{soil} = \delta^{26}Mg_{ex}^{A} \times [Mg]_{ex}^{A} \times m_{soil} + \delta^{26}Mg_{solu}^{A} \times [Mg]_{solu}^{A} \times m_{solu} \quad (2\text{-A-2})$$

For the adsorption experiments, both the $MgCl_2$ solution and the exchangeable Mg of the soil sample used for this experiment contributed Mg to the reaction. In this case equations (2-A-3) and (2-A-4) were used to calculate the Mg concentration and isotope composition of the adsorbed Mg.

$$[Mg]_{solu}^{B} \times m_{solu} + [Mg]_{ex}^{B} \times m_{soil} = [Mg]_{ex}^{A} \times m_{soil} + [Mg]_{solu}^{A} \times m_{solu} \quad (2\text{-A-3})$$

$$\delta^{26}Mg_{solu}^{B} \times [Mg]_{solu}^{B} \times m_{solu} + \delta^{26}Mg_{ex}^{B} \times [Mg]_{ex}^{B} \times m_{soil} = \delta^{26}Mg_{ex}^{A} \times [Mg]_{ex}^{A} \times m_{soil} + \delta^{26}Mg_{solu}^{A} \times [Mg]_{solu}^{A} \times m_{solu} \quad (2\text{-A-4})$$

Table S2-1: Element concentrations, Mg isotopic composition of bulk regolith, clay-sized fraction and separated mineral samples.

Sample	IGSN†	Depth	Major elements (ICP-OES)						Mg isotopes (MC-ICP-MS)				
		m	Al_2O_3 %	CaO %	Fe_2O_3 %	K_2O %	MgO %	Na_2O %	$\delta^{26}Mg$	2SD	$\delta^{25}Mg$	2SD	n*
Bulk regolith													
DC1-1	GFDUH00LU	0.4	16	0.47	6.5	2.5	2.2	1.2	0.06	0.04	0.05	0.05	4
DC1-2	GFDUH00LY	1.2	16	0.37	7.1	2.6	2.5	1.1	n.d.	n.d.	n.d.	n.d.	
DC1-3	GFDUH00M1	1.9	15	0.41	7.2	2.7	2.6	1.1	n.d.	n.d.	n.d.	n.d.	
DC1-3-Replicate	GFDUH00M1	1.9	15	0.39	6.7	2.5	2.4	1.1	n.d.	n.d.	n.d.	n.d.	
DC1-4	GFDUH00M5	2.7	15	0.49	6.5	2.6	2.4	1.2	0.02	0.03	0.02	0.02	4
DC1-5	GFDUH00MB	3.4	15	0.49	6.6	2.8	2.5	1.3	0.06	0.01	0.02	0.04	4
DC1-6	GFDUH00MD	4.4	14	0.55	6.0	2.5	2.2	1.3	0.06	0.05	0.03	0.02	4
DC1-7	GFDUH00MF	5.7	15	0.55	6.5	2.7	2.4	1.4	n.d.	n.d.	n.d.	n.d.	
DC1-7-Replicate	GFDUH00MF	5.7	15	0.56	6.7	2.7	2.4	1.4	n.d.	n.d.	n.d.	n.d.	
DC1-8	GFDUH00N5	7.6	17	9.3	11	1.6	5.8	2.1	n.d.	n.d.	n.d.	n.d.	
DC1-9	GFDUH00N8	10.1	16	4.1	8.8	2.6	4.3	2.7	n.d.	n.d.	n.d.	n.d.	
DC1-10	GFDUH00N9	12.9	16	5.4	7.9	2.1	3.3	3.0	-0.17	0.06	-0.10	0.03	4
DC1-11	GFDUH00NB	16.3	16	6.3	8.8	1.8	3.8	2.9	-0.23	0.03	-0.11	0.03	4
DC1-12	GFDUH00NC	18.4	16	5.7	7.1	2.0	3.4	3.2	-0.16	0.05	-0.07	0.02	4
DC1-13	GFDUH00ND	19.5	16	6.3	6.8	2.3	3.2	3.2	-0.19	0.06	-0.10	0.02	4
DC1-13-Replicate	GFDUH00ND	19.5	16	6.6	7.2	2.4	3.2	3.3	-0.19	0.03	-0.11	0.02	
Clay sized fraction #													
Clay-1	GFDUH00LU	0.4	14	0.05	7.5	1.2	1.9	0.13	0.11	0.07	0.06	0.02	4
Clay-2	GFDUH00HJ	1.0	19	0.06	11	1.7	2.4	0.17	0.09	0.05	0.05	0.02	4
Clay-3	GFDUH00HN	1.8	23	0.08	10	3.2	2.5	0.23	0.09	0.03	0.04	0.03	4
Clay-4	GFDUH00HR	2.4	22	0.08	9.7	3.1	2.5	0.22	0.09	0.04	0.06	0.05	4
Clay-5	GFDUH00HT	2.8	18	0.07	8.6	2.7	2.1	0.17	0.14	0.09	0.09	0.03	4
Clay-6	GFDUH00MB	3.4	20	0.10	9.2	3.3	2.9	0.35	0.08	0.04	0.05	0.03	4
Clay-7	GFDUH00MD	4.4	22	0.11	11	3.7	3.3	0.42					
Seperated minerals $													
Quartz and Feldspar	GFDUH00ND	19.5	17	4.5	1.4	2.0	0.67	4.4	-0.42	0.07	-0.35	0.03	4
Chlorite	GFDUH00ND	19.5	17	5.7	16	1.7	7.8	1.7	-0.13	0.09	-0.50	0.06	4
Hornblende	GFDUH00ND	19.5	18	6.1	12	1.8	5.2	2.8	-0.21	0.05	-0.40	0.02	4
Biotite	GFDUH00ND	19.5	12	0.93	16	4.1	8.1	0.29	-0.08	0.05	-0.38	0.04	4
Reference													
SRM2709a			14	2.8	4.9	2.6	2.4	1.5	-0.12	0.04	-0.08	0.07	4
SRM2709a			13	2.6	4.6	2.4	2.2	1.4	-0.12	0.01	-0.06	0.02	4
SRM2709a			13	2.6	4.6	2.4	2.3	1.5	-0.17	0.04	-0.09	0.04	4
Certified or recommended values ^			**14 ± 0.3**	**2.7 ± 0.1**	**4.8 ± 0.1**	**2.5 ± 0.07**	**2.4 ± 0.03**	**1.6 ± 0.04**	**-0.15**	**0.03**	**-0.08**	**0.02**	
SGR-1			n.d.	n.d.	n.d.	n.d.	n.d.	n.d.	-0.97	0.02	-0.49	0.01	4
SGR-1			n.d.	n.d.	n.d.	n.d.	n.d.	n.d.	-0.98	0.05	-0.49	0.02	4
SGR-1			n.d.	n.d.	n.d.	n.d.	n.d.	n.d.	-0.96	0.02	-0.50	0.05	4
Certified or recommended values ^									**-1.00**	**0.08**	**-0.51**	**0.03**	

† IGSN (International Geo Sample Number). Metadata of samples are available under: www.igsn.org by adding the IGSN after igsn.org, e.g. igsn.org/

* n means replicates of a sample measured by MC-ICP-MS

Clay-sized fraction was separated from bulk regolith using a centrifuge

$ Minerals were seperated from bedrock at 19.5 m depth

^ Recommended values for comparision are from Shalev et al., (2018). doi.org/10.1111/ggr.12208 and Teng, 2017. doi.org/10.2138/rmg.2017.82.7

Table S2-2: Discharge of creek water, major element concentrations and Mg isotopic composition of creek water, subsurface flow, and groundwater samples.

Sample	IGSN†	Sampling Date	Sample type	Discharge#	Major elements (ICP-OES)				Mg isotopes (MC-ICP-MS)				
				l/s	Na µmol/l	Mg µmol/l	K µmol/l	Ca µmol/l	δ^{26}Mg	2SD	δ^{25}Mg	2SD	n*
Open rainfall													
	GFJUB0065	01/02/2016	Open rainfall		N.A	N.A	N.A	N.A	-1.73	0.03	-0.90	0.03	3
Throughfall													
	GFJUB0066	01/02/2016	Throughfall		N.A	N.A	N.A	N.A	-1.92	0.04	-0.97	0.01	2
creek water													
FVA-1	GFJUB0067	11/04/2015	creek water	2.8	113	50	12	117	-0.53	0.04	-0.26	0.01	4
FVA-1-Replicate		12/04/2015	creek water						-0.55	0.10	-0.27	0.07	4
FVA-2	GFJUB0068	15/06/2015	creek water	2.0	87	51	19	136	-0.56	0.07	-0.28	0.05	4
FVA-2-Replicate		16/06/2015	creek water						-0.56	0.04	-0.28	0.03	4
FVA-3	GFJUB0069	15/07/2015	creek water	0.2	134	67	14	186	-0.52	0.03	-0.28	0.04	4
FVA-4	GFJUB006A	17/08/2015	creek water	0.1	130	78	13	211	-0.51	0.06	-0.27	0.05	4
FVA-5	GFJUB006B	15/09/2015	creek water	0.1	129	82	11	222	-0.56	0.12	-0.29	0.06	4
FVA-6	GFJUB006C	15/10/2015	creek water	0.2	127	84	10	226	-0.54	0.10	-0.30	0.04	4
FVA-7	GFJUB006D	15/11/2015	creek water	0.3	129	88	11	242	-0.54	0.03	-0.28	0.03	4
FVA-8	GFJUB006E	21/11/2015	creek water	2.3	102	78	25	189	-0.55	0.05	-0.27	0.06	4
FVA-9	GFJUB006F	17/12/2015	creek water	0.8	119	64	12	174	-0.55	0.06	-0.27	0.01	4
FVA-10	GFJUB006G	01/02/2016	creek water	0.9	103	49	10	123	-0.57	0.05	-0.29	0.03	4
FVA-11	GFJUB006H	15/02/2016	creek water	4.4	99	47	10	116	-0.51	0.08	-0.27	0.03	4
FVA-12	GFJUB006J	25/02/2016	creek water	2.8	100	48	10	119	-0.57	0.05	-0.30	0.04	4
Subsurface flow (0-15 cm)													
SF1-1	GFJUB006K	15/06/2015	Subsurface flow		36	105	276	298	-0.74	0.03	-0.38	0.03	3
SF1-2	GFJUB006L	16/08/2015	Subsurface flow		31	89	256	234	-0.79	0.05	-0.39	0.02	4
SF1-3	GFJUB006M	14/09/2015	Subsurface flow		31	115	206	371	-0.78	0.07	-0.40	0.07	4
SF1-4	GFJUB006N	16/11/2015	Subsurface flow		62	184	295	593	-0.79	0.03	-0.40	0.02	4
SF1-5	GFJUB006P	20/11/2015	Subsurface flow		14	35	145	122	-0.78	0.05	-0.41	0.05	4
SF1-6	GFJUB006Q	01/02/2016	Subsurface flow		26	17	68	56	-0.84	0.10	-0.44	0.07	4
SF1-7	GFJUB006R	25/02/2016	Subsurface flow		21	20	72	70	-0.86	0.03	-0.45	0.05	4
Subsurface flow (15-150 cm)													
SF2-1	GFJUB006S	15/06/2015	Subsurface flow		46	46	68	83	-0.60	0.07	-0.32	0.05	4
SF2-2	GFJUB006T	16/08/2015	Subsurface flow		28	49	101	110	-0.81	0.10	-0.42	0.07	4
SF2-3	GFJUB006U	20/11/2015	Subsurface flow		27	48	71	99	-0.61	0.07	-0.30	0.04	4
SF2-4	GFJUB006V	25/02/2016	Subsurface flow		31	19	39	43	-0.65	0.06	-0.34	0.02	4
Groundwater													
GW-1	GFJUB006W	11/04/2015	Groundwater		127	65	18	222	-0.56	0.06	-0.27	0.03	4
GW-2	GFJUB006X	15/07/2015	Groundwater		136	95	17	451	-0.54	0.06	-0.28	0.04	4
GW-3	GFJUB006Y	15/09/2015	Groundwater		129	93	18	456	-0.56	0.04	-0.30	0.04	4
GW-4	GFJUB006Z	20/11/2015	Groundwater		139	99	21	489	-0.58	0.03	-0.30	0.03	4
GW-5	GFDIC0009	17/12/2015	Groundwater		136	94	18	452	-0.55	0.06	-0.28	0.06	4
GW-6	GFDIC0008	25/02/2016	Groundwater		120	70	15	267	-0.54	0.07	-0.27	0.09	4
Reference													
SLRS-6			Reference		109	89	16	213	-1.23	0.03	-0.64	0.04	4
SLRS-6			Reference		113	92	16	221	-1.20	0.06	-0.63	0.01	4
SLRS-6			Reference						-1.27	0.02	-0.63	0.03	4
Certified or recommended values ^					**120 ± 10**	**89 ± 2**	**17 ± 1**	**219 ± 5**	**-1.22**	**0.06**	**-0.64**	**0.04**	

† IGSN (International Geo Sample Number). Metadata of samples are available under: www.igsn.org by adding the IGSN after igsn.org, e.g. igsn.org/

Discharge data from Sohrt et al., (2019) doi.org/10.3389/ffgc.2019.00085

* n means replicates of a sample measured by MC-ICP-MS

^ Recommended values for comparision are from Shalev et al., (2018). doi.org/10.1111/ggr.12208

Table S2-3: Element concentrations and Mg isotopic composition of plant samples.

		Element concentrations (ICP-OES)								Mg isotopes (MC-ICP-MS)					Description
sample	IGSN†	Al µg/g	Ca µg/g	Fe µg/g	K µg/g	Mg µg/g	Na µg/g	P µg/g	Sr µg/g	δ^{26}Mg	2SD	δ^{25}Mg	2SD	n*	
Leaves															
BF-L-1	GFDIC0006	49	7374	74	9870	1852	30	1628	22	-0.27	0.05	-0.15	0.07	4	Mature beech leaves, 1 m above ground
BF-L-1-Re	GFDIC0006									-0.33	0.09	-0.18	0.04	4	
BF-L-2	GFDIC0007	33	6212	55	7158	1818	16	1422	23	-0.35	0.02	-0.18	0.05	4	Mature beech leaves, 6 m above ground
BF-L-2-Re	GFDIC0007									-0.41	0.05	-0.20	0.05	4	
BF-L-3	GFDIC0005	42	5139	65	9155	1075	24	2504	20	-0.34	0.05	-0.15	0.04	4	Young beech leaves, 2 m above ground
BF-L-4	GFDIC0004	54	7408	72	7439	1319	18	1648	27	-0.27	0.04	-0.11	0.03	4	Young beech leaves, 3 m above ground
BF-L-5	GFDIC0003	228	5154	65	5913	810	78	1253	16	-0.74	0.07	-0.39	0.03	4	Young spruce needles, 4 m above ground
BF-L-5-Re	GFDIC0003	226	5711	53	4676	696	97	923	15	-0.87	0.04	-0.46	0.06	4	
Twigs															
BF-T-1	GFDIC0002	34	5761	25	2095	620	25	677	32	-0.49	0.06	-0.23	0.04	4	Mature beech branches, 1 m above ground
BF-T-2	GFDIC0001	12	1644	12	3152	230	37	814	10	-0.49	0.04	-0.24	0.02	4	Mature beech branches, 6 m above ground
Tree rings															
R-1	GFDUH00NH	12	9717	393	6745	1631	35	199	74	-0.39	0.06	-0.22	0.04	4	Tree ring samples from mature beech
R-2	GFDUH00NH	16	11141	166	12374	1680	63	524	80	-0.41	0.06	-0.21	0.03	4	Tree ring samples from mature beech
R-3	GFDUH00NH	15	14076	492	8786	1842	84	456	96	-0.46	0.05	-0.22	0.03	4	Tree ring samples from mature beech
R-4	GFDUH00NH	14	12549	305	6506	1549	105	456	101	-0.61	0.07	-0.33	0.03	4	Tree ring samples from mature beech
R-5	GFDUH00NH	22	13514	530	9942	1922	116	554	116	-0.55	0.10	-0.29	0.05	4	Tree ring samples from mature beech
Reference															
SRM1515		265	14325	72	12229	2439	26	1479	22	-1.16	0.02	-0.61	0.06	4	
SRM1515		297	13911	68	12308	2360	26	1477	22	-1.22	0.04	-0.62	0.02	4	
SRM1515		322	14971	73	12903	2510	28	1583	24	-1.21	0.13	-0.63	0.06	4	
SRM1515		**285**	**15250**	**83**	**16080**	**2710**	**24.4**	**1593**	**25**	**-1.22**	**0.03**	**-0.62**	**0.03**		Certified or recommended values ^

† IGSN (International Geo Sample Number). Metadata of samples are available under: www.igsn.org by adding the IGSN after igsn.org, e.g. igsn.org/

* n means replicates of a sample measured by MC-ICP-MS

^ Recommended values for comparision are from Shalev et al., (2018). doi.org/10.1111/ggr.12208

Table S4: Element concentrations and Mg isotopic composition of regolith exchangeable fraction.

			Major elments (ICP-OES)					Mg isotopes (MC-ICP-MS)				
Sample	IGSN†	Depth m	Al µg/g	K µg/g	Ca µg/g	Mg µg/g	Na µg/g	δ^{26}Mg	2SD	δ^{25}Mg	2SD	n*
EX1	GFDUH00HE	0.2	54	219	605	125	14	-0.60	0.05	-0.32	0.02	4
EX2	GFDUH00J1	0.4	31	47	120	27	13	-0.52	0.04	-0.25	0.03	4
EX3	GFDUH00J2	0.6	47	32	75	17	14	-0.51	0.04	-0.26	0.05	4
EX4	GFDUH00HH	0.8	47	27	54	8.9	13	-0.62	0.06	-0.33	0.03	4
EX5	GFDUH00HJ	1.0	33	21	33	5.1	11	-0.63	0.06	-0.32	0.04	4
EX5-Re	GFDUH00HJ	1.0						-0.64	0.04	-0.32	0.04	4
EX6	GFDUH00HK	1.2	22	23	28	4.7	11	-0.62	0.04	-0.32	0.04	4
EX7	GFDUH00HL	1.4	16	25	29	7.0	9.2	-0.72	0.08	-0.36	0.05	4
EX8	GFDUH00HM	1.6	16	27	28	7.9	9.0	-0.66	0.09	-0.35	0.03	4
EX9	GFDUH00HN	1.8	9.8	29	57	16	11	-0.56	0.06	-0.30	0.03	4
EX10	GFDUH00HP	2.0	11	29	74	26	12	-0.61	0.03	-0.32	0.01	4
EX11	GFDUH00JA	2.2	4.6	33	109	48	14	-0.56	0.03	-0.30	0.04	4
EX12	GFDUH00HR	2.4	1.6	48	238	97	14	-0.50	0.03	-0.25	0.04	4
EX13	GFDUH00HS	2.6	0.34	55	384	147	15	-0.44	0.07	-0.23	0.05	4
EX14	GFDUH00HT	2.8	0.30	63	600	196	16	-0.41	0.08	-0.20	0.04	4
EX15	GFDUH00M5	2.7	<LOD	78	744	270	19	-0.50	0.03	-0.27	0.03	4
EX16	GFDUH00MB	3.4	<LOD	56	698	239	19	-0.51	0.09	-0.25	0.04	4
EX16-Re	GFDUH00MB	3.4						-0.53	0.08	-0.27	0.03	4
EX17	GFDUH00MC	3.8	<LOD	69	1066	305	19	-0.52	0.18	-0.25	0.11	4
EX18	GFDUH00MD	4.4	<LOD	77	1114	303	20	-0.56	0.09	-0.27	0.05	4
EX19	GFDUH00ME	5.0	<LOD	67	861	304	20	-0.46	0.08	-0.23	0.05	4
EX20	GFDUH00MF	5.7	<LOD	47	684	225	14	-0.50	0.06	-0.26	0.04	4
EX21	GFDUH00MG	6.4	<LOD	69	863	280	18	-0.50	0.11	-0.24	0.05	4
Reference												
SLRS-6								-1.21	0.04	-0.63	0.05	4
SLRS-6								-1.20	0.13	-0.63	0.05	4
Certified or recommended values ^								**-1.22**	**0.06**	**-0.64**	**0.04**	

<LOD: below limit of determination limit

† IGSN (International Geo Sample Number). Metadata of samples are available under: www.igsn.org by adding the IGSN after igsn.org, e.g. igsn.org/

* n means replicates of a sample measured by MC-ICP-MS

^ Recommended values for comparision are from Shalev et al., (2018). doi.org/10.1111/ggr.12208

Table S5: Characteristics of soil for adsorption and desorption experiment

IGSN[†]	Soil type	parent rock	Texture	pH($CaCl_2$)	TC	LOI[#]	CEC[*]	$[Mg]_{ex}$[^]	$\delta^{26}Mg_{ex}$[$]	
					(mg/g)	(wt%)	(mEq/100g)	(µg/g)	(‰)	2sd
GFDIC0000	Dystric Cambisol	paragneiss	27% clay, 33% silt, 40% sand	4.1	149	15	5.3	125	-0.6	0.05

LOI: loss on ignition.

* CEC: cation exchange capacity.

^ [Mg]ex: concentration of exchangeable Mg.

$ $\delta^{26}Mg_{ex}$: Mg isotope composition of the exchangeable fraction.

TC: total carbon.

Table S6: Mg isotope compositions on adsorption and desorption experiments.

Experiment No.	pH	Solution before reaction						Solution after reaction						Exchangeable fraction after reaction*			
		Ca (μg/g)	Mg (μg/g)	δ^{26}Mg (‰)	2SD	δ^{25}Mg (‰)	2SD	Ca (μg/g)	Mg (μg/g)	δ^{26}Mg (‰)	2SD	δ^{26}Mg (‰)	2SD	Mg (μg/g)	δ^{26}Mg (‰)	2SD	$\Delta_{solu-exch}$
Mg desorption experiment on soil																	
S-D-1	6.2	0.00	-	n.d.	n.d.	n.d.	n.d.	6.7	2.5	-0.66	0.03	-0.33	0.01	99	-0.60	0.06	-0.06
S-D-2	6.2	0.52	-	n.d.	n.d.	n.d.	n.d.	7.6	2.3	-0.61	0.12	-0.30	0.05	101	-0.59	0.08	-0.02
S-D-3	6.2	1.1	-	n.d.	n.d.	n.d.	n.d.	7.2	2.3	n.d.	n.d.	n.d.	n.d.	101	n.d.	n.d.	n.d.
S-D-4	6.2	2.2	-	n.d.	n.d.	n.d.	n.d.	8.4	2.6	-0.63	0.10	-0.33	0.04	98	-0.58	0.08	-0.05
S-D-5	6.2	6.3	-	n.d.	n.d.	n.d.	n.d.	10.0	2.9	n.d.	n.d.	n.d.	n.d.	95	n.d.	n.d.	n.d.
S-D-6	6.2	11	-	n.d.	n.d.	n.d.	n.d.	13	3.4	n.d.	n.d.	n.d.	n.d.	90	n.d.	n.d.	n.d.
S-D-7	6.2	22	-	n.d.	n.d.	n.d.	n.d.	17	3.8	-0.63	0.07	-0.32	0.02	86	-0.59	0.08	-0.04
S-D-8	6.2	38	-	n.d.	n.d.	n.d.	n.d.	27	4.8	n.d.	n.d.	n.d.	n.d.	76	n.d.	n.d.	n.d.
S-D-9	6.2	54	-	n.d.	n.d.	n.d.	n.d.	39	5.0	-0.63	0.03	-0.31	0.02	74	-0.59	0.07	-0.04
S-D-10	3.2	0.00	-	n.d.	n.d.	n.d.	n.d.	12	4.0	-0.67	0.01	-0.33	0.05	84	-0.57	0.06	-0.10
S-D-11	3.2	0.70	-	n.d.	n.d.	n.d.	n.d.	13	4.2	-0.66	0.03	-0.34	0.05	82	-0.57	0.07	-0.09
S-D-12	3.2	3.5	-	n.d.	n.d.	n.d.	n.d.	14	4.4	-0.64	0.05	-0.32	0.05	80	-0.58	0.07	-0.06
S-D-13	3.2	9.5	-	n.d.	n.d.	n.d.	n.d.	17	4.5	-0.64	0.04	-0.34	0.02	79	-0.58	0.07	-0.06
S-D-14	3.2	16	-	n.d.	n.d.	n.d.	n.d.	21	4.6	-0.66	0.03	-0.32	0.05	78	-0.56	0.07	-0.10
Mg adsorption experiment on soil																	
S-A-1	6.2	-	0.00	-0.09	0.05	-0.05	0.02	6.7	2.5	-0.66	0.03	-0.33	0.01	99	-0.58	0.06	-0.08
S-A-2	6.2	-	0.60	-0.09	0.05	-0.05	0.02	8.7	2.9	-0.59	0.09	-0.30	0.08	101	-0.57	0.07	-0.01
S-A-3	6.2	-	1.2	-0.09	0.05	-0.05	0.02	8.6	3.0	-0.57	0.04	-0.29	0.05	107	-0.55	0.06	-0.02
S-A-4	6.2	-	3.5	-0.09	0.05	-0.05	0.02	8.6	3.8	-0.53	0.04	-0.27	0.06	121	-0.48	0.06	-0.05
S-A-5	6.2	-	5.8	-0.09	0.05	-0.05	0.02	11	5.1	-0.45	0.09	-0.22	0.06	131	-0.43	0.08	-0.01
S-A-6	6.2	-	12	-0.09	0.05	-0.05	0.02	11	7.6	-0.31	0.14	-0.16	0.08	168	-0.37	0.11	0.05
S-A-7	6.2	-	24	-0.09	0.05	-0.05	0.02	13	14	-0.27	0.15	-0.12	0.10	227	-0.25	0.13	-0.02
S-A-8	6.2	-	38	-0.09	0.05	-0.05	0.02	17	21	-0.23	0.10	-0.11	0.10	288	-0.21	0.11	-0.01
S-A-9	6.2	-	61	-0.09	0.05	-0.05	0.02	18	38	-0.20	0.07	-0.11	0.05	349	-0.15	0.10	-0.05
S-A-10	3.2	-	0.00	-0.09	0.05	-0.05	0.02	12	4.0	-0.67	0.01	-0.33	0.05	84	-0.57	0.06	-0.10
S-A-11	3.2	-	0.64	-0.09	0.05	-0.05	0.02	13	4.4	-0.63	0.04	-0.31	0.01	86	-0.55	0.07	-0.08
S-A-12	3.2	-	3.0	-0.09	0.05	-0.05	0.02	14	6.1	-0.53	0.05	-0.27	0.02	93	-0.48	0.08	-0.05
S-A-13	3.2	-	8.4	-0.09	0.05	-0.05	0.02	17	9.5	-0.39	0.08	-0.20	0.04	113	-0.40	0.10	0.01
S-A-14	3.2	-	19	-0.09	0.05	-0.05	0.02	21	16	-0.27	0.04	-0.14	0.03	154	-0.32	0.08	0.05

n.d=not determined

* Exchangeable concentrations and Mg isootpe compositions after reaction were calculated by following mass balance. Uncertainty was estimated by error propagation.

$$[Mg]^{B}_{ex} \times m_{soil} = [Mg]^{A}_{ex} \times m_{soil} + [Mg]^{A}_{solu} \times m_{solu}$$

$$\delta^{26}Mg^{B}_{ex} \times [Mg]^{B}_{ex} \times m_{soil} = \delta^{26}Mg^{A}_{ex} \times [Mg]^{A}_{ex} \times m_{soil} + \delta^{26}Mg^{A}_{solu} \times [Mg]^{A}_{solu} \times m_{solu}$$

Chapter 3

Identifying pathways for dissolved Li from its isotopic composition during weathering in a temperate forested catchment

Abstract

In a temperate forested headwater catchment (Conventwald, Black Forest, Germany), we have investigated Li isotopic composition (δ^7Li) variation in time-series subsurface flow (0-15 cm depth), groundwater (>8 m) and creek water samples. All water samples (6.5 to 20.4 ‰) are enriched in ^{7}Li compared to bedrock (~ -1.3 ‰) and regolith (~ -1.7 ‰). Both subsurface flow and creek water show seasonal variation in δ^7Li, while groundwater exhibits negligible δ^7Li variation. Li budget estimation shows that atmospheric deposition and biological processes have negligible influence on Li cycling. Viewed in the context of our measurements of bedrock, bulk regolith, clay-sized fraction, vegetation and exchangeable fraction of regolith, we suggest that δ^7Li variation in different water reservoirs indicate different chemical evolution pathways. δ^7Li in shallow subsurface flow (0-15 cm) became more positive with increasing Li concentration, and a binary mixing process could be identified with two endmembers being throughfall and soil solution. Groundwater exhibited negligible δ^7Li variation despite Li concentration and groundwater table fluctuation, which most likely reflects a buffering effect of the deep exchangeable pool. In creek water samples, δ^7Li covaried with proportion of Li remaining in the solution. This fractionation could be attributed to Li incorporation into, or adsorption to, secondary minerals. However, despite the heavy δ^7Li ($\Delta^7Li_{dissolved\text{-}bedrock}$ =16.1 ‰ to 21.5 ‰) exported in dissolved form, saprolite and soil are isotopically almost identical to bedrock. A reservoir enriching in ^{6}Li is missing. This missing reservoir might be fine particles that have been exported in subsurface flow during geological time. In summary, our study has identified three different pathways for dissolved δ^7Li evolution, implying that Critical Zone of different structures and hydrological conditions may see different evolution regimes in riverine δ^7Li.

3.1. Introduction:

Critical Zone science is the study of integrated Earth surface processes at multiple spatial and temporal scales and across natural and anthropogenic gradients. A key consideration of Critical Zone research is mass transfer between different compartments. Isotope tools have been proven powerful tracers quantifying mass fluxes between vegetation, bedrock, soil and water (Bouchez et al., 2013). Among these isotopes, lithium (Li) is mainly hosted in silicate minerals (Kısakűrek et al.,

2005) and thought to be insensitive to biological processes (Lemarchand et al., 2010). As a result, its isotope ratio has been proven as ideal tracer for silicate chemical weathering (e.g. Huh et al., 1998a; Pistiner and Henderson, 2003; Misra and Froelich, 2012; Dellinger et al., 2015).

Since pioneering research now decades ago (Huh et al., 1998), numerous field studies and lab experiments have been carried out on the behaviour of Li isotopes during silicate weathering, which have greatly deepened our understanding of the Li isotope fractionation taking place when water, primary minerals, and secondary solids interact. Generally speaking, during secondary mineral formation or Li adsorption onto oxides or clay mineral surfaces the light isotope ^{6}Li is favoured, relatively enriching the corresponding subsurface- or river water in heavy ^{7}Li. As a consequence, the $^{7}Li/^{6}Li$ ratio in soil or sediment, as the weathering residue, is lower than bedrock while this ratio in fluid is higher.

The fractionation factors associate with these processes have been experimentally quantified in several studies (Vigier et al., 2008; Wimpenny et al., 2010, 2015; Hindshaw et al., 2019; Li and Liu, 2020). These experiments have indicated that the magnitude of fractionation depends on whether Li is incorporated into a structural site ($\Delta^{7}Li_{solid\text{-}solution}$ = -10 ‰ to -21.5 ‰; Vigier et al., 2008; Hindshaw et al., 2019) or adsorbed onto exchangeable sites ($\Delta^{7}Li_{solid\text{-}solution}$= -36 ‰ to ~ 0 ‰; Pistiner and Henderson, 2003; Wimpenny et al., 2015; Li and Liu, 2020). The highly variable $\delta^{7}Li$ fractionation factors during adsorption results from different complexation mechanisms, with outer-sphere complexation inducing little fractionation and inner-sphere inducing larger fractionation. The global $\delta^{7}Li$ difference between dissolved Li in large rivers (23 ‰, flux weighted, Huh et al., 1998) and average continental crust (0 ± 2 ‰, Teng et al., 2004) is 23.9 ± 3.1 ‰ ($\Delta^{7}Li_{river\text{-}continent}$, 1σ error). This value is consistent with the experimentally determined Li fractionation factor during Li incorporation into octahedral sites (-21.5 ± 1.1 ‰, Hindshaw et al., 2019), suggesting that to a first order, Li incorporation into the octahedral site might dominate fractionation at a global scale (Hindshaw et al., 2019). However, it was also suggested that kinetic adsorption process with fractionation factor $\alpha \sim 0.992$ could explain field observation in the worldwide rivers (Li and Liu, 2020).

Given that $^{7}Li/^{6}Li$ is so sensitive to the processes that incorporate Li into solids, the system is a powerful tracer to explore the geological and hydrologic processes and settings of the Critical Zone, and thus the weathering regime (Huh et al., 1998, 2001; Kısakűrek et al., 2005; Vigier et al., 2009; Huh et al. 2001, Pogge von Strandmann and Henderson 2015;Wanner et al., 2014; Liu et al., 2015). Since the Li uptake flux by plants is insignificant as compared to weathering (Lemarchand et al., 2010), from a mass balance perspective, it is now widely accepted that the riverine $\delta^{7}Li$ is mainly determined by the fraction of Li incorporated into secondary solids relative to the flux of Li dissolved from primary minerals (e.g. Millot et al., 2010; Lemarchand et al., 2010; Pogge von Strandmann et al., 2012). Using a steady state mass balance

model, Bouchez et al. (2013) inferred that "congruent weathering" of Li (minor or negligible Li isotope fractionation of dissolved Li relative to bedrock) should be observed in two endmember scenarios: 1) very low denudation rate settings where both primary and secondary minerals are dissolved, or 2) very high denudation rate settings where secondary phases that can incorporate Li are not formed in sufficient amounts to impact the dissolved Li efflux. The largest Li isotope fractionations seen within a catchment should therefore take place at intermediate denudation rates. This conceptual framework has since been shown to be consistent with observations of dissolved δ^7Li in large catchments such as the Amazon (Dellinger et al., 2015).

Within a catchment, a large variation in δ^7Li in time series water samples was observed (e.g. Henchiri et al., 2016; Liu et al., 2015), suggesting hydrological control on Li fractionation, in addition to lithological and tectonic forces. One way to explain this is that heavy rainfall might alter flow paths and thus change the Li sources. Study has shown that soil solutions from different compartments of a single regolith profile exhibited different Li fractionation regimes (Golla et al., 2021). Therefore, in responds to hydrological condition variation, changing Li sources would result in variation in δ^7Li in outlet runoff (Lemarchand et al., 2010; Henchiri et al., 2016; Fries et al., 2019). Residence time of water and temperature variation are also suggested as other factors controlling δ^7Li fractionation in a specific catchment (Liu et al., 2015; Gou et al., 2019). To further interrogate the role of water flow for Li isotope fractionation, we conducted a detailed study in a small, mono-lithological catchment (Conventwald, the Black Forest, Germany). We collected time-series creek water samples, time-series subsurface flow (0-15 cm depth), and groundwater samples to trace δ^7Li in dissolved Li through time. Seasonal patterns in these samples were investigated, along with measurements of bedrock, vegetation, bulk regolith, clay-sized fraction, and the exchangeable fraction of regolith. Our measurements reveal diverse patterns of variation in each compartment: although water samples are all enriched in ^{7}Li compared to bedrock, time series of subsurface flow, groundwater and creek water show strongly divergent patterns. We evaluate the diverse causal drivers for these disparate δ^7Li trends in different compartments, adding another example (see also e.g. Golla et al. 2021) that any Critical Zone site can comprise multiple distinct 'reactors' – often with very different fractionation regimes – that contribute very differently to the integrated catchment-scale dissolved Li budget.

3.2. Field setting

Samples were collected from an instrumented forest site "Conventwald" (48°02′0N, 7°96′0E), located in the Black Forest, southern Germany (see Uhlig and von Blanckenburg, 2019; Uhlig et al., 2020). This observatory is operated as part of the long-term forest ecosystem monitoring program "International Co-operative Program on assessment and monitoring of air pollution effects on forests (ICP Forest Level II)" and represents also one of the study sites of the DFG priority program SPP 1685 "Ecosystem Nutrition—Forest Strategies for limited Phosphorus

Resources". The monitored creek catchment has an area of 0.077 km² and the average elevation is ~840 m a.s.l.. Mean annual temperature at the study site is 6.8 ˚C, and mean annual precipitation is 1395 mm/a. The underlying bedrock is paragneiss, which was developed from metamorphosed sedimentary rock in the Precambrian. Weathered bedrock was found at ~7 m depth and unweathered bedrock was encountered at ~16 m depth during a core-drilling campaign at the site (Uhlig and von Blanckenburg,2019). The soil type is a hyperdystric skeletic folic Cambisol with a loamy or sandy loamy texture and a mor-type moder forest floor atop. A detailed description is provided by Lang et al. (2017). Although the study site was not glaciated during the Quaternary, periglacial slope deposits developed during the last glacial maximum. The uppermost metre of soil had a rock fragment content of ~70%. The vegetation is mainly composed of European beech (*Fagus sylvatica*, ~40%) and Norway spruce (*Picea abies*, ~45%).

3.3. Methods

3.3.1. Sampling

The sampling strategy was presented in detail by Uhlig and von Blanckenburg (2019) for regolith samples and Sohrt et al. (2019) for water samples. Briefly, shallow regolith was sampled at depth increments of 20 cm in a 3 m deep trench. Deeper regolith beyond 3 m was retrieved using diesel-powered wireline core-drilling to ~20 m. Time series water samples were collected from 01.03.2015 to 25.02.2016. Open rainfall and throughfall were collected bi-weekly in bulk containers coved by a netting mesh. Creek discharge was collected daily at midnight by an autosampler. Groundwater was sampled daily in the well installed after drilling by an autosampler. The groundwater table level was monitored by a pressure probe installed 8.5 m below the surface. Subsurface water from subsurface flow collectors installed at various depths in soil and subsoil (see Bachmain and Weiler 2012) was collected at three depths intervals: 0-15 cm, 15-150 cm, and 150-320 cm. Due to limited availability of water samples from 15-150cm and 150-320 cm, we only analyzed the 0-15 cm subsurface flow samples in this study. All the water samples were acidified and stored at 4 ˚C before analysis. Living wood, beech leaves and spruce needles were collected from representative mature and young trees, and then oven dried before chemical treatment.

3.3.2. Extraction of the exchangeable fraction, separation of clay-sized fraction, and separation of primary minerals

Soil and saprolite samples were first oven-dried and sieved to < 2 mm. 2 g of the selected samples were accurately weighed and added to 15 ml acid-cleaned polypropylene centrifuge tubes pre-filled with 14 ml of a 1 M NH_4OAc solution. Samples were agitated, and the resulting suspensions shaken on a hotdog roller at 60 rpm for 3 hours. After reaction, the suspensions were centrifuged at 4200 rpm for 30 min, before the supernatant was pipetted off into a syringe and filtered through a 0.2 μm acetate filter. Solutions were then split into two separate aliquots

for major element concentration and Li isotope analysis. Afterwards, the NH_4OAc-extracted soil and saprolite samples were rinsed twice by Milli-Q water. The clay-sized fractions of these samples were then separated by centrifugation following the USGS method (Poppe et al., 2001). To evaluate the Li isotopic composition of minerals in bedrock, bedrock was first crushed and then sieved to 125 μm - 1 mm. The felsic minerals (mainly quartz and feldspar) were first removed using a magnet separator. Hornblende, chlorite, and biotite were hand-picked under a microscope. Chlorite and biotite grains, formed from metamorphosed hornblende, generally contained trace relicts of hornblende.

3.3.3. Analytical methods

All measurements were performed in the Helmholtz Laboratory for the Geochemistry of the Earth Surface (HELGES) at GFZ Potsdam. Soil, saprolite, the extracted clay-sized fraction, primary minerals, and bedrock were dissolved by acid digestion using a mixture of concentrated HF and HNO_3 in PFA vials. Aqua regia was also applied to assist digestion after HF and HNO_3 treatment. Li concentrations of the filtered supernatant, water samples, and acid digested solution were analyzed by measured by iCap Q-ICP-MS (Thermo Fisher). The precision and accuracy of resulting concentrations were evaluated by replicate analyses of reference materials. Uncertainties are close to 5 % for most samples. For plant samples and water samples having low Li concentration (<1 ppb), uncertainties are generally higher (~10 %) based on external reproductivity. For Li isotope measurements, the digested solutions were dried and taken up in 0.2 M HCl for cation exchange chromatography. 3.0 mL of Bio-Rad AG 50W X12 (200-400 mesh) was loaded in BRAND 50 ml pipette PP columns (I.D. 6.4 mm, resin height 9.32 cm in MQ-H_2O). The matrix was eluted with 26 ml 0.2 M HCl and Li was collected in 23.5 ml 0.2 M HCl. The purified Li fractions were evaporated to dryness and taken up in 1 mL of 0.3 M HNO_3. Purity and quantitative Li yield was assessed by Q-ICP-MS, with Li yield better than 98%.

Lithium isotope ratios were measured on an MC-ICP-MS (Thermo Fisher Scientific Neptune Plus) equipped with a Jet Interface (Jet sample and X skimmer cones). Sample solutions were nebulized into an ESI Apex desolvating sample introduction system. Instrumental mass bias was corrected using the sample-standard bracketing technique, against LSVEC lithium carbonate (Qi et al., 1997). An individual measurement consisted of 10 cycles of 4.2 s integration time, with ^{7}Li and ^{6}Li signals detected simultaneously in Faraday cups L4 and H4, equipped with 10^{11} Ω amplifiers. Prior to analysis the Li concentration in the sample solutions were adjusted to match the bracketing standard solution at 20 ng/mL in 0.2 M HNO_3. Samples were measured two to four times during each session. For extracted exchangeable fractions and some water samples where Li content is low, sample solutions and bracketing standard solutions were adjust to ~2 ng/ml in 0.2M HNO_3 for isotope measurement. Internal precisions for these low Li samples (better than 1 ‰) are generally worse than high Li samples (better than 0.5 ‰). Background

signals (<20 mv) were monitored with 0.2 M HNO_3 and subtracted from sample signal intensities. Reference materials LSVEC and in house Li_2CO_3, $LiNO_3$ are used to gauge intermediate reproductivity and SLRS-6 (river water, 24.0 ± 0.3 ‰), OSIL (seawater, 30.9 ± 1.5 ‰), SRM2709a (soil, -0.2 ± 0.1 ‰), BHVO-2 (basalt, 4.9 ± 0.7 ‰) were routinely monitored to gauge external reproducibility (see Tables S3-1to S3-4).

3.4. Results

3.4.1. Li mass loss and δ^7Li in solids and the exchangeable fraction

Results of [Li] and δ^7Li analysis in regolith solids are given in Table S3-1. τ^{Li} (calculated as $\frac{Li_{sample}/Zr_{sample}}{Li_{bedrock}/Zr_{bedrock}} - 1$) suggests ~50 % of Li loss in the saprolite and soil (Fig. 3-1). Paragneiss bedrock yielded δ^7Li of ~-1.3 ‰. Of the separated minerals amphibole (-1.3 ‰) and chlorite (-1.4 ‰) are isotopically similar to bulk bedrock, whereas biotite (-0.7 ‰) and felsic minerals (-0.1 ‰) are slightly heavier than bulk bedrock. δ^7Li shows negligible variation throughout the regolith, with values being almost indistinguishable from bedrock δ^7Li. The clay-sized fraction is relatively enriched in lighter Li isotopes, with δ^7Li ranging from (-3.5 to -5.4 ‰). [Li] and δ^7Li measurements from the exchangeable Li extracted with NH_4OAc are given in Table S3-4 and show systematic variations in terms of both Li concentration and δ^7Li. The highest δ^7Li (22.5 ‰) is found in the topsoil. δ^7Li gradually decreases from the surface to ~ 1.8 m depth (2.5 ‰), followed by a shift towards heavier δ^7Li at 2.5 m depth (12 ‰). Below ~2.5 m, δ^7Li remains largely invariant (~10 ‰).

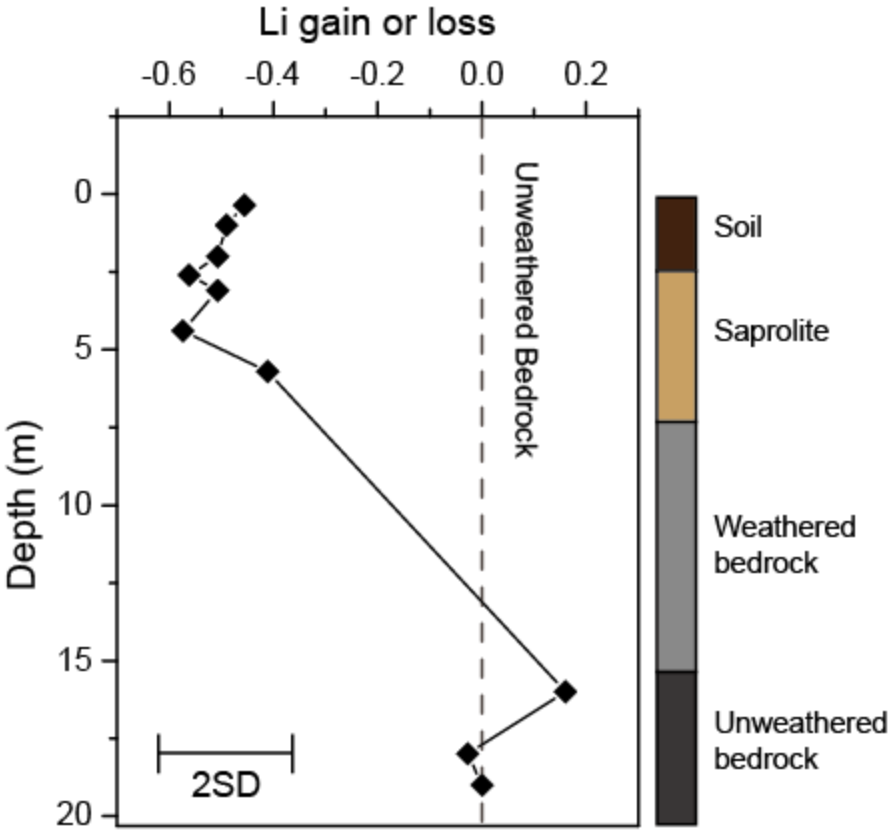

Fig. 3-1 Li gain or loss (τ^{Li}) of the weathering regolith. Error bar (24%, two standard deviation) from propagation of external analytical uncertainty (±9% for Zr (Uhlig and von Blanckenburg 2019) and ±5% for Li concentration measurement).

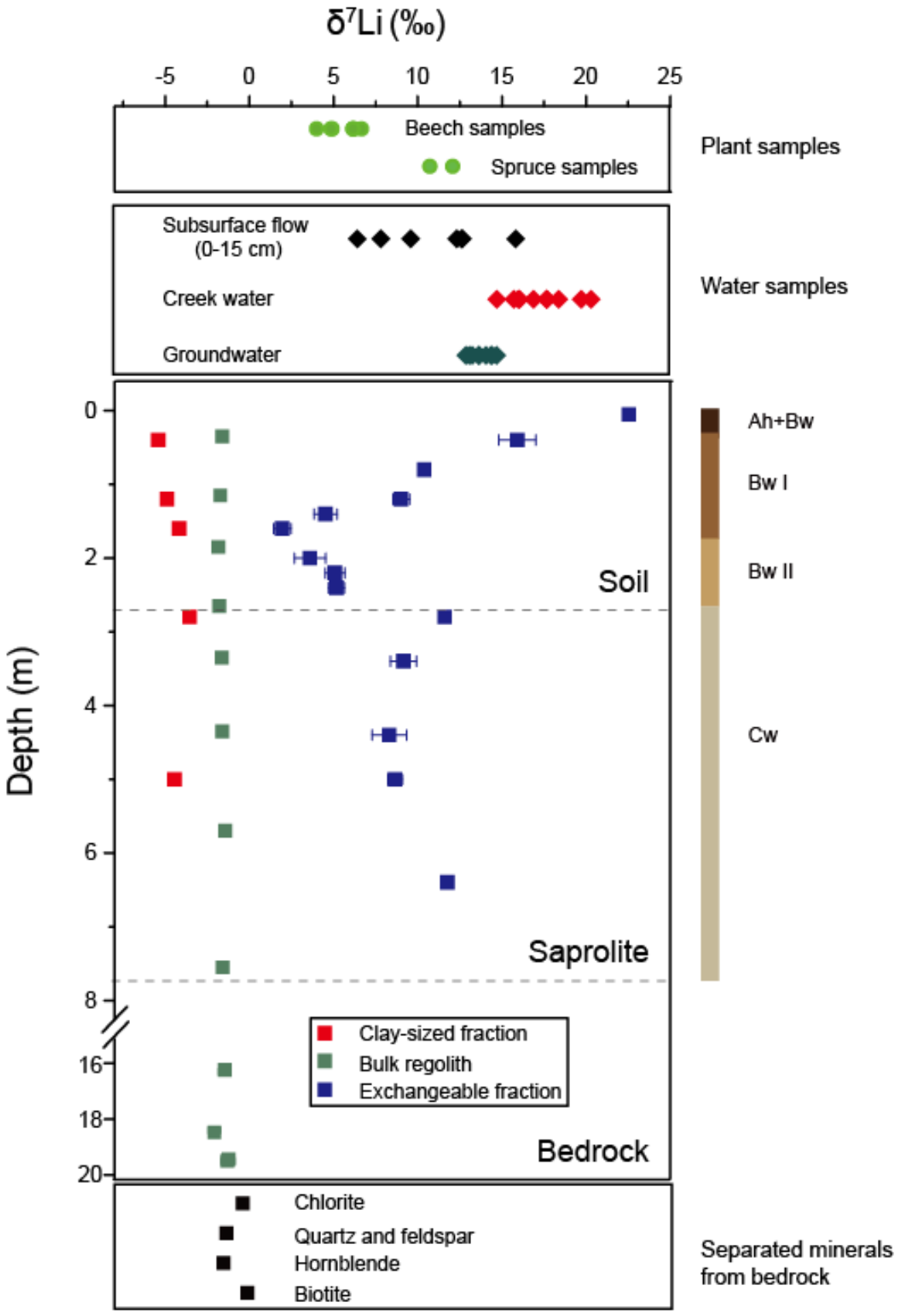
δ7Li (‰)
-5
0
5
10
15
20
25
Beech samples
Spruce samples
Plant samples
Subsurface flow
(0-15 cm)
Creek water
Groundwater
Water samples
Depth (m)
0
2
4
6
8
16
18
20
Soil
Saprolite
Bedrock
Clay-sized fraction
Bulk regolith
Exchangeable fraction
Ah+Bw
Bw I
Bw II
Cw
Chlorite
Quartz and feldspar
Hornblende
Biotite
Separated minerals
from bedrock

Fig. 3-2 δ^7Li of all components measured in this study. Uncertainty shown for the exchangeable fraction represents two standard deviations of 3 replicate measurements. The uncertainty of the other samples is smaller than the symbol size. External precision for reference material is reported in Table S3-1 to S3-4 and section 3.3.3. Ah, Bw, Cw: Soil horizons according to IUSS/ISRIC/FAO 2006.

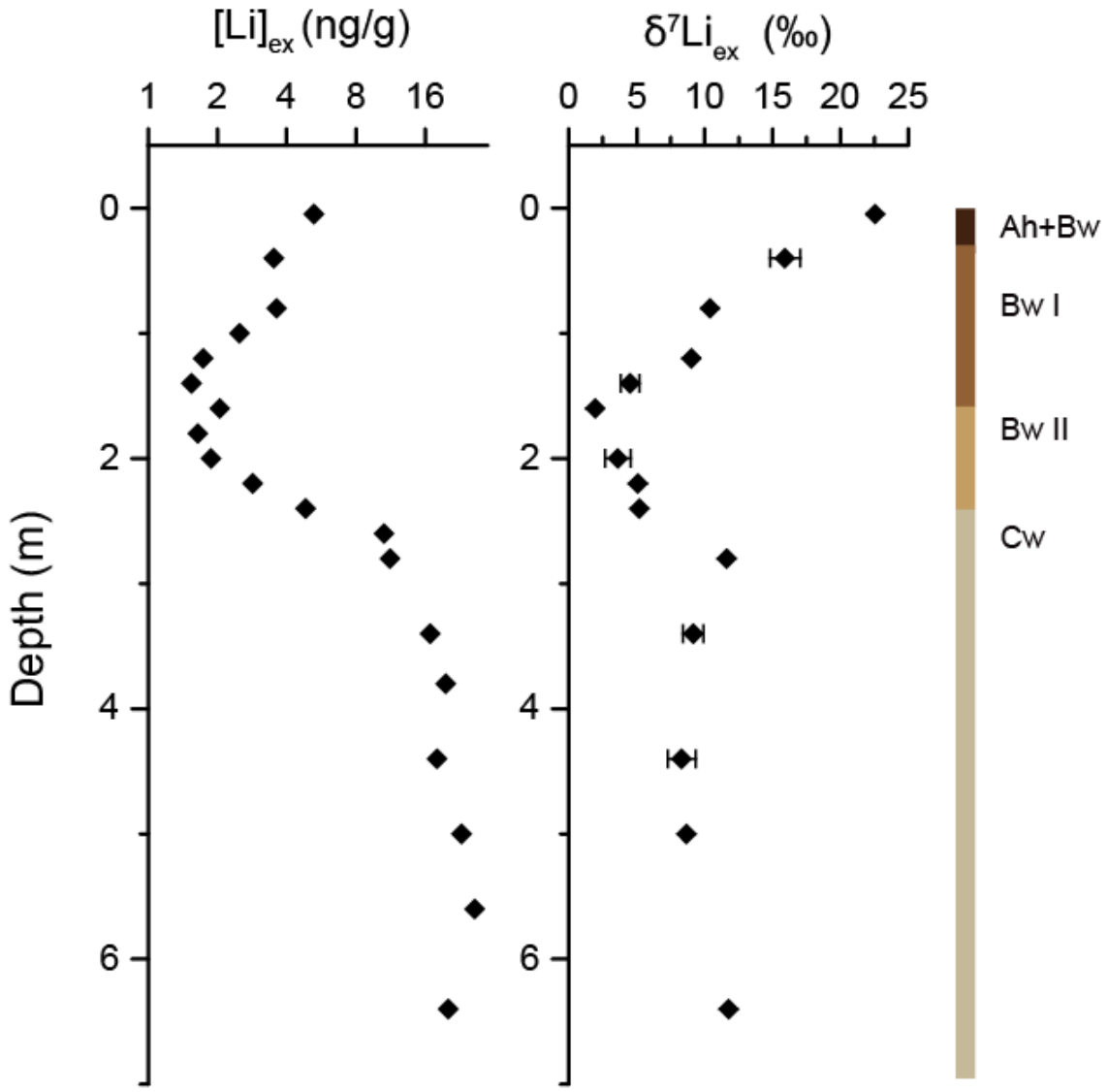

Fig. 3-3 Li concentration ($[Li]_{ex}$), and isotopic composition (δ^7Li_{ex}) of the regolith exchangeable fraction (extracted by 1 N NH_4OAc). Uncertainty shown for the exchangeable fraction represents two standard deviations of 3 replicate

measurements. Analytical uncertainty for Li concentration measurement is better than 5 % based on repeat measurement of reference materials.

3.4.2. Li concentration and δ^7Li of time series water samples

Water from throughfall is very diluted in [Li] (6.7 nmol/l) that has δ^7Li of 8.4 ‰. This isotopic composition might indicate the interaction of rain containing Li from sea spray (~31 ‰) with Saharan dust (δ^7Li = -0.7 ‰, Clergue et al., 2015). [Li] of subsurface flow (0-15 cm) ranges from 18.2 to 152.9 nmol/l. δ^7Li of subsurface flow (15 cm) shows the largest variation, ranging from 6.5 to 15.9 ‰. [Li] of groundwater is much higher on average than subsurface flow samples, ranging from 180.2 to 330.9 nmol/l. Although there is considerable variability in the [Li] of groundwater, its isotopic composition remains almost invariant (13.9 ± 1.22 ‰, n = 9) throughout a hydrological year. [Li] of creek water is similar to groundwater, ranging from 157.2 to 241.7 nmol/l, while its δ^7Li is similar to or heavier than groundwater, ranging from 14.8 to 20.4 ‰.

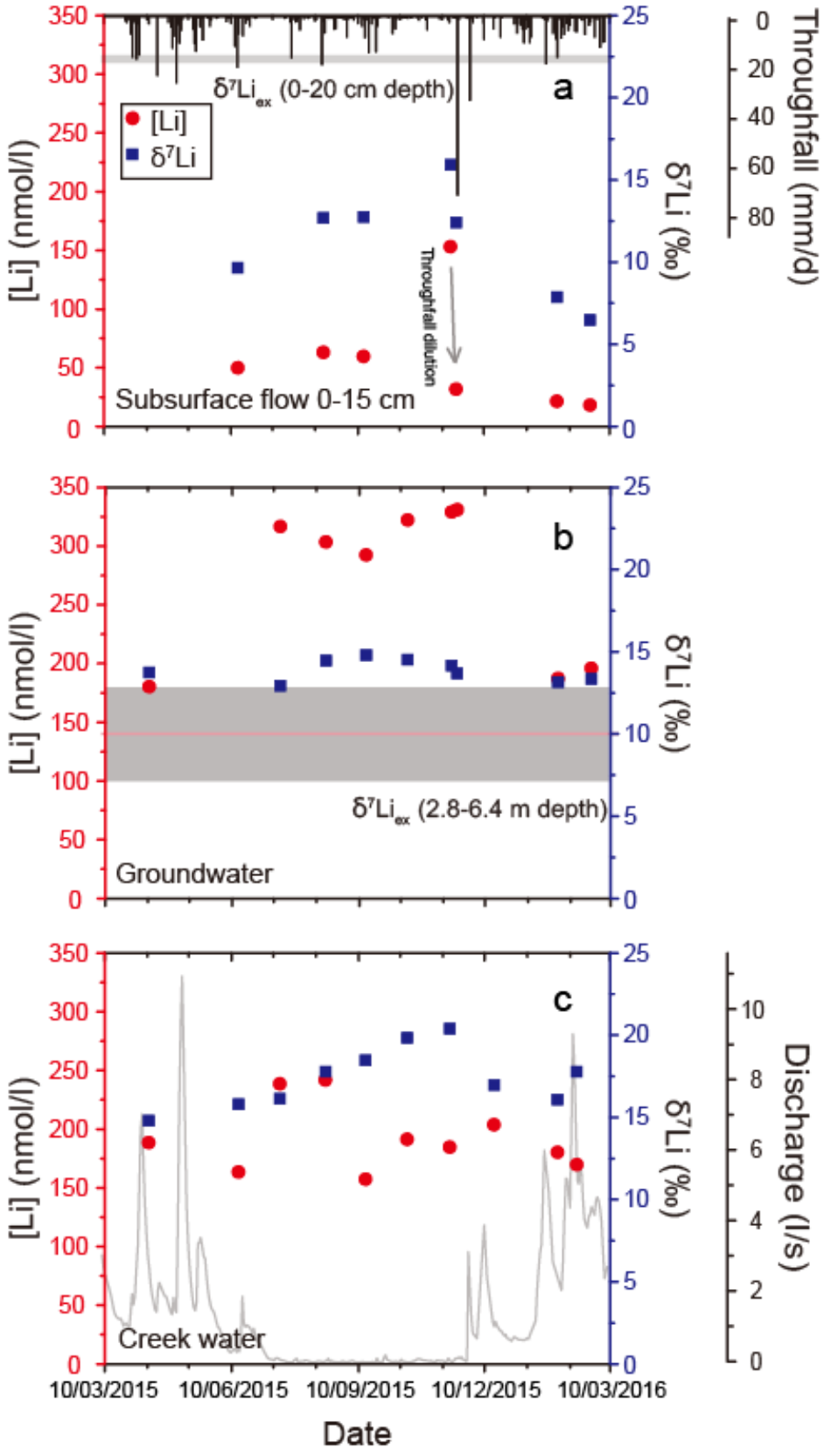
a
b
c
[Li] (nmol/l)
δ7Li (‰)
Throughfall (mm/d)
Discharge (l/s)
δ7Li_ex (0-20 cm depth)
[Li]
δ7Li
Throughfall dilution
Subsurface flow 0-15 cm
δ7Li_ex (2.8-6.4 m depth)
Groundwater
Creek water
10/03/2015
10/06/2015
10/09/2015
10/12/2015
10/03/2016
Date

Fig. 3-4 Li concentration ([Li]) and Li isotope composition (δ^7Li) of time-series water samples. Throughfall and creek water discharge are also shown in the background of panel a and c. δ^7Li measurement uncertainties (estimated as 2s.d. of replicate measurements) are smaller than the symbol size. Horizonal grey bars of panel a and b shows the δ^7Li of regolith exchangeable fraction at corresponding depth.

3.4.3. δ^7Li of plant samples

Beech leaves and twig samples have Li concentrations ranging from 2 to 7 ng/g, and show similar δ^7Li (5.5 ± 1.9 ‰, n = 6). Spruce needles have both higher Li concentration (~ 20 ng/g) and δ^7Li (average of 11.4 ‰, n = 2) than beech samples (Fig. 3-2, 3-5).

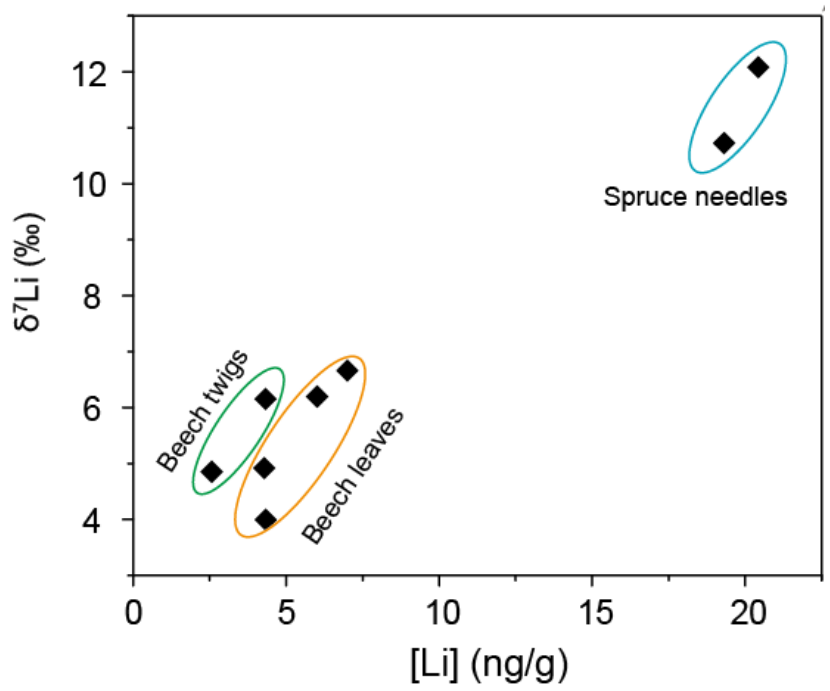

Fig. 3-5 Li concentration and isotope composition of plant samples. δ^7Li measurements uncertainties (estimated as 2s.d. of replicate measurements) are smaller than the symbol size.

3.5. Discussion

3.5.1. Negligible impact of plant activity and atmospheric deposition on Li budget of the catchment

We first present an evaluation of the influence of wet precipitation and plant uptake on the catchment's Li budget. Table 3-1 shows the glossary of metrics and equations used for calculation of metrics in this study. Fig. 3-6 shows the estimated budget of all Critical Zone processes involving a transfer of Li. The annual Li wet deposition budget was calculated by multiplying the annual precipitation flux with the Li concentration in the open rainfall. The chemical weathering flux is deduced from the denudation rate (Uhlig and von Blanckenburg, 2019) and Li depletion (τ^{Li}, Fig. 1), and is ~ 460 times higher than wet deposition. Thus, we suggest that the contribution of wet deposition to the runoff of Li at this site is negligible.

Table 3-1 Glossary of metrics in this study.

Name	Description	Calculation		Interpretation
Li inventories (in g m^{-2})				
I_{bulk}^{Li}	Inventory of bulk Li of regolith	$I_{bulk}^{Li} = \int_0^Z [Li_{bulk}]_z \times \rho d_z$	(3.1)	Z is the depth of the weathering profile and ρ is the density of bulk regolith. $[Li_{bulk}]_z$ is the Li concentration of bulk regolith at depth z.
I_{ex}^{Li}	Inventory of exchangeable Li of regolith	$I_{ex}^{Li} = \int_0^Z [Li_{ex}]_z \times \rho d_z$	(3.2)	Calculated the same way as I_{bulk}^{Li} , the only difference is using Li concentration of exchangeable fraction rather than that of bulk regolith.
Li fluxes (in g m^{-2} yr^{-1})				
D	Denudation rate			Denudation rate is estimated from cosmogenic nuclides (Uhlig and von Blanckenburg, 2019).
D^{Li}	Denudation rate of Li	$D^{Li} = D \times [Li]_{Bedrock}$	(3.3)	$[Li]_{Bedrock}$ means Li concentration in the bedrock.
RP^{Li}	Regolith production rate of Li	$\mathrm{RP}^{Li} = D^{Li}$	(3.4)	In steady state, regolith production rate is the same as denudation rate.
$W_{Regolith}^{Li}$	Regolith weathering rate of Li	$W_{Regolith}^{Li} = D \times [\mathrm{Li}]_{Bedrock} \times (-\tau^{Li})$	(3.5)	Net solubilisation flux of Li from regolith. See for calculation of $-\tau^{Li}$.
$E_{Regolith}^{Li}$	Regolith erosion Rate of Li	$E_{Regolith}^{Li} = D \times [\mathrm{Li}]_{Bedrock} \times (1 + \tau^{Li})$	(3.6)	Erosion flux of Li from regolith. $E_{Regolith}^{Li} + W_{Regolith}^{Li} = D^{Li}$
U^{Li}	Plant uptake rate of Li	$U^{Li} = \frac{NPP \times [\mathrm{Li}]_{tree}}{[C]_{tree}}$	(3.7)	Where $[C]_{tree}$ denotes carbon concentration in dry mass (~50%). NPP means net primary productivity, which is approximately half of GPP (gross primary production)
Dep_{wet}^{Li}	Wet deposition of Li	$Dep_{wet}^{Li} = [Li]_{precipitation} \times F_{precipitation}$	(3.8)	$F_{precipitation}$denotes annual flux of precipitation and $[Li]_{precipitation}$ means Li concentration in precipitation.
Li mass fractions and flux ratios (dimensionless)				
τ^{Li}	Elemental mass transfer coefficient	$\tau^{Li} = \frac{[Li]_{Regolith}}{[Zr]_{Regolith}} \times \frac{[Zr]_{Bedrock}}{[Li]_{Bedrock}} - 1$	(3.9)	Fractional mass loss or gain of an element relative to bedrock.
DEE^{Li}	Dissolved export efficiency of Li	$DEE^{Li} = \frac{W_{River}^{Li}}{W_{Regolith}^{Li}}$	(3.10)	Ratio of flux of Li found in dissolved river export (W_{River}^{Li}) relative to the flux released by weathering in regolith ($W_{Regolith}^{Li}$).

DEE_{Na}^{Li}	Na-Normalised dissolved export efficiency of Li	$DEE_{Na}^{Li} = \frac{W_{river}^{Li}/W_{river}^{Na}}{W_{regolith}^{Li}/W_{regolith}^{Na}} = \frac{(\frac{[Li]}{[Na]})_{river}/(\frac{[Li]}{[Na]})_{bedrock}}{\tau_{Zr}^{Li}/\tau_{Zr}^{Na}}$	(3.11)	Ratio is normalised by the conservative element Na so that the ratio is independent of rate estimates.

The biological influence on the Li budget of a catchment is generally thought be minor , as Li is regarded to be a non -essential element for plants and its concentration in plant tissues is low (Lemarchand et al., 2010; Clergue et al., 2015). At Coventwald, we estimate the plant uptake flux of Li by multiplying the local biomass growth rate of 1260 ± 60 g m^{-2} yr^{-1} (from global GPP data from Uhlig and von Blanckenburg 2019; and assuming NPP is about 50% of GPP (Chapin et al ., 2012) and that carbon amounts to 50% of biomass) with the average Li concentrations in plants (Table S3-3). We note that this represents only a rough estimate as we use the Li concentration in leaves to represent the bulk tree, in conjunction with a coarse-resolution GPP model. Regardless, the calculated plant uptake flux amounts to only 1 % of the chemical weathering flux, which confirms its likely negligible influence on the catchment Li budget.

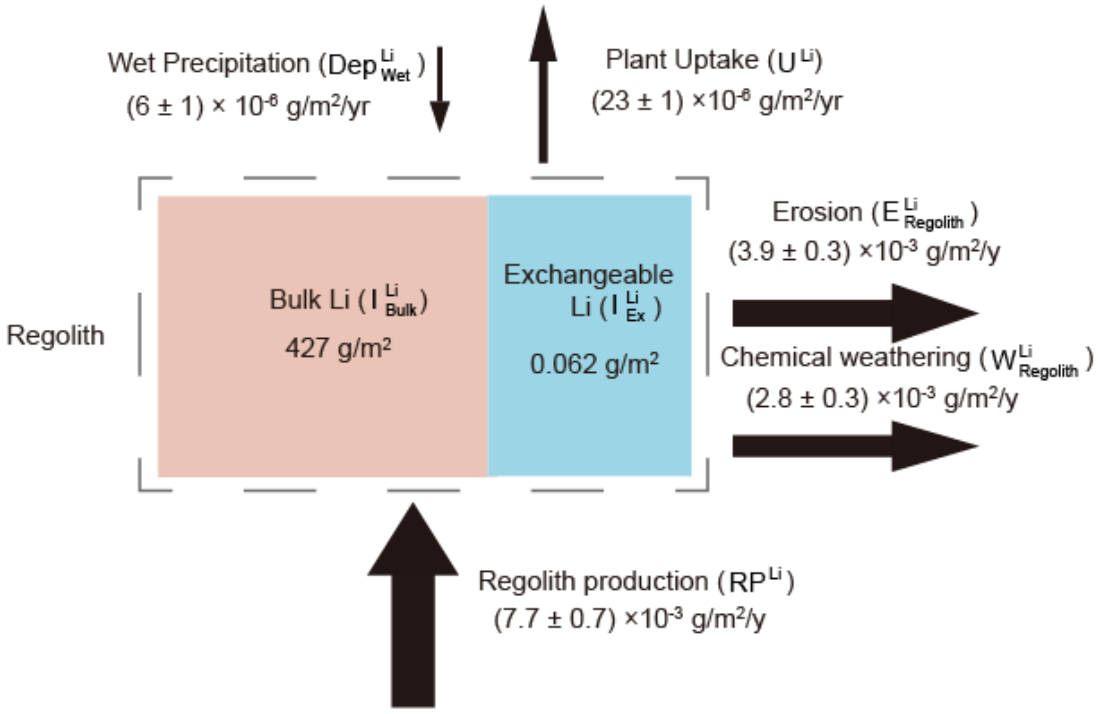

Fig. 3-6 Estimated inventory and fluxes for Li at the Conventwald site.

3.5.2. Li isotope fractionation during plant uptake

A challenge of evaluating δ^7Li fractionation during uptake in the field is to identify the δ^7Li of the nutrient source. Lemarchand et al., (2010) and Clergue et al., (2015) suggest that little isotope fractionation occurs during plant uptake by comparing

plant δ^7Li to soil solution δ^7Li. However, Li et al., (2020) found heterogenous δ^7Li of different plant tissues, and isotope fractionation during Li translocation was inferred. In this study, beech leaves and spruce needles exhibit different Li isotopic compositions. Using isotope proxies $^{87}Sr/^{86}Sr$ and $^{10}Be(meteoric)/^{9}Be$, Uhlig et al., (2020) identified that plants started to uptake nutrient from ~3 m depth in this research area. Spruce needles show similar δ^7Li to that of deep (>3 m) exchangeable pool (Fig. 3-2), indicating negligible isotope fractionation if this exchangeable fraction is the source. However, beech leaves and branches exhibit more negative δ^7Li. One explanation for the discrepancy is that beech trees may uptake nutrient from shallower depth. Exchangeable Li from 1.5 m to 2.5 m depth has similar δ^7Li to beech tissues δ^7Li. Little isotope fractionation could be inferred if beech uptake nutrient from this depth interval. However, as our sampling strategy did not cover the whole tree tissues, we could not exclude the possibility that δ^7Li was fractionated during translocation within beech tree, as proposed by Li et al., (2020).

3.5.3. Li isotopic fractionation during weathering and clay formation

Although ~50 % of Li contained in parent rock was lost by weathering at a depth from 0 to 6 m (Fig. 3-1), the regolith shows negligible Li isotopic fractionation relative to parent rock (Fig. 3-2). Although regolith with invariant δ^7Li at different depths has previously been reported (e.g. Lemarchand et al., 2010; Ryu et al., 2014), this finding is nonetheless surprising, not least since water samples at this site are significantly enriched in ^{7}Li. We investigated whether the increase in $^7Li/^6$Li in water is due to preferential dissolution of minerals that differ in δ^7Li, since XRD analysis (Uhlig and von Blanckenburg, 2019) and Mg isotope measurements on these same samples (Cai et al., in review) has revealed the preferential dissolution of horenblende in the regolith. However, we find Li isotopic compositions are relatively homogenous in different primary minerals (Fig. 3-2), and so preferential dissolution should not induce a shift in isotope ratios. Instead, it is likely that secondary mineral formation is key in driving the observed patterns. The clay-sized fraction separated from bulk soil and saprolite exhibits higher Li concentrations and more negative δ_7Li than the bulk regolith (Table S3-1, Fig. 3-2). This observation is compatible with the formation of secondary minerals that preferentially incorporate $_6$Li. The fraction of Li-bearing secondary minerals could be approximated via mass balance:

$$\delta^7 Li_{soil} = (1 - f^{Li}_{secondary}) \times \delta^7 Li_{bedrock} + f^{Li}_{secondary} \times \delta^7 Li_{secondary} \qquad (3.12)$$

where $\delta^7 Li_{bedrock}$ represent the mean δ^7Li value of bedrock (-1.3 ‰), $\delta^7 Li_{secondary}$ is the most positive δ^7Li value of our separated clay-sized fraction (-5.4 ‰), and $f^{Li}_{secondary}$ is the relative proportion of neoformed secondary minerals. As $\delta^7 Li_{soil}$ is almost identical to $\delta^7 Li_{bedrock}$, calculated $f_{secondary}$ is only ~9 %. This is a maximum estimation as we use the most positive δ^7Li value of our separated clay-sized fraction and true secondary mineral is expected to have more

negative δ^7Li than the clay-size fraction (which may still contain some component of primary Li).

3.5.4. Isotope fractionation between exchangeable Li and dissolved Li

The weakly-bound exchangeable fraction of regolith is sometimes regarded as an alternative record of the chemistry of soil solution (e.g. Bullen and Chadwick., 2016; Li and Liu, 2020). However, investigation into exchangeable Li and its isotopic composition in the Critical Zone are sparse, and whether dissolved δ^7Li could be reconstituted by corresponding exchangeable δ^7Li remains unknown yet. Our previous Mg isotope study on the same batch of samples (Cai et al., in review) has indicated that there is negligible isotopic fractionation during Mg exchange, and that the Mg isotopic composition of groundwater and creek water have almost identical Mg isotopic composition to deep regolith exchangeable pool. However, studies on Li adsorption onto different geological matrices have shown highly variable fractionation factors. Although the NH_4OAc (or other such extraction reagents used in other studies) extracted fraction is called "exchangeable", Hindshaw et al., (2019) indicated that this fraction may also contain loosely bound Li from different coordination environments, and that these may be associated with different fractionation factors (-0.2 ± 1.9 ‰ and 15.0 ± 13.2 ‰ for outer-sphere and pseudo-hexagonal sites respectively, in the case of saponite). In addition, Li adsorption experiments using different minerals as adsorbent have also shown contrasting magnitude of fractionation, with $\Delta^7Li_{adsorbed\text{-}solution}$ ranging from ~ 0 ‰ to -36 ‰ (Pistiner and Henderson, 2003; Hindshaw et al., 2019; Pogge von Strandmann et al., 2019; Li and Liu, 2020). Further study is required to better understand mechanisms of Li adsorption and δ^7Li fractionation during exchange processes. Here, to evaluate whether the exchangeable fraction could serve as an alternative record of dissolved δ^7Li in field research, we briefly compared dissolved δ^7Li with corresponding exchangeable δ^7Li. Deep groundwater (collected at ~8 m depth) exhibited invariant δ^7Li, and the corresponding deep (>3 m) regolith exchangeable fraction also shows small δ^7Li variation. Our empirical $\Delta^7Li_{exchangeable\text{-}solution}$ between deep exchangeable pool and deep groundwater is ~ -4 ‰. XRD analysis at this site has identified chlorite and biotite as main phyllosilicates (Uhlig and von Blanckenburg, 2019), and we suspect that these minerals constitute the main hosts for exchangeable cations. Although no isotope fractionation factor for Li adsorption onto chlorite or biotite has been reported yet, Millot and Girard (2007) observed that dissolved δ^7Li only slightly increased by 3.8 ± 1.0 ‰ after an exchanging experiment with chlorite, which might suggest small isotopic fractionation between dissolved Li and adsorbed Li. Therefore, we suggest that our groundwater δ^7Li is likely to be in equilibrium with exchangeable δ^7Li of deep regolith and there is a small isotopic fractionation between dissolved and adsorbed pools.

Subsurface flow (0-15 cm), however, shows large δ^7Li variation (6.5 to 15.9 ‰) and shows significantly lower values than the δ^7Li of topsoil exchangeable Li (22.5 ‰). Topsoil is highly enriched in organic matter, which is suspected to be a major host

for exchangeable cations. On the basis of humic acid-Li interaction experiments (Li et al., 2020), Li adsorption onto organic matter is expected to favour ^{6}Li, but a specific fractionation factor is not known (indeed, fractionations would likely be strongly compound-specific). Mg isotope investigation at this site (Cai et al., in review) indicates the Mg isotope composition of subsurface flow (15cm) is not fully buffered by the corresponding exchangeable Mg hosted in shallow soil, due to limited interaction time. Since Li takes longer to reach exchange equilibrium than Mg (Pogge von Strandmann et al., 2019; Li and Liu, 2020), we thus infer that $\delta^{7}Li$ in subsurface flow has similarly not yet equilibrated with the exchangeable fraction.

3.5.5. Controlling factors of Li concentration and $\delta^{7}Li$ of water samples

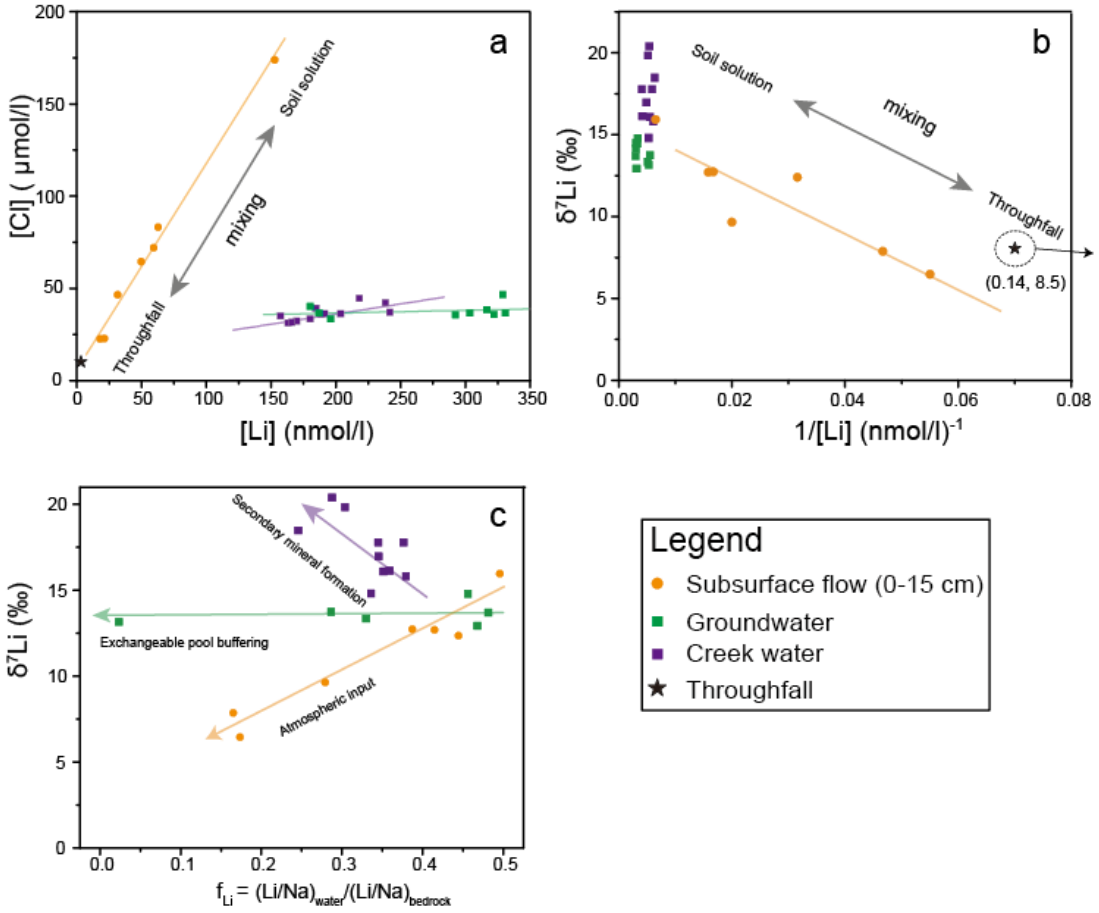

Fig. 3-7 Binary plots of a) [Li] vs. [Cl], b) [Li] vs. $\delta^{7}Li$ and c) the proportion of Li remaining in solution (f_{Li}) vs. $\delta^{7}Li$ (f_{Li} is calculated as $(Li/Na)_{water}/(Li/Na)_{bedrock}$, see text for details). Cl is regarded as a conservative element here. Arrows are illustrative. $\delta^{7}Li$ measurements uncertainties are smaller than the symbol size.

a) ***Subsurface flow (0-15 cm)***

Given its shallow depth, water in subsurface flow at 15 cm depth is likely influenced by both evapotranspiration and dilution by rain fall. To account for these effects, we normalised Li concentration to [Cl] which can be considered to be chemically inert

(e.g. Lemarchand et al., 2010; Tipper et al., 2012). Fig. 3-7a shows the covariation of [Li] and [Cl] (data from Sohrt et al., 2019). Cl concentration is lowest in the throughfall samples. All other water samples are more enriched in Cl, suggesting the influence of evapotranspiration. The subsurface flow samples also exhibit the largest δ^7Li and variation (Fig. 3-7b). We suspect that this δ^7Li variation is due to binary mixing of soil solution and throughfall rather than chemical reaction. For instance, we observed throughfall exerting a direct influence on the subsurface flow geochemistry: the sample collected on the 20/11/2015 was significantly diluted due to heavy throughfall that day (Fig. 3-4), and Li and Cl concentration decreased by three times compared to the sample collected 4 days earlier. The δ^7Li of this sample also became more negative, approaching the δ^7Li of throughfall. A linear Li-Cl relationship and 1/Li- δ^7Li (Fig. 3-7) are also good evidence of two-end-member mixing. In such a scenario, throughfall – depleted in Cl and ^{7}Li – would be one endmember. The other endmember – enriched in Cl and ^{7}Li – would have undergone evapotranspiration and chemical alteration. We infer that this endmember might be soil solution, originating from pre-event old water and have long residence time for evapotranspiration and alteration. During rainfall event, this old, stationary soil solution was expected to be flushed by new, diluted rainfall as to generate subsurface flow. Although not sampled in this study, previous research has found that top 10 cm soil solution are most significantly affected by evapotranspiration due to the shallow depth (Zhao et al., 2013) therefore have high Cl concentration, and exhibited more positive^{7}Li, as a result of ^{6}Li incorporation into secondary minerals (Lemarchand et al., 2010; Clergue et al., 2015). The evidence that clay-sized fraction in our study site is enriched in the light Li isotope supports this assertion.

One may still argue that the δ^7Li variation in subsurface flow is due to chemical alteration (i.e. adsorption or incorporation) rather than mixing. An alternative way to test this is the f_{Li}- δ^7Li plot. Because Na is generally not incorporated into secondary phases during weathering, Li/Na in water samples can be used as a tracer for Li adsorption or incorporation. The proportion of Li remaining in solution (f_{Li}) after secondary mineral formation is calculated as:

$$f_{Li} = \frac{(\frac{Li}{Na})_{water}}{(\frac{Li}{Na})_{bedrock}} \qquad (3.13)$$

assuming that the initial dissolved Li/Na ratio is identical to that of bedrock. For the 15 cm subsurface flow samples, a positive relationship between f_{Li} and δ^7Li was observed. As more Li incorporated into secondary minerals ($or\ low\ f_{Li}$) would drive dissolved δ^7Li more positive, the positive relationship we observed is the opposite of the expected negative f_{Li}- δ^7Li pattern in other studies (e.g. Dellinger et al., 2015; Liu et al., 2015). Therefore, we suggest that large δ^7Li variation in subsurface flow is highly unlikely to be attributable to chemical alteration, and that a mixing process is more likely the cause.

In summary, the subsurface flow is generated by mixing of throughfall (depleted in Cl and ^{7}Li) and stationary soil solution. The soil solution itself is enriched in Cl and more ^{7}Li, due to evapotranspiration and chemical alteration.

b) *Groundwater*

Groundwater has a longer residence time than shallow subsurface flow (Kim et al., 2014), which means there is a higher likelihood that solutes reach thermodynamic equilibrium with reacting solids (Maher, 2010). In this study site, groundwater has much higher Li content compared to shallow subsurface flow, and low and uniform Cl concentrations. Consequently, groundwater Li/Cl does not follow the trend of surface water (Fig. 3-7a), suggesting groundwater Li chemistry is not set by rate of throughfall input at the surface. Groundwater Li concentration at our site does covary with the level of the groundwater table, however, with lower Li concentration in periods of a high groundwater table, characteristic of dilution (Fig. 3-8). This relationship is not linear: when the level of the ground water table increased from ~ 8.5 m to ~6.5 m below ground, the Li concentration decreased only very slightly. Given the Li isotopic composition remained invariant (at ~13.9 ‰) throughout a hydrological year despite changes in groundwater level and Li concentration – correspondingly resulting in horizontal relationship in the f_{Li}- δ^{7}Li plot – this non-linearity is unlikely to have been caused by Li gain or loss via dissolution or incorporation. Instead, we suggest that during water table highstands, the exchangeable pool of the deep regolith can release further Li to the groundwater and thus 'buffer' the concentration (and isotope composition) of the groundwater. We note that identical Mg isotopes measured in groundwater and deep regolith at this site (Cai et al., in review) indicates that Mg in the groundwater is similarly sourced from the regolith exchangeable pool (specifically the exchangeable sites of chlorite or biotite).

The process that sets the high ^{7}Li/^{6}Li in the exchangeable pool – and thus the ground water also – is attributed to the preferential incorporation of ^{6}Li into secondary minerals. This is evidenced by the δ^{7}Li of clay-sized fraction and exchangeable fraction showing opposite trends (Fig. 3-2, 3-3), which might indicate that the more Li incorporated into the clay minerals, the heavier the Li in the exchangeable pool gets.

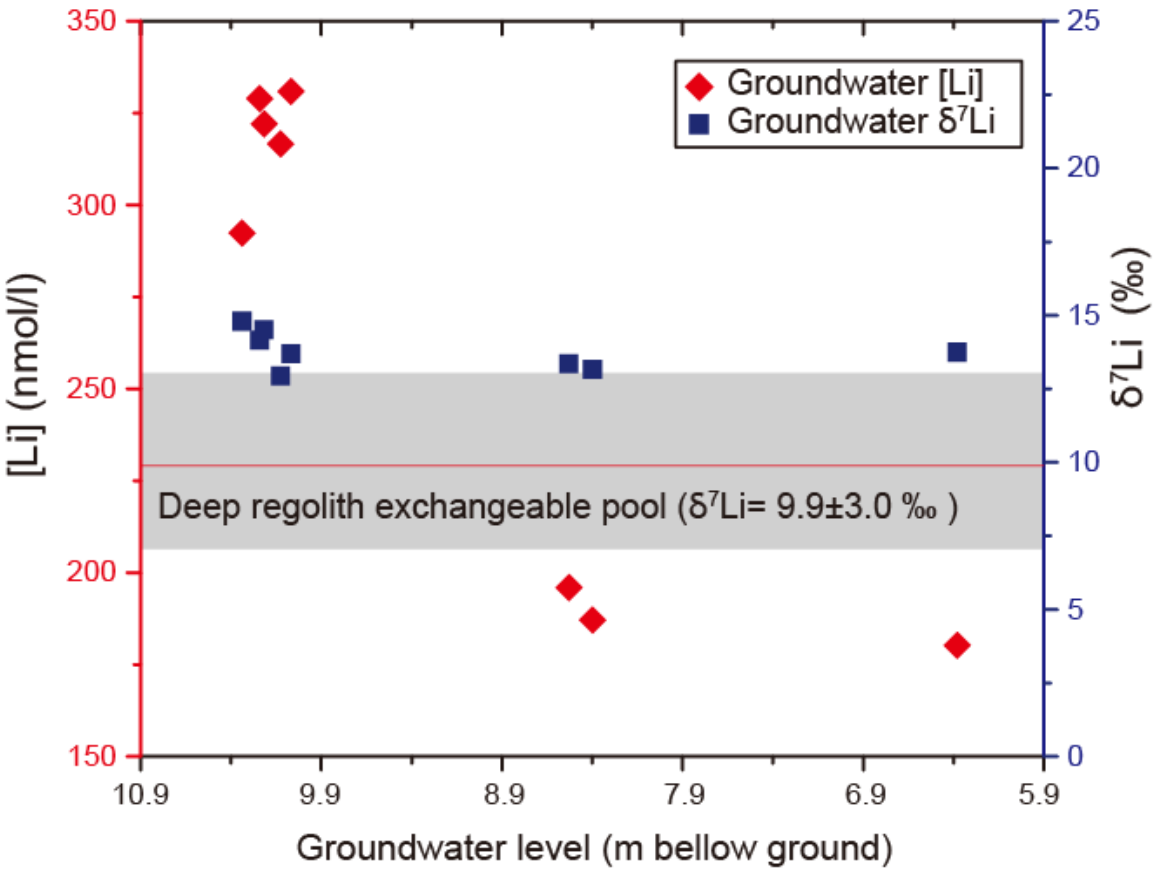

Fig. 3-8 Li concentrations [Li] and Li isotopes [δ^7Li] variation of groundwater in response to groundwater level change.

c) ***Creek water***

The Li/Cl relationships for creek water, like groundwater, are distinct from subsurface flow (Fig. 3-6). However, δ^7Li values of creek water (14.8 to 20.4 ‰) are similar to, or more positive than, groundwater samples (~13.9 ‰). Endmember mixing models have indicated that groundwater is the major source feeding creek water at this site (Sohrt et al., 2019). Compared to groundwater, the higher ^{7}Li/^{6}Li ratio in creek water samples could be either due to further reaction between fluid and solids in the creek channel, or changes in Li sources. The latter would manifest itself in a relationship between δ^7Li and discharge, assuming the contribution of Li from different depths or sources is related to discharge (Lemarchand et al., 2010; Henchiri et al., 2016). However, this relationship is not evident (Fig. 3-4c). We thus assume that variation of δ^7Li in the creek water is due to further fluid/solid reactions. Indeed, Fig. 3-6 suggest that δ^7Li_{creek} is negatively correlated with f_{Li}, consistent with worldwide river water trend (Liu et al., 2015; Dellinger et al., 2015; Pogge von Strandmann et al., 2017). A batch fractionation model (not shown) gives a fractionation factor of 0.970. This study supports published hypotheses that

continued δ^7Li fractionation occurs during river water downstream evolution (e.g. Liu et al., 2015).

3.5.6. A missing Li export path

From a mass balance perspective, bulk soil, as the counterpart of water, should be depleted in the elements or isotopes originally contained in bedrock that water samples are enriched in, provided that the system is in steady state. In this study, subsurface flow, groundwater, and creek water are all enriched in heavy ^{7}Li, which means that water is continuously removing ^{7}Li in preference to ^{6}Li from the regolith. However, the regolith δ^7Li is statistically indistinguishable from that in bedrock (Fig. 3-2) and also shows negligible Li isotope variation. Bouchez et al. (2013) developed a mass balance model considering the involved compartments that quantitatively described the dissolved loss of an element:

$$\frac{W^{Li}}{D^{Li}} = \frac{\delta^7 Li_{soil} - \delta^7 Li_{rock}}{\delta^7 Li_{soil} - \delta^7 Li_{water}} \qquad (3.14)$$

Where W^{Li} and D^{Li} are the weathering flux and denudation flux of Li respectively.

Since at Coventwald soil is almost identical to bedrock in δ^7Li, the calculated $\frac{W^{Li}}{D^{Li}}$ is very small. Using creek water δ^7Li that ranges from 14.8 to 20.4 ‰, we calculated $\frac{W^{Li}}{D^{Li}}$ value of 1.8 ± 1.5 % (2SD) to 2.4 ± 1.1% (2SD) (calculated uncertainty was propagated from measurement uncertainty of water and soil samples using Monte Carlo method).

We can compare this isotope-derived dissolved export fraction $\frac{W^{Li}}{D^{Li}}$ with the fraction of Li lost from regolith as determined by concentration measurements, i.e., $-\tau^{Li}$, which gives a value of ~50%. These two numbers are clearly inconsistent.

An alternative approach to this question is to quantitively compare the instantaneous element export flux (using river chemistry) and long-term Li export flux (using regolith chemistry) as "dissolved export efficiency" (or DEE, Table 3-1, Uhlig et al., 2017) which is calculated as (see also Table 3-1):

$$DEE^{Li} = \frac{W^{Li}_{river}}{W^{Li}_{regolith}} \qquad (3.10)$$

where W^{Li}_{river} represents the dissolved river flux of Li and $W^{Li}_{regolith}$ the net solubilisation of Li from regolith (solubilisation from bedrock minus incorporation into secondary solids). To obtain a metric that is independent of timescale effects and without the need to know absolute values for weathering fluxes, W^{Li}_{river} and $W^{Li}_{regolith}$ are normalized by W^{Na}_{river} and $W^{Na}_{regolith}$ respectively (see also Table 3-1):

$$DEE_{Na}^{Li} = \frac{W_{river}^{Li}/W_{river}^{Na}}{W_{regolith}^{Li}/W_{regolith}^{Na}} = \frac{(\frac{[Li]}{[Na]})river/(\frac{[Li]}{[Na]})bedrock}{\tau_{Zr}^{Li}/\tau_{Zr}^{Na}} \quad . (3.11)$$

A DEE^{Li} of 1 means that fluxes are balanced, a value < 1 indicates that a fraction of the flux is missing. The calculated DEE_{Na}^{Li} ranges from 38% to 60%, suggesting that of Li solubilized from regolith, only ~38% to 60% appears dissolved in the stream water (assuming the export of Na reflects congruent dissolution from rock).

In summary, both isotope- (W/D vs τ) and element-based (DEE) mass balances show a missing export pathway of Li that is enriched in ^{6}Li. Such a discrepancy is not only seen in our study site, however. In a catchment in France, regolith also shows negligible δ^{7}Li variation compared to the bedrock despite 80% Li loss by chemical weathering, and runoff being substantially enriched in ^{7}Li (Lemarchand et al., 2010). Similarly, in the SSHCZO (Susquehanna Shale Hills Critical Zone Observatory), both runoff and soil are characterized by higher δ^{7}Li values than bedrock (Steinhoefel et al., 2021). Besides Li, for other elements like Mg, similar discrepancies have been observed. Ma et al. (2015) observed that both soil and stream have lighter δ^{26}Mg than bedrock. Bolou-Bi et al., (2012); Tipper et al., (2012); Uhlig et al., (2017) also found isotopically light riverine δ^{26}Mg with bulk soil being almost isotopically indistinguishable to bedrock, despite the large Mg depletion in the soil. We are seeing a consistent picture in that not all elements released in the weathering zone appear in river discharge.

So far, the explanations suggested for this discrepancy include: 1) export of plant litter or coarse wood debris which are not sampled (Uhlig et al., 2017), or 2) fine particles like clays that have been removed from the system in the subsurface over geological time (Ma et al., 2015; Steinhoefel et al., 2021). As Li is not a nutritive element and bio-uptake accounts for an only negligible amount of Li flux compared to weathering (Fig. 3-6), the first hypothesis is not likely here. The missing Li export pathway in this study might be export of fine particulate matter (that has not been sampled) in the subsurface flow. Other candidate explanations include the export of colloid-bound Li, which was filtered out before our water analysis. Another explanation is that the bedrock in the catchment is heterogeneous, which would introduce a bias in the element-based estimates of DEE^{Li}. It is unlikely, however, that heterogeneous bedrock simultaneously results in a DEE < 1 in several different study sites. Since this discrepancy is now a more common observation in Critical Zone research, future studies are required to further investigate this problem.

3.6. Conclusions

We have investigated δ^{7}Li in different compartments of the Critical Zone in a temperate forested catchment. Wet precipitation and biological processes have a negligible influence on the Li weathering budget. Secondary mineral formation is the main process fractionating dissolved Li. Yet time series data on subsurface flow,

groundwater, and creek water differ in their δ^7Li, and also vary through a hydrological year. A binary mixing of throughfall and soil solution explains the correlated Li concentration and δ^7Li variation in subsurface flow, whereas the invariance of δ^7Li in groundwater most likely reflects the buffering process of the deep exchangeable pool. δ^7Li in creek water is covaries with the proportion of Li remaining in the solution, suggesting that Li isotope fractionation occurs in rivers with ^{6}Li being preferentially incorporated into secondary solids. Our result elucidated that water in different depths may subject to different geological processes, and thus the structure of the Critical Zone is a crucial consideration when considering water chemistry. However, the Li isotope budget in this catchment is not balanced and a reservoir enriched in ^{6}Li is missing. Since unbalanced export budgets are an increasingly frequent observation in several recent studies, more work is required to further explore this issue.

Table S3-1: Element concentrations, Li isotopic composition of bulk regolith, clay-sized fraction and separated mineral samples.

Sample	IGSN†	Depth	Major elements (ICP-OES)						ICP-MS	Li isotopes (MC-ICP-MS)		
		m	Al_2O_3	CaO	Fe_2O_3	K_2O	MgO	Na_2O	Li	δ^7Li	2SD	n*
			%	%	%	%	%	%	µg/g			
Bulk regolith												
DC1-1	GFDUH00LU	0.4	15.5	0.5	6.5	2.5	2.2	1.2	63.4	-1.6	0.0	3
DC1-2	GFDUH00LY	1.2	15.9	0.4	7.1	2.6	2.5	1.1	68.4	-1.7	0.1	3
DC1-3	GFDUH00M1	1.9	15.5	0.4	7.2	2.7	2.6	1.1	66.4	-1.8	0.0	3
DC1-3-Replicates	GFDUH00M1	1.9	14.8	0.4	6.7	2.5	2.4	1.1	64.1			
DC1-4	GFDUH00M5	2.7	14.6	0.5	6.5	2.6	2.4	1.2	63.1	-1.8	0.1	3
DC1-5	GFDUH00MB	3.4	15.1	0.5	6.6	2.8	2.5	1.3	65.2	-1.6	0.2	3
DC1-6	GFDUH00MD	4.4	13.9	0.6	6.0	2.5	2.2	1.3	61.6	-1.6	0.0	3
DC1-7	GFDUH00MF	5.7	14.7	0.5	6.5	2.7	2.4	1.4	65.5	-1.4	0.1	3
DC1-7-Replicates	GFDUH00MF	5.7	15.1	0.6	6.7	2.7	2.4	1.4	92.8			
DC1-8	GFDUH00N5	7.6	17.3	9.3	11.2	1.6	5.8	2.1	32.4	-1.6	0.1	3
DC1-9	GFDUH00N8	9.6	16.1	4.1	8.8	2.6	4.3	2.7	43.6			
DC1-10	GFDUH00N9	12.9	16.5	5.4	7.9	2.1	3.3	3.0	65.7			
DC1-11	GFDUH00NB	16.3	16.5	6.3	8.8	1.8	3.8	2.9	61.3	-1.4	0.1	3
DC1-12	GFDUH00NC	18.4	16.4	5.7	7.1	2.0	3.4	3.2	59.5	-2.1	0.1	3
DC1-13	GFDUH00ND	19.5	16.0	6.3	6.8	2.3	3.2	3.2	63.6	-1.2	0.1	3
DC1-13-replicates	GFDUH00ND	19.5	16.4	6.6	7.2	2.4	3.2	3.3	67.4	-1.3	0.0	3
Clay sized fraction #												
Clay-1	GFDUH00LU	0.4	14.3	0.0	7.5	1.2	1.9	0.1	87.5	-5.4	0.0	3
Clay-2	GFDUH00HJ	1	19.5	0.1	11.0	1.7	2.4	0.2	111.2	-4.9	0.4	3
Clay-3	GFDUH00HN	1.8	23.4	0.1	10.4	3.2	2.5	0.2	109.8	-4.2	0.3	3
Clay-4	GFDUH00HR	2.4	21.8	0.1	9.7	3.1	2.5	0.2	95.0			
Clay-5	GFDUH00HT	2.8	18.0	0.1	8.6	2.7	2.1	0.2	88.2	-3.5	0.4	3
Clay-6	GFDUH00MB	3.4	19.9	0.1	9.2	3.3	2.9	0.3	85.3			
Clay-7	GFDUH00MD	5.1	21.7	0.1	10.8	3.7	3.3	0.4	98.5	-4.4	0.3	3
Seperated minerals $												
Quartz and Feldspar	GFDUH00ND	19.5	17.5	4.5	1.4	2.0	0.7	4.4	44.3	-0.4	0.2	3
Chlorite	GFDUH00ND	19.5	16.7	5.7	16.4	1.7	7.8	1.7	94.4	-1.3	0.5	2
Hornblende	GFDUH00ND	19.5	17.7	6.1	11.8	1.8	5.2	2.8	84.9	-1.5	0.1	3
Biotite	GFDUH00ND	19.5	11.6	0.9	16.3	4.1	8.1	0.3	170.5	-0.1	0.0	3
Reference												
SRM2709a			13.6	2.8	4.9	2.6	2.4	1.5	55.7	-0.3	0.1	3
SRM2709a			12.7	2.6	4.6	2.4	2.2	1.4	52.5	-0.2	0.6	3
SRM2709a			13.0	2.6	4.6	2.4	2.3	1.5	54.7			
Certified or recommended values ^			**13.9 ± 0.3**	**2.7 ± 0.1**	**4.8 ± 0.1**	**2.5 ± 0.07**	**2.4 ± 0.03**	**1.6 ± 0.04**	**51.4**	**-0.2**	**0.0**	
BHVO-2									4.8	5.1	0.2	3
BHVO-2										5.2	0.7	3
BHVO-2										4.5	0.2	3
Certified or recommended values ^									**4.7**	**4.2**	**0.1**	

† IGSN (International Geo Sample Number). Metadata of samples are available under: www.igsn.org by adding the IGSN after igsn.org, e.g. igsn.org/

* n means replicates of a sample measured by MC-ICP-MS

Clay-sized fraction was separated from bulk regolith using a centrifuge

$ Minerals were seperated from bedrock at 19.5 m depth

^ Recommended values for comparision are from Weynell et al., (2017). 10.1016/j.gca.2017.06.026

Table S3-2: Discharge of creek water, major element concentrations and Li isotopic composition of creek water, subsurface flow, and groundwater samples.

Sample	IGSN†	Date	Sample type	Discharge#	Major elements (ICP-OES)				ICP-MS	Li isotopes (MC-ICP-MS)		
				l/s	Na µmol/l	Mg µmol/l	K µmol/l	Ca µmol/l	Li nmol/l	δ^7Li	2SD	n*
Throughfall												
	GFJUB0066	01/02/2016	Throughfall		N.A	N.A	N.A	N.A	6.7	8.5	0.0	2
creek water												
FVA-1	GFJUB0067	11/04/2015	creek water	2.8	113.0	50.4	12.2	117.4	188.4	14.8	0.1	3
FVA-2	GFJUB0068	15/06/2015	creek water	2.0	86.8	50.9	18.6	136.0	163.4	15.8	0.1	3
FVA-3	GFJUB0069	15/07/2015	creek water	0.2	133.9	67.2	13.7	186.3	238.4	16.1	0.0	3
FVA-4	GFJUB006A	17/08/2015	creek water	0.1	129.5	77.8	12.8	211.4	241.7	17.8	0.1	3
FVA-5	GFJUB006B	15/09/2015	creek water	0.1	128.8	81.9	10.8	221.9	157.2	18.5	0.3	3
FVA-6	GFJUB006C	15/10/2015	creek water	0.2	126.9	83.5	9.8	226.0	191.2	19.8	0.1	3
FVA-7	GFJUB006D	15/11/2015	creek water	0.3	129.3	88.2	10.9	242.1	184.6	20.4	0.4	3
FVA-8	GFJUB006E	21/11/2015	creek water	2.3	101.8	77.6	25.1	189.1	218.2			3
FVA-9	GFJUB006F	17/12/2015	creek water	0.8	118.9	64.3	12.3	173.8	203.7	17.0	0.4	3
FVA-10	GFJUB006G	01/02/2016	creek water	0.9	103.3	49.3	10.4	123.0	180.1	16.1	0.1	3
FVA-11	GFJUB006H	15/02/2016	creek water	4.4	99.1	47.3	10.2	115.9	169.7	17.8	0.1	3
FVA-12	GFJUB006J	25/02/2016	creek water	2.8	99.7	48.4	9.8	119.5	166.1			
Subsurface flow (0.1m)												
SF1-1	GFJUB006K	15/06/2015	Subsurface flow		36.0	105.2	275.6	297.5	49.9	9.7	0.7	3
SF1-2	GFJUB006L	16/08/2015	Subsurface flow		30.6	88.9	256.0	233.6	63.0	12.7	0.4	3
SF1-3	GFJUB006M	14/09/2015	Subsurface flow		31.1	115.0	206.0	370.9	59.6	12.7	0.1	3
SF1-4	GFJUB006N	16/11/2015	Subsurface flow		62.2	183.6	295.0	592.8	152.9	15.9	0.2	3
SF1-5	GFJUB006P	20/11/2015	Subsurface flow		14.4	35.5	145.2	121.9	31.6	12.4	0.1	3
SF1-6	GFJUB006Q	01/02/2016	Subsurface flow		26.1	16.6	68.0	56.4	21.4	7.9	0.1	3
SF1-7	GFJUB006R	25/02/2016	Subsurface flow		21.1	19.9	71.8	69.9	18.2	6.5	0.7	3
Groundwater												
GW-1	GFJUB006W	11/04/2015	Groundwater		126.8	65.1	18.5	222.4	180.2	13.7	0.3	3
GW-2	GFJUB006X	15/07/2015	Groundwater		136.4	95.5	16.9	450.8	316.6	12.9	0.4	3
GW-3	GFJUB006Y	15/09/2015	Groundwater		129.2	93.5	18.0	455.8	292.3	14.8	0.4	3
GW-4	GFJUB006Z	20/11/2015	Groundwater		138.6	98.7	20.9	489.0	330.9	13.7	0.4	3
GW-5	GFDIC0009	17/12/2015	Groundwater		136.3	94.2	18.0	452.3	314.2			
GW-6	GFDIC0008	25/02/2016	Groundwater		119.7	69.7	14.6	266.9	195.9	13.3	0.6	3
Reference												
SLRS-6 (river water)		Reference			109.3	88.9	15.6	212.7	74.2	24.2	0.5	4
SLRS-6 (river water)		Reference			113.5	91.6	16.2	221.0	82.1	24.1	0.4	4
SLRS-6 (river water)		Reference							83.7	23.7	1.5	4
Certificated or recommended values for comparision					**120 ± 10**	**89 ± 2**	**17 ± 1**	**219 ± 5**				
OSIL (Atlantic Seawater)										29.9	0.4	3
OSIL (Atlantic Seawater)										31.6	0.1	3
OSIL (Atlantic Seawater)										31.3	0.1	3
Certificated or recommended values for comparision										**30.7**	**0.4**	

† IGSN (International Geo Sample Number). Metadata of samples are available under: www.igsn.org by adding the IGSN after igsn.org, e.g. igsn.org/

Discharge data from Sohrt et al., (2019) doi.org/10.3389/ffgc.2019.00085

* n means replicates of a sample measured by MC-ICP-MS

^ Recommended values for comparision are from Yang et al., (2015). doi.org/10.4224/crm.2015.slrs-6 and Bryant et al., (2003). doi.org/10.1039/B212083F

Table S3-3: Element concentrations and Li isotopic composition of plant samples.

		Elements concnetration (ICP-OES)								ICP-MS	Li isotopes (MC-ICP-MS)			Description
sample	IGSN†	Al µg/g	Ca µg/g	Fe µg/g	K µg/g	Mg µg/g	Na µg/g	P µg/g	Sr µg/g	Li ng/g	δ^7Li	2SD	n*	
Leaves														
BF-L-1	GFDIC0006	48.8	7373.7	74.2	9870.0	1852.0	29.9	1627.8	21.8	4.3	4.9	0.2	3	Mature beech leaves,1m above ground
BF-L-2	GFDIC0007	32.5	6212.0	55.5	7157.9	1817.6	16.4	1421.6	22.7	4.3	4.0	0.1	3	Mature beech leaves,6m above ground
BF-L-3	GFDIC0005	41.8	5138.8	65.4	9154.7	1075.1	23.8	2503.9	19.8	6.0	6.2	0.2	3	Young beech leaves,2m above ground
BF-L-4	GFDIC0004	53.7	7407.7	71.8	7439.4	1319.0	18.3	1648.1	27.2	7.0	6.7	0.3	3	Young beech leaves,3m above ground
BF-L-5	GFDIC0003	227.8	5153.7	65.1	5913.1	809.5	78.0	1252.9	15.8	19.3	10.7	0.1	3	Young spruce leaves, 4m above ground
BF-L-5-Re	GFDIC0003	226.3	5711.2	52.7	4676.2	696.1	96.7	922.5	15.5	20.4	12.1	0.2	3	
Twigs														
BF-T-1	GFDIC0002	34.0	5761.3	24.8	2095.5	619.8	25.0	676.9	31.8	4.3	6.2	0.2	3	Mature beech branches,1m above ground
BF-T-2	GFDIC0001	12.5	1644.3	11.6	3152.2	230.2	37.1	814.5	10.5	2.6	4.9	0.2	3	Mature beech branches,6m above ground
Reference														
SRM1515		265.1	14325.4	71.8	12229.4	2439.3	25.9	1478.9	21.9	143.0	-0.8	0.4	3	
SRM1515		296.7	13910.6	68.3	12308.0	2360.3	25.6	1477.2	22.0		-1.1	0.2	3	
SRM1515		321.5	14971.1	73.2	12903.0	2510.5	27.8	1582.8	23.7					
SRM1515		**284.5**	**15250**	**82.7**	**16080**	**2710**	**24.4**	**1593**	**25**					Certificated or recommended values for comparision

† IGSN (International Geo Sample Number). Metadata of samples are available under: www.igsn.org by adding the IGSN after igsn.org, e.g. igsn.org/

* n means replicates of a sample measured by MC-ICP-MS

^ Recommended values for comparision are from Nist Certificate of Analysis

Table S3-4: Element concentrations and Li isotopic composition of regolith exchangeable fraction.

			Major elements (ICP-OES)					ICP-MS	Li isotopes (MC-ICP-MS)		
Sample	IGSN†	Depth	Al	K	Ca	Mg	Na	Li	δ^7Li	2SD	n*
		m	µg/g	µg/g	µg/g	µg/g	µg/g	ng/g			
EX1	GFDUH00HE	0.2	53.8	218.5	605.1	124.8	13.5	5.3	22.5	0.3	3
EX2	GFDUH00J1	0.4	30.8	47.2	120.2	27.4	12.9	3.5	15.9	1.1	3
EX3	GFDUH00J2	0.6	46.7	31.7	75.4	16.8	13.8				3
EX4	GFDUH00HH	0.8	46.9	26.5	53.6	8.9	12.7	3.6	10.4	0.3	3
EX5	GFDUH00HJ	1	33.0	21.3	32.6	5.1	11.1	2.5			3
EX6	GFDUH00HK	1.2	21.8	23.0	27.9	4.7	11.0	1.7	9.0	0.5	3
EX7	GFDUH00HL	1.4	15.6	25.1	29.2	7.0	9.2	1.5	4.5	0.7	3
EX8	GFDUH00HM	1.6	16.3	27.5	27.9	7.9	9.0	2.0	2.0	0.5	3
EX9	GFDUH00HN	1.8	9.8	29.1	56.7	16.5	11.2	1.6			3
EX10	GFDUH00HP	2	11.3	28.9	73.5	26.4	12.0	1.9	3.6	0.9	3
EX11	GFDUH00JA	2.2	4.6	32.7	108.5	48.2	14.0	2.8	5.1	0.6	3
EX12	GFDUH00HR	2.4	1.6	47.8	238.4	97.0	13.9	4.8	5.2	0.5	3
EX13	GFDUH00HS	2.6	0.3	54.7	384.3	147.3	14.9	10.6			3
EX14	GFDUH00HT	2.8	0.3	62.8	600.3	196.5	15.7	11.2	11.6	0.3	3
EX16	GFDUH00MB	3.4	<LOD	56.3	698.1	238.8	19.1	16.8	9.2	0.8	3
EX17	GFDUH00MC	3.8	<LOD	68.9	1066.3	304.6	19.0	19.7			3
EX18	GFDUH00MD	4.4	<LOD	76.8	1114.4	303.2	19.7	18.0	8.3	1.0	3
EX19	GFDUH00ME	5	<LOD	67.3	861.0	304.2	20.1	23.1	8.6	0.4	3
EX20	GFDUH00MF	5.6	<LOD	47.2	684.3	224.7	14.3	26.3			
EX21	GFDUH00MG	6.4	<LOD	69.0	863.0	279.5	18.0	20.1	11.8	0.3	3
Reference											
SLRS-6									24.1	0.4	4
SLRS-6									23.9	0.9	2

<LOD: below limit of determination limit

† IGSN (International Geo Sample Number). Metadata of samples are available under: www.igsn.org by adding the IGSN after igsn.org, e.g. igsn.org/

* n means replicates of a sample measured by MC-ICP-MS

Chapter 4

Summary and outlook

7.1. Summary

This doctorate research applied Li and Mg isotope tools to Critical Zone research in a small, forested catchment underlain by paragneiss (Conventwald, Germany). Li and Mg isotopes ratios of bedrock, bulk regolith, the exchangeable fraction, vegetation and water samples were investigated and factors controlling isotope fractionation were discussed.

A research gap closed is presented by determination of the Mg isotope fractionation during adsorption. While Mg isotope fractionation during dissolution, secondary mineral formation and bio-uptake has been extensively investigated under controlled experiments conditions (e.g. Black et al., 2008; Bolou-Bi et al., 2010; Li et al., 2020; Wimpenny et al., 2010; Hindshaw et al., 2020), adsorption and desorption associated fractionation remain poorly understood (Wimpenny et al., 2014). This research filled this gap by conducting a series of batch exchange experiments using soil samples from Conventwald, revealing that negligible isotope fractionation occurs during Mg exchange processes. The adsorption mechanism of Mg onto soil was thus inferred to be outer-sphere complexation which does not induce covalent bond formation. These experimental results explain our field observation well as subsurface flow samples that have similar δ^{26}Mg values to the regolith exchangeable fraction at the respective sampling depths. Groundwater and creek water also show δ^{26}Mg values that are identical to those of the exchangeable fraction.

Therefore, the new isotope evidence supports previous hypotheses suggesting that cation concentrations in runoff are buffered by the regolith exchangeable pool during high discharge (e.g. Clow and Mast 2010; Kim et al., 2017). More importantly, this research disclosed the potential of using δ^{26}Mg in the regolith exchangeable pool as biological and geological processes tracer. The large pool of Mg in the exchangeable fraction of the deep regolith (>3 m) is isotopically light and most likely reflects the isotope composition of the Mg residue in soil water after secondary mineral formation - a process which often favours heavy Mg isotopes (e.g. Liu et al., 2014; Teng et al., 2010). Superimposed on this effect, the exchangeable fraction in the shallow regolith (0-3 m depth) shows a strong imprint of biological cycling. Mg isotopes thus provide an exact depth image of the geogenic (weathering) and the organic (bio-cycled) nutrient cycle. In summary, combination of field research and lab experiments in this research informs about processes fractionating Mg in the Critical Zone – with the role of the exchangeable

pool highlighted as particularly important – and further demonstrates the potential of Mg isotopes as a tool in tracing weathering processes the deep regolith.

Another important result is the attribution of different Li isotope ratios with depth of fluid in terms of secondary mineral formation and buffering by the exchangeable pool. Li input-output fluxes were first estimated and the result support previous suggestions that wet precipitation and bio-uptake constitute negligible Li fluxes as compared to weathering (Lemarchand et al., 2010; Clergue et al., 2015). Thus Li isotopes effectively serve as a tracer exclusively for chemical weathering. An initial important finding is that the various water compartments strongly differ in their Li isotope composition. In creek water samples, δ^7Li are the more positive the more Li is incorporated in the secondary phase, consistent with previous research (e.g. Dellinger et al., 2015; Liu et al., 2015). In contrast, groundwater exhibited negligible δ^7Li variation even in the face of Li concentration and groundwater table fluctuation. This variation pattern, which has not been reported in previous research, I attribute to buffering process of exchangeable pool. δ^7Li in shallow subsurface flow (0-15 cm) became more positive with increasing Li concentration, and a binary mixing process could be identified with two endmembers being new throughfall and pre-event soil solution.

Finally, despite all water samples being enriched in ^{7}Li, soil samples (which constitute the weathering residue), were not enriched in ^{6}Li to balance the ^{7}Li loss. This might indicate that a pool enriched in ^{6}Li is missing. This unbalanced isotope cycling in the Critical Zone is widely observed in different geological settings, and for different isotope systematics. Several hypotheses were put forward to explain this discrepancy. For example, colloids which were filtered out after water sample collection might contain a non-negligible amount of cations, and thus might be the missing isotope pool. Another potential missing pool might be fine particulate matter, which could be continuously removed from Critical Zone by subsurface flow. It is also likely that our sampling strategy is just a snapshot of weathering processes, and conceivably might not represent a steady-state situation. However, due to the lack of certain evidence, more work needs to be done in the future to verify these hypotheses.

7.2. Implications for future studies:

In the following section, I summarize some research gaps that emerged from this study and raise scientific questions worth further investigation.

7.2.1. A better understanding of plant uptake-induced isotope fractionation

Mg is intensively involved in biological recycling. Yet determining Mg isotope fractionation factors of plant uptake from field data is challenging. The difficulty lies in the lack of Mg uptake flux data and inaccurate estimation of the overall δ^{26}Mg of a whole plant. For example, tree leaves and branches are often pooled so as to represent the whole plant (e.g. Bolou-Bi et al., 2012; Mavromatis et al., 2014).

However, our research indicated that the trunk – the main Mg reservoir of the tree – is variable in terms of δ^{26}Mg and shows different δ^{26}Mg as compared to leaves and twigs. Biased estimation of whole plant δ^{26}Mg would arise if this pool is ignored. In addition, roots are not considered in our study due to the notorious difficulty in sample collection and chemical pre-treatment for isotope analysis. Future research could develop more comprehensive sampling strategy and to better constrain this issue.

In terms of Li isotopes, growth experiments have not, to my knowledge, been conducted yet to investigate Li isotope fractionation by plant activity. Results of previous field research are still non-conclusive on whether Li isotopes are fractionated during uptake and translocation (Lemarchand et al., 2010; Clergue et al., 2015; Li et al., 2020). A series of hydroponic growth experiments using a variety of model plant species could be done to answer this question.

7.2.2. Developing exchangeable Mg isotopes as new proxy tracing nutrient recycling

It was observed that strongly recycled nutrients (e.g. P, K, Mg) are generally more concentrated in topsoil exchangeable fraction, which was widely attributed to the "bio-uplift effect" (Jobbágy and Jackson, 2001; Porder and Chadwick, 2009; Bullen and Chadwick, 2016). In this study, I verified that Mg isotopes could serve as additional proxy constraining this effect. The variation of exchangeable δ^{26}Mg with regolith depth allows one to identify the depth from which plants start uptaking nutrients and to evaluate the effect of uptake and organic matter decomposition at different depths. Since this study is the first report of exchangeable δ^{26}Mg data at high depth resolution, similar work is encouraged in future critical zone research to further explore this proxy. For Barium, vertical distributions of exchangeable Barium isotopes of Hawai'i regolith were found to be also dictated by median annual precipitation (Bullen and Chadwick, 2016). Whether different environmental factors (e.g. precipitation, temperature etc.) also impact the vertical distribution of exchangeable δ^{26}Mg remains unknown. In addition, as exchangeable δ^{26}Mg also reflects bioactivity, it is worth determining exchangeable δ^{26}Mg of paleosol to investigate nutrient utilization in geological time.

7.2.3. Isotopes in exchangeable Mg as an indicator of cation sources in runoff?

In this study, cations in groundwater and runoff originate from deep regolith where abiotic processes dominate, as evidenced by Mg isotopes. Although there is evident biological influence on the shallower soil column, this is not reflected in the outlet runoff chemistry. However, different regimes have been observed in other catchments with runoff δ^{26}Mg changing significantly with discharge (Bolou-Bi et al., 2012; Mavromatis et al., 2014). These authors inferred that δ^{26}Mg variations in the runoff were due to the changing source from shallow depth (biological recycled Mg) to deep depth (abiotic weathering released). However, no direct evidence was provided in their studies. In this research, I propose that exchangeable δ^{26}Mg could

provide an exact depth image of the geogenic (weathering) and the organic (bio-cycled) nutrient cycle, which makes tracing the source of Mg in runoff possible. By providing additional regolith exchangeable δ^{26}Mg data, future research could verify the hypothesis that variation of runoff δ^{26}Mg responding to rainfall is due to changing sources.

7.2.4. Li isotope fractionation during exchange process

In this thesis, I experimentally determined the isotopic fractionation of Mg during adsorption and desorption using soil from this research site, but I did not carry out the same experiment for Li. Using a variety of geological materials as adsorbent, previous research has resulted in a range of fractionation factors during adsorption (e.g. Pistiner and Henderson, 2003; Wimpenny et al., 2015; Li and Liu, 2020). Unlike for Mg, where exchange equilibrium is attained within hours, much longer time is required (days to months, e.g. Li and Liu et al., 2020; Pogge von Strandmann et al., 2019; Zhang et al., 2021a) to reach Li exchange equilibrium. Therefore, whether the measured fractionation factor under constrained lab conditions could be effectively extrapolated to field studies remains unclear as 1) major minerals hosting exchangeable sites are less well-constrained in the field; and 2) the reaction time is generally unknown. In this thesis, I report the first field measurements of paired exchangeable and dissolved δ^{7}Li and observed that the difference in δ^{7}Li between groundwater and corresponding regolith exchangeable fraction is generally the same in different seasons, which might be an indication of Li exchange being in isotopic equilibrium. However, shallow subsurface flow samples varied significantly in δ^{7}Li and clearly suggest non-equilibrium fractionation with respect to the exchangeable pool. Therefore, compared to Mg isotopic systematics, the extent to which the regolith exchangeable pool can buffer water δ^{7}Li, and on what timescales, is still unknown. Further study is encouraged to explore this subject.

7.2.5. The imbalance of isotopes cycling in the Critical Zone

As discussed in Chapter 3, the cycling of Li isotopes in the Conventwald could not be balanced, as a pool enriched in ^{6}Li appears to be missing. Actually, numerous field studies have observed similar unbalanced isotope budgets (for Sr, Mg, Li, Fe, B etc) in the Critical Zone (e.g. Ma et al., 2015; Oeser and von Blanckenburg et al., 2020; Steihoefel et al., 2021). von Blanckenburg et al., (2021) have concluded four explanations for such imbalance in elemental fluxes. These include: 1) methodological artefacts; 2) perturbation of the steady state in fluxes; 3) element fractionation along hillslopes or at depth; and 4) a hidden pathway or pool. Future research could take these explanations as guidelines to investigate why isotope cycling in the Critical Zone is imbalanced. So far, the mostly adopted explanation for the discrepancy in isotope cycling is that a hidden pathway or pool was not sampled. For example, Uhlig et al., (2017) suggested that removal of coarse woody debris might account for the unidentified export of heavy Mg isotopes. Similarly, Oeser and von Blanckenburg, (2021) attributed the loss of ^{86}Sr to erosion of fractionated organic solids (i.e. leaf litter and woody debris). Fine particulates

transported by subsurface flow were also proposed as reservoirs potentially hosting the missing light B (Noireaux et al., (2021), heavy Mg (Ma et al., 2015) and light Li (Steihoefel et al., 2021) isotopes respectively. In addition, colloids, which were filtered out after water sample collection, might also present such a missing reservoir at our site. Isotopic constraints on these samples are still a blind spot in research. Future Critical Zone research should take these reservoirs into account.

References

Aciego S. M., Riebe C. S., Hart S. C., Blakowski M. A., Carey C. J., Aarons S. M., Dove N. C., Botthoff J. K., Sims K. W. W. and Aronson E. L. (2017) Dust outpaces bedrock in nutrient supply to montane forest ecosystems. *Nat Commun* **8**, 14800.

Anderson D. W. (1988) The Effect of Parent Material and Soil Development on Nutrient Cycling in Temperate Ecosystems. *Biogeochemistry* **5**, 71–97.

Anderson S. P., Dietrich W. E., Torres R., Montgomery D. R. and Loague K. (1997) Concentration-discharge relationships in runoff from a steep, unchanneled catchment. *Water Resources Research* **33**, 211–225.

Attiwill P. M. (1968) The Loss of Elements from Decomposing Litter. *Ecology* **49**, 142–145.

Bachmair, S., and Weiler, M. (2012). Technical Report on Experimental Hillslope Hydrology, Hydronotes. University of Freiburg, Freiburg, Germany

Bagard M.-L., West A. J., Newman K. and Basu A. R. (2015) Lithium isotope fractionation in the Ganges–Brahmaputra floodplain and implications for groundwater impact on seawater isotopic composition. *Earth and Planetary Science Letters* **432**, 404–414.

Bastviken D., Thomsen F., Svensson T., Karlsson S., Sandén P., Shaw G., Matucha M. and Öberg G. (2007) Chloride retention in forest soil by microbial uptake and by natural chlorination of organic matter. *Geochimica et Cosmochimica Acta* **71**, 3182–3192.

Berner R. A. (1992) Weathering, plants, and the long-term carbon cycle. Geochimica et Cosmochimica Acta 56, 3225–3231.

Bern C. R. and White A. F. (2011) A model for assessing, quantifying, and correcting for index element mobility in weathering studies. *Applied Geochemistry* **26**, S9–S11.

Black J. R., Epstein E., Rains W. D., Yin Q. Z. and Casey W. H. (2008) Magnesium-isotope Fractionation During Plant Growth. *Environmental Science & Technology* **42**, 7831–7836.

Bolou-Bi E. B., Poszwa A., Leyval C. and Vigier N. (2010) Experimental determination of magnesium isotope fractionation during higher plant growth. *Geochimica et Cosmochimica Acta* **74**, 2523–2537.

Bolou-Bi E. B., Vigier N., Poszwa A., Boudot J.-P. and Dambrine E. (2012) Effects of biogeochemical processes on magnesium isotope variations in a forested catchment in the Vosges Mountains (France). *Geochimica et Cosmochimica Acta* **87**, 341–355.

Bouchez J., Blanckenburg F. von and Schuessler J. A. (2013) Modeling novel stable isotope ratios in the weathering zone. *Am J Sci* **313**, 267–308.

Brantley S. L., Goldhaber M. B. and Ragnarsdottir K. V. (2007) Crossing Disciplines and Scales to Understand the Critical Zone. *Elements* **3**, 307–314.

Brantley S. L., Megonigal J. P., Scatena F. N., Balogh-Brunstad Z., Barnes R. T., Bruns M. A., Cappellen P. V., Dontsova K., Hartnett H. E., Hartshorn A. S., Heimsath A., Herndon E., Jin L., Keller C. K., Leake J. R., Mcdowell W. H., Meinzer F. C., Mozdzer T. J., Petsch S., Pett-Ridge J., Pregitzer K. S., Raymond P. A., Riebe C. S., Shumaker K., Sutton-Grier A., Walter R. and Yoo K. (2011) Twelve testable hypotheses on the geobiology of weathering. *Geobiology* **9**, 140–165.

Brenot A., Cloquet C., Vigier N., Carignan J. and France-Lanord C. (2008) Magnesium isotope systematics of the lithologically varied Moselle river basin, France. *Geochimica et Cosmochimica Acta* **72**, 5070–5089.

Brimhall G. H. and Dietrich W. E. (1987) Constitutive mass balance relations between chemical composition, volume, density, porosity, and strain in metasomatic hydrochemical systems: Results on weathering and pedogenesis. *Geochimica et Cosmochimica Acta* **51**, 567–587.

Buendía C., Kleidon A. and Porporato A. (2010) The role of tectonic uplift, climate, and vegetation in the long-term terrestrial phosphorous cycle. *Biogeosciences* **7**, 2025–2038.

Bullen T. and Chadwick O. (2016) Ca, Sr and Ba stable isotopes reveal the fate of soil nutrients along a tropical climosequence in Hawaii. Chemical Geology 422, 25–45.

Cai D., Henehan M. J., Uhlig D. and von Blanckenburg F. (2022) Mg isotope composition of runoff is buffered by the regolith exchangeable pool. Geochimica et Cosmochimica Acta 321, 99–114.

Campbell D. H., Clow D. W., Ingersoll G. P., Mast M. A., Spahr N. E. and Turk J. T. (1995) Processes Controlling the Chemistry of Two Snowmelt-Dominated Streams in the Rocky Mountains. *Water Resources Research* **31**, 2811–2821.

Caves Rugenstein J. K., Ibarra D. E. and von Blanckenburg F. (2019) Neogene

cooling driven by land surface reactivity rather than increased weathering fluxes. *Nature* **571**, 99–102.

Chadwick O. A., Derry L. A., Vitousek P. M., Huebert B. J. and Hedin L. O. (1999) Changing sources of nutrients during four million years of ecosystem development. *Nature* **397**, 491–497.

Chapela Lara M., Buss H. L., Pogge von Strandmann P. A. E., Schuessler J. A. and Moore O. W. (2017) The influence of critical zone processes on the Mg isotope budget in a tropical, highly weathered andesitic catchment. *Geochimica et Cosmochimica Acta* **202**, 77–100.

Chapin SF, Matson PA, Vitousek PM (2012) Principles of terrestrial ecosystem ecology, Second. Springer New York Dordrecht Heidelberg London

Charlet L. and Sposito G. (1989) Bivalent Ion Adsorption by an Oxisol. *Soil Science Society of America Journal* **53**, 691–695.

Clergue C., Dellinger M., Buss H. L., Gaillardet J., Benedetti M. F. and Dessert C. (2015) Influence of atmospheric deposits and secondary minerals on Li isotopes budget in a highly weathered catchment, Guadeloupe (Lesser Antilles). *Chemical Geology* **414**, 28–41.

Clow D. W. and Mast M. A. (2010) Mechanisms for chemostatic behavior in catchments: Implications for CO_2 consumption by mineral weathering. *Chemical Geology* **269**, 40–51.

Dellinger M., Gaillardet J., Bouchez J., Calmels D., Galy V., Hilton R. G., Louvat P. and France-Lanord C. (2014) Lithium isotopes in large rivers reveal the cannibalistic nature of modern continental weathering and erosion. *Earth and Planetary Science Letters* **401**, 359–372.

Dellinger M., Gaillardet J., Bouchez J., Calmels D., Louvat P., Dosseto A., Gorge C., Alanoca L. and Maurice L. (2015) Riverine Li isotope fractionation in the Amazon River basin controlled by the weathering regimes. *Geochimica et Cosmochimica Acta* **164**, 71–93.

Dessert C., Lajeunesse E., Lloret E., Clergue C., Crispi O., Gorge C. and Quidelleur X. (2015) Controls on chemical weathering on a mountainous volcanic tropical island: Guadeloupe (French West Indies). *Geochimica et Cosmochimica Acta* **171**, 216–237.

Drouet Th., Herbauts J., Gruber W. and Demaiffe D. (2005) Strontium isotope composition as a tracer of calcium sources in two forest ecosystems in Belgium. *Geoderma* **126**, 203–223.

Ehleringer J. R. and Dawson T. E. (1992) Water uptake by plants: perspectives from stable isotope composition. *Plant, Cell & Environment* **15**, 1073–1082.

Flesch G. D., Anderson A. R. and Svec H. J. (1973) A secondary isotopic standard for $^{6}Li/^{7}Li$ determinations. *International Journal of Mass Spectrometry and Ion Physics* **12**, 265–272.

Ford Cochran M. and Berner R. A. (1996) Promotion of chemical weathering by higher plants: field observations on Hawaiian basalts. *Chemical Geology* **132**, 71–77.

Frey B., Rieder S. R., Brunner I., Plötze M., Koetzsch S., Lapanje A., Brandl H. and Furrer G. (2010) Weathering-Associated Bacteria from the Damma Glacier Forefield: Physiological Capabilities and Impact on Granite Dissolution. *Applied and Environmental Microbiology* **76**, 4788–4796.

Fries D. M., James R. H., Dessert C., Bouchez J., Beaumais A. and Pearce C. R. (2019) The response of Li and Mg isotopes to rain events in a highly-weathered catchment. *Chemical Geology* **519**, 68–82.

Gaillardet J., Dupré B., Louvat P. and Allègre C. J. (1999) Global silicate weathering and CO_2 consumption rates deduced from the chemistry of large rivers. *Chemical Geology* **159**, 3–30.

Ganor J., Roueff E., Erel Y. and Blum J. D. (2005) The dissolution kinetics of a granite and its minerals—Implications for comparison between laboratory and field dissolution rates. *Geochimica et Cosmochimica Acta* **69**, 607–621.

Gou L.-F., Jin Z., Pogge von Strandmann P. A. E., Li G., Qu Y.-X., Xiao J., Deng L. and Galy A. (2019) Li isotopes in the middle Yellow River: Seasonal variability, sources and fractionation. *Geochimica et Cosmochimica Acta* **248**, 88–108.

Hasenmueller E. A., Gu X., Weitzman J. N., Adams T. S., Stinchcomb G. E., Eissenstat D. M., Drohan P. J., Brantley S. L. and Kaye J. P. (2017) Weathering of rock to regolith: The activity of deep roots in bedrock fractures. *Geoderma* **300**, 11–31.

van der Heijden G., Legout A., Midwood A. J., Craig C.-A., Pollier B., Ranger J. and Dambrine E. (2013) Mg and Ca root uptake and vertical transfer in soils assessed by an *in situ* ecosystem-scale multi-isotopic (^{26}Mg & ^{44}Ca) tracing experiment in a beech stand (Breuil-Chenue, France). *Plant Soil* **369**, 33–45.

Henchiri S., Gaillardet J., Dellinger M., Bouchez J. and Spencer R. G. M. (2016) Riverine dissolved lithium isotopic signatures in low-relief central Africa and

their link to weathering regimes. *Geophysical Research Letters* **43**, 4391–4399.

Hindshaw R. S., Reynolds B. C., Wiederhold J. G., Kretzschmar R. and Bourdon B. (2011) Calcium isotopes in a proglacial weathering environment: Damma glacier, Switzerland. *Geochimica et Cosmochimica Acta* **75**, 106–118.

Hindshaw R. S., Teisserenc R., Le Dantec T. and Tananaev N. (2019a) Seasonal change of geochemical sources and processes in the Yenisei River: A Sr, Mg and Li isotope study. *Geochimica et Cosmochimica Acta* **255**, 222–236.

Hindshaw R. S., Tosca R., Goût T. L., Farnan I., Tosca N. J. and Tipper E. T. (2019b) Experimental constraints on Li isotope fractionation during clay formation. *Geochimica et Cosmochimica Acta* **250**, 219–237.

Hindshaw R. S., Tosca R., Tosca N. J. and Tipper E. T. (2020) Experimental constraints on Mg isotope fractionation during clay formation: Implications for the global biogeochemical cycle of Mg. *Earth and Planetary Science Letters* **531**, 115980.

Huh Y., Chan L.-H. and Chadwick O. A. (2004) Behavior of lithium and its isotopes during weathering of Hawaiian basalt. *Geochemistry, Geophysics, Geosystems* **5**.

Huh Y., Chan L.-H. and Edmond J. M. (2001) Lithium isotopes as a probe of weathering processes: Orinoco River. *Earth and Planetary Science Letters* **194**, 189–199.

Huh Y., Chan L.-H., Zhang L. and Edmond J. M. (1998) Lithium and its isotopes in major world rivers: implications for weathering and the oceanic budget. *Geochimica et Cosmochimica Acta* **62**, 2039–2051.

James J., Littke K., Bonassi T. and Harrison R. (2016) Exchangeable cations in deep forest soils: Separating climate and chemical controls on spatial and vertical distribution and cycling. *Geoderma* **279**, 109–121.

Jobbágy E. G. and Jackson R. B. (2001) The distribution of soil nutrients with depth: Global patterns and the imprint of plants. *Biogeochemistry* **53**, 51–77.

Jobbágy E. G. and Jackson R. B. (2004) The Uplift of Soil Nutrients by Plants: Biogeochemical Consequences Across Scales. *Ecology* **85**, 2380–2389.

Jongmans A. G., van Breemen N., Lundström U., van Hees P. A. W., Finlay R. D., Srinivasan M., Unestam T., Giesler R., Melkerud P.-A. and Olsson M. (1997) Rock-eating fungi. *Nature* **389**, 682–683.

Kim H., Dietrich W. E., Thurnhoffer B. M., Bishop J. K. B. and Fung I. Y. (2017) Controls on solute concentration-discharge relationships revealed by simultaneous hydrochemistry observations of hillslope runoff and stream flow: The importance of critical zone structure. *Water Resour. Res.* **53**, 1424–1443.

Kimmig S. R., Holmden C. and Bélanger N. (2018) Biogeochemical cycling of Mg and its isotopes in a sugar maple forest in Québec. *Geochimica et Cosmochimica Acta*.

Kısakűrek B., James R. H. and Harris N. B. W. (2005) Li and δ^7Li in Himalayan rivers: Proxies for silicate weathering? *Earth and Planetary Science Letters* **237**, 387–401.

Kump L. R., Brantley S. L. and Arthur M. A. (2000) Chemical Weathering, Atmospheric CO_2, and Climate. *Annual Review of Earth and Planetary Sciences* **28**, 611–667.

Lang F., Krüger J., Amelung W., Willbold S., Frossard E., Bünemann E. K., Bauhus J., Nitschke R., Kandeler E., Marhan S., Schulz S., Bergkemper F., Schloter M., Luster J., Guggisberg F., Kaiser K., Mikutta R., Guggenberger G., Polle A., Pena R., Prietzel J., Rodionov A., Talkner U., Meesenburg H., Wilpert K. von, Hölscher A., Dietrich H. P. and Chmara I. (2017) Soil phosphorus supply controls P nutrition strategies of beech forest ecosystems in Central Europe. *Biogeochemistry* **136**, 5–29.

Lee C.-T. A., Morton D. M., Little M. G., Kistler R., Horodyskyj U. N., Leeman W. P. and Agranier A. (2008) Regulating continent growth and composition by chemical weathering. *PNAS* **105**, 4981–4986.

Lemarchand E., Chabaux F., Vigier N., Millot R. and Pierret M.-C. (2010) Lithium isotope systematics in a forested granitic catchment (Strengbach, Vosges Mountains, France). *Geochimica et Cosmochimica Acta* **74**, 4612–4628.

Li G. and West A. J. (2014) Evolution of Cenozoic seawater lithium isotopes: Coupling of global denudation regime and shifting seawater sinks. *Earth and Planetary Science Letters* **401**, 284–293.

Li W., Beard B. L., Li C. and Johnson C. M. (2014) Magnesium isotope fractionation between brucite [$Mg(OH)_2$] and Mg aqueous species: Implications for silicate weathering and biogeochemical processes. *Earth and Planetary Science Letters* **394**, 82–93.

Li W. and Liu X.-M. (2020) Experimental investigation of lithium isotope fractionation during kaolinite adsorption: Implications for chemical

weathering. *Geochimica et Cosmochimica Acta* **284**, 156–172.

Li W., Liu X.-M. and Chadwick O. A. (2020) Lithium isotope behavior in Hawaiian regoliths: Soil-atmosphere-biosphere exchanges. *Geochimica et Cosmochimica Acta* **285**, 175–192.

Li W., Liu X.-M., Wang K. and Koefoed P. (2021) Lithium and potassium isotope fractionation during silicate rock dissolution: An experimental approach. *Chemical Geology* **568**, 120142.

Liu X.-M., Rudnick R. L., McDonough W. F. and Cummings M. L. (2013) Influence of chemical weathering on the composition of the continental crust: Insights from Li and Nd isotopes in bauxite profiles developed on Columbia River Basalts. Geochimica et Cosmochimica Acta 115, 73–91.

Liu X.-M., Teng F.-Z., Rudnick R. L., McDonough W. F. and Cummings M. L. (2014) Massive magnesium depletion and isotope fractionation in weathered basalts. *Geochimica et Cosmochimica Acta* **135**, 336–349.

Liu X.-M., Wanner C., Rudnick R. L. and McDonough W. F. (2015) Processes controlling δ^7Li in rivers illuminated by study of streams and groundwaters draining basalts. *Earth and Planetary Science Letters* **409**, 212–224.

Lucas Y. (2001) The Role of Plants in Controlling Rates and Products of Weathering: Importance of Biological Pumping. *Annual Review of Earth and Planetary Sciences* **29**, 135–163.

Ma L., Teng F.-Z., Jin L., Ke S., Yang W., Gu H.-O. and Brantley S. L. (2015) Magnesium isotope fractionation during shale weathering in the Shale Hills Critical Zone Observatory: Accumulation of light Mg isotopes in soils by clay mineral transformation. *Chemical Geology* **397**, 37–50.

Maher K. (2010) The dependence of chemical weathering rates on fluid residence time. *Earth and Planetary Science Letters* **294**, 101–110.

Maher K., Johnson N. C., Jackson A., Lammers L. N., Torchinsky A. B., Weaver K. L., Bird D. K. and Brown G. E. (2016) A spatially resolved surface kinetic model for forsterite dissolution. *Geochimica et Cosmochimica Acta* **174**, 313–334.

Manaka T., Araoka D., Yoshimura T., Hossain H. M. Z., Nishio Y., Suzuki A. and Kawahata H. (2017) Downstream and seasonal changes of lithium isotope ratios in the Ganges-Brahmaputra river system. *Geochemistry, Geophysics, Geosystems* **18**, 3003–3015.

Markewitz D., Davidson E. A., Figueiredo R. de O., Victoria R. L. and Krusche A. V. (2001) Control of cation concentrations in stream waters by surface soil processes in an Amazonian watershed. *Nature* **410**, 802–805.

Martinelli L. A., Piccolo M. C., Townsend A. R., Vitousek P. M., Cuevas E., McDowell W., Robertson G. P., Santos O. C. and Treseder K. (1999) Nitrogen stable isotopic composition of leaves and soil: Tropical versus temperate forests. *Biogeochemistry* **46**, 45–65.

Mavromatis V., Prokushkin A. S., Pokrovsky O. S., Viers J. and Korets M. A. (2014) Magnesium isotopes in permafrost-dominated Central Siberian larch forest watersheds. *Geochimica et Cosmochimica Acta* **147**, 76–89.

Miller E. K., Blum J. D. and Friedland A. J. (1993) Determination of soil exchangeable-cation loss and weathering rates using Sr isotopes. *Nature* **362**, 438–441.

Millot R., Guerrot C. and Vigier N. (2004) Accurate and High-Precision Measurement of Lithium Isotopes in Two Reference Materials by MC-ICP-MS. Geostandards and Geoanalytical Research 28, 153–159.

Millot R. and Girard J. P. (2007) Lithium isotope fractionation during adsorption onto mineral surfaces. Clays Nat. Eng. Barriers Radioact. Waste Confin. 3rd Int. Meet.,307–308.

Millot R., Scaillet B. and Sanjuan B. (2010a) Lithium isotopes in island arc geothermal systems: Guadeloupe, Martinique (French West Indies) and experimental approach. *Geochimica et Cosmochimica Acta* **74**, 1852–1871.

Millot R., Vigier N. and Gaillardet J. (2010b) Behaviour of lithium and its isotopes during weathering in the Mackenzie Basin, Canada. *Geochimica et Cosmochimica Acta* **74**, 3897–3912.

Misra S. and Froelich P. N. (2012) Lithium Isotope History of Cenozoic Seawater: Changes in Silicate Weathering and Reverse Weathering. *Science* **335**, 818–823.

Noireaux J., Sullivan P. L., Gaillardet J., Louvat P., Steinhoefel G. and Brantley S. L. (2021) Developing boron isotopes to elucidate shale weathering in the critical zone. Chemical Geology 559, 119900.

Novak M., Andronikov A., Kram P., Curik J., Veselovsky F., Stepanova M., Prechova E., Sebek O. and Bohdalkova L. (2021) Time-series of δ^{26}Mg values in a headwater catchment reveal decreasing magnesium isotope variability from precipitation to runoff. *Hydrological Processes* **35**, e14116.

Oeser R. A. and von Blanckenburg F. (2020) Do degree and rate of silicate weathering depend on plant productivity? *Biogeosciences* **17**, 4883–4917.

Oeser R. A. and von Blanckenburg F. (2020) Strontium isotopes trace biological activity in the Critical Zone along a climate and vegetation gradient. Chemical Geology 558, 119861.

O'Leary M. H. (1988) Carbon Isotopes in Photosynthesis. *BioScience* **38**, 328–336.

Opfergelt S., Burton K. W., Georg R. B., West A. J., Guicharnaud R. A., Sigfusson B., Siebert C., Gislason S. R. and Halliday A. N. (2014) Magnesium retention on the soil exchange complex controlling Mg isotope variations in soils, soil solutions and vegetation in volcanic soils, Iceland. *Geochimica et Cosmochimica Acta* **125**, 110–130.

Page B. D., Bullen T. D. and Mitchell M. J. (2008) Influences of calcium availability and tree species on Ca isotope fractionation in soil and vegetation. *Biogeochemistry* **88**, 1–13.

Pawlik Ł., Phillips J. D. and Šamonil P. (2016) Roots, rock, and regolith: Biomechanical and biochemical weathering by trees and its impact on hillslopes—A critical literature review. *Earth-Science Reviews* **159**, 142–159.

Penniston-Dorland S., Liu X.-M. and Rudnick R. L. (2017) Lithium Isotope Geochemistry. *Reviews in Mineralogy and Geochemistry* **82**, 165–217.

Pistiner J. S. and Henderson G. M. (2003) Lithium-isotope fractionation during continental weathering processes. *Earth and Planetary Science Letters* **214**, 327–339.

Poppe, L.J., Paskevich, V.F., Hathaway, J.C. and Blackwood, D.S., (2001). A laboratory manual for X-ray powder diffraction. US Geological Survey open-file report, 1(041), 1-88.

Pogge von Strandmann P. A. E., Burton K. W., James R. H., van Calsteren P., Gíslason S. R. and Mokadem F. (2006) Riverine behaviour of uranium and lithium isotopes in an actively glaciated basaltic terrain. *Earth and Planetary Science Letters* **251**, 134–147.

Pogge von Strandmann P. A. E., Burton K. W., James R. H., van Calsteren P., Gislason S. R. and Sigfússon B. (2008) The influence of weathering processes on riverine magnesium isotopes in a basaltic terrain. *Earth and Planetary Science Letters* **276**, 187–197.

Pogge von Strandmann P. A. E., Burton K. W., Opfergelt S., Eiríksdóttir E. S.,

Murphy M. J., Einarsson A. and Gislason S. R. (2016) The effect of hydrothermal spring weathering processes and primary productivity on lithium isotopes: Lake Myvatn, Iceland. *Chemical Geology* **445**, 4–13.

Pogge von Strandmann P. A. E., Fraser W. T., Hammond S. J., Tarbuck G., Wood I. G., Oelkers E. H. and Murphy M. J. (2019a) Experimental determination of Li isotope behaviour during basalt weathering. *Chemical Geology* **517**, 34–43.

Pogge von Strandmann P. A. E. and Henderson G. M. (2015) The Li isotope response to mountain uplift. *Geology* **43**, 67–70.

Pogge von Strandmann P. A. E., Schmidt D. N., Planavsky N. J., Wei G., Todd C. L. and Baumann K.-H. (2019b) Assessing bulk carbonates as archives for seawater Li isotope ratios. *Chemical Geology* **530**, 119338.

Pokharel R., Gerrits R., Schuessler J. A. and von Blanckenburg F. (2019) Mechanisms of olivine dissolution by rock-inhabiting fungi explored using magnesium stable isotopes. *Chemical Geology* **525**, 18–27.

Pokharel R., Gerrits R., Schuessler J. A., Frings P. J., Sobotka R., Gorbushina A. A. and von Blanckenburg F. (2018) Magnesium Stable Isotope Fractionation on a Cellular Level Explored by Cyanobacteria and Black Fungi with Implications for Higher Plants. *Environ. Sci. Technol.* **52**, 12216–12224.

Porder S. and Chadwick O. A. (2009) Climate and soil-age constraints on nutrient uplift and retention by plants. Ecology 90, 623–636.

Porder S., Vitousek P. M., Chadwick O. A., Chamberlain C. P. and Hilley G. E. (2007) Uplift, Erosion, and Phosphorus Limitation in Terrestrial Ecosystems. *Ecosystems* **10**, 159–171.

Powers J. S., Becklund K. K., Gei M. G., Iyengar S. B., Meyer R., O' Connell C. S., Schilling E. M., Smith C. M., Waring B. G. and Werden L. K. (2015) Nutrient addition effects on tropical dry forests: a mini-review from microbial to ecosystem scales. *Front. Earth Sci.* **3**.

Qi H. P., Taylor P. D. P., Berglund M. and De Bièvre P. (1997) Calibrated measurements of the isotopic composition and atomic weight of the natural Li isotopic reference material IRMM-016. *International Journal of Mass Spectrometry and Ion Processes* **171**, 263–268.

Riebe C. S., Kirchner J. W., Granger D. E. and Finkel R. C. (2001) Strong tectonic and weak climatic control of long-term chemical weathering rates. *Geology* **29**, 511–514.

Robinson B. H., Yalamanchali R., Reiser R. and Dickinson N. M. (2018) Lithium as an emerging environmental contaminant: Mobility in the soil-plant system. *Chemosphere* **197**, 1–6.

Rodstedth M., Ståhlberg C., Sandén P. and Öberg G. (2003) Chloride imbalances in soil lysimeters. *Chemosphere* **52**, 381–389.

Roering J. J., Marshall J., Booth A. M., Mort M. and Jin Q. (2010) Evidence for biotic controls on topography and soil production. *Earth and Planetary Science Letters* **298**, 183–190.

Ryu J.-S., Jacobson A. D., Holmden C., Lundstrom C. and Zhang Z. (2011) The major ion, $\delta^{44/40}$Ca, $\delta^{44/42}$Ca, and $\delta^{26/24}$Mg geochemistry of granite weathering at pH=1 and T=25°C: power-law processes and the relative reactivity of minerals. *Geochimica et Cosmochimica Acta* **75**, 6004–6026.

Ryu J.-S., Vigier N., Decarreau A., Lee S.-W., Lee K.-S., Song H. and Petit S. (2016) Experimental investigation of Mg isotope fractionation during mineral dissolution and clay formation. *Chemical Geology* **445**, 135–145.

Ryu J.-S., Vigier N., Lee S.-W., Lee K.-S. and Chadwick O. A. (2014) Variation of lithium isotope geochemistry during basalt weathering and secondary mineral transformations in Hawaii. *Geochimica et Cosmochimica Acta* **145**, 103–115.

Saenger C. and Wang Z. (2014) Magnesium isotope fractionation in biogenic and abiogenic carbonates: implications for paleoenvironmental proxies. *Quaternary Science Reviews* **90**, 1–21.

Scalley T. H., Scatena F. N., Moya S. and Lugo A. E. (2012) Long-term dynamics of organic matter and elements exported as coarse particulates from two Caribbean montane watersheds. *Journal of Tropical Ecology* **28**, 127–139.

Scatena F. N. and Lugo A. E. (1995) Geomorphology, disturbance, and the soil and vegetation of two subtropical wet steepland watersheds of Puerto Rico. *Geomorphology* **13**, 199–213.

Schmitt A.-D., Vigier N., Lemarchand D., Millot R., Stille P. and Chabaux F. (2012) Processes controlling the stable isotope compositions of Li, B, Mg and Ca in plants, soils and waters: A review. *Comptes Rendus Geoscience* **344**, 704–722.

Schöll L. V., Hoffland E. and Breemen N. V. (2006a) Organic anion exudation by ectomycorrhizal fungi and *Pinus sylvestris* in response to nutrient deficiencies. *New Phytologist* **170**, 153–163.

Schöll L. V., Smits M. M. and Hoffland E. (2006b) Ectomycorrhizal weathering of the soil minerals muscovite and hornblende. *New Phytologist* **171**, 805–814.

Schott J., Mavromatis V., Fujii T., Pearce C. R. and Oelkers E. H. (2016) The control of carbonate mineral Mg isotope composition by aqueous speciation: Theoretical and experimental modeling. *Chemical Geology* **445**, 120–134.

Schollenberger C. J. and Simon R. H. (1945) Determination of exchange capacity and exchangeable bases in soil—ammonium acetate method. Soil Science 59, 13–24.

Schuessler J. A., Kämpf H., Koch U. and Alawi M. (2016) Earthquake impact on iron isotope signatures recorded in mineral spring water. *Journal of Geophysical Research: Solid Earth* **121**, 8548–8568.

Shalev N., Farkaš J., Fietzke J., Novák M., Schuessler J. A., Strandmann P. A. E. P. von and Törber P. B. (2018) Mg Isotope Interlaboratory Comparison of Reference Materials from Earth-Surface Low-Temperature Environments. *Geostandards and Geoanalytical Research* **42**, 205–221.

Sohrt J., Uhlig D., Kaiser K., von Blanckenburg F., Siemens J., Seeger S., Frick D. A., Krüger J., Lang F. and Weiler M. (2019) Phosphorus Fluxes in a Temperate Forested Watershed: Canopy Leaching, Runoff Sources, and In-Stream Transformation. *Front. For. Glob. Change* **2**, 85.

Steinhoefel G., Brantley S. L. and Fantle M. S. (2021) Lithium isotopic fractionation during weathering and erosion of shale. *Geochimica et Cosmochimica Acta* **295**, 155–177.

Teng F.-Z. (2017) Magnesium Isotope Geochemistry. *Reviews in Mineralogy and Geochemistry* **82**, 219–287.

Teng F.-Z., Li W.-Y., Rudnick R. L. and Gardner L. R. (2010) Contrasting lithium and magnesium isotope fractionation during continental weathering. Earth and Planetary Science Letters 300, 63–71.

Teng F.-Z., McDonough W. F., Rudnick R. L., Dalpé C., Tomascak P. B., Chappell B. W. and Gao S. (2004) Lithium isotopic composition and concentration of the upper continental crust. Geochimica et Cosmochimica Acta 68, 4167–4178

Tipper E. T., Galy A. and Bickle M. J. (2008) Calcium and magnesium isotope systematics in rivers draining the Himalaya-Tibetan-Plateau region: Lithological or fractionation control? *Geochimica et Cosmochimica Acta* **72**, 1057–1075.

Tipper E. T., Galy A. and Bickle M. J. (2006a) Riverine evidence for a fractionated reservoir of Ca and Mg on the continents: Implications for the oceanic Ca cycle. *Earth and Planetary Science Letters* **247**, 267–279.

Tipper E. T., Galy A., Gaillardet J., Bickle M. J., Elderfield H. and Carder E. A. (2006b) The magnesium isotope budget of the modern ocean: Constraints from riverine magnesium isotope ratios. *Earth and Planetary Science Letters* **250**, 241–253.

Tipper E. T., Lemarchand E., Hindshaw R. S., Reynolds B. C. and Bourdon B. (2012) Seasonal sensitivity of weathering processes: Hints from magnesium isotopes in a glacial stream. *Chemical Geology* **312–313**, 80–92.

Trivedi P. and Axe L. (2001) Predicting Divalent Metal Sorption to Hydrous Al, Fe, and Mn Oxides. *Environ. Sci. Technol.* **35**, 1779–1784.

Uhlig D., Amelung W. and Blanckenburg F. von (2020) Mineral Nutrients Sourced in Deep Regolith Sustain Long-Term Nutrition of Mountainous Temperate Forest Ecosystems. *Global Biogeochemical Cycles* **34**, e2019GB006513.

Uhlig D. and von Blanckenburg F. (2019) How Slow Rock Weathering Balances Nutrient Loss During Fast Forest Floor Turnover in Montane, Temperate Forest Ecosystems. *Front. Earth Sci.* **7**.

Uhlig D., Schuessler J. A., Bouchez J., Dixon J. L. and von Blanckenburg F. (2017) Quantifying nutrient uptake as driver of rock weathering in forest ecosystems by magnesium stable isotopes. *Biogeosciences* **14**, 3111–3128.

Verney-Carron A., Vigier N. and Millot R. (2011) Experimental determination of the role of diffusion on Li isotope fractionation during basaltic glass weathering. *Geochimica et Cosmochimica Acta* **75**, 3452–3468.

Vigier N., Decarreau A., Millot R., Carignan J., Petit S. and France-Lanord C. (2008) Quantifying Li isotope fractionation during smectite formation and implications for the Li cycle. *Geochimica et Cosmochimica Acta* **72**, 780–792.

Vigier N., Gislason S. R., Burton K. W., Millot R. and Mokadem F. (2009) The relationship between riverine lithium isotope composition and silicate weathering rates in Iceland. *Earth and Planetary Science Letters* **287**, 434–441.

Vigier N. and Goddéris Y. (2015) A new approach for modeling Cenozoic oceanic lithium isotope paleo-variations: the key role of climate. *Climate of the Past* **11**, 635–645.

Vitousek P. M. and Sanford R. L. (1986) Nutrient Cycling in Moist Tropical Forest. *Annual Review of Ecology and Systematics* **17**, 137–167.

von Blanckenburg F., von Wiren N., Guelke M., Weiss D. J. and Bullen T. D. (2009) Fractionation of Metal Stable Isotopes by Higher Plants. Elements 5, 375–380.

von Blanckenburg, F., Schuessler, J.A., Bouchez, J., Frings, P.J., Uhlig, D., Oelze, M., Frick, D.A., Hewawasam, T., Dixon, J.E., Norton, K., 2021. Rock weathering and nutrient cycling along an erodosequence. American Journal of Science 321. doi: 10.2475/08.2021.01

Wang Q.-L., Chetelat B., Zhao Z.-Q., Ding H., Li S.-L., Wang B.-L., Li J. and Liu X.-L. (2015) Behavior of lithium isotopes in the Changjiang River system: Sources effects and response to weathering and erosion. *Geochimica et Cosmochimica Acta* **151**, 117–132.

Wanner C., Sonnenthal E. L. and Liu X.-M. (2014) Seawater δ^7Li: A direct proxy for global CO_2 consumption by continental silicate weathering? *Chemical Geology* **381**, 154–167.

White A. F., Blum A. E., Bullen T. D., Vivit D. V., Schulz M. and Fitzpatrick J. (1999) The effect of temperature on experimental and natural chemical weathering rates of granitoid rocks. *Geochimica et Cosmochimica Acta* **63**, 3277–3291.

Wimpenny J., Burton K. W., James R. H., Gannoun A., Mokadem F. and Gíslason S. R. (2011) The behaviour of magnesium and its isotopes during glacial weathering in an ancient shield terrain in West Greenland. *Earth and Planetary Science Letters* **304**, 260–269.

Wimpenny J., Colla C. A., Yin Q.-Z., Rustad J. R. and Casey W. H. (2014) Investigating the behaviour of Mg isotopes during the formation of clay minerals. *Geochimica et Cosmochimica Acta* **128**, 178–194.

Wimpenny J., Colla C. A., Yu P., Yin Q.-Z., Rustad J. R. and Casey W. H. (2015) Lithium isotope fractionation during uptake by gibbsite. *Geochimica et Cosmochimica Acta* **168**, 133–150.

Wimpenny J., Gíslason S. R., James R. H., Gannoun A., Pogge Von Strandmann P. A. E. and Burton K. W. (2010) The behaviour of Li and Mg isotopes during primary phase dissolution and secondary mineral formation in basalt. *Geochimica et Cosmochimica Acta* **74**, 5259–5279.

Yu Z., Chen H. Y. H., Searle E. B., Sardans J., Ciais P., Peñuelas J. and Huang Z.

(2020) Whole soil acidification and base cation reduction across subtropical China. *Geoderma* **361**, 114107.

Zhang J.-W., Zhao Z.-Q., Yan Y.-N., Cui L.-F., Wang Q.-L., Meng J.-L., Li X.-D. and Liu C.-Q. (2021) Lithium and its isotopes behavior during incipient weathering of granite in the eastern Tibetan Plateau, China. *Chemical Geology* **559**, 119969.

Zhang L., Chan L.-H. and Gieskes J. M. (1998) Lithium isotope geochemistry of pore waters from ocean drilling program Sites 918 and 919, Irminger Basin. *Geochimica et Cosmochimica Acta* **62**, 2437–2450.

Zhang X., Saldi G. D., Schott J., Bouchez J., Kuessner M., Montouillout V., Henehan M. and Gaillardet J. (2021) Experimental constraints on Li isotope fractionation during the interaction between kaolinite and seawater. *Geochimica et Cosmochimica Acta* **292**, 333–347.